

(NASA-CR-149107) SIMPLIFIED SIMULATION
MODELS FOR CONTROL STUDIES OF TURBOJET
ENGINES (Notre Dame Univ.) - 93 p HC A05/MF
A01 CSCI 21E

N77-10061

Unclas
G3/07 08035



Department of

ELECTRICAL ENGINEERING



UNIVERSITY OF NOTRE DAME, NOTRE DAME, INDIANA

SIMPLIFIED SIMULATION MODELS FOR CONTROL
STUDIES OF TURBOJET ENGINES*

Thomas C. Brennan and R. Jeffrey Leake
Department of Electrical Engineering
University of Notre Dame
Notre Dame, Indiana 46556

Technical Report No. EE-757

November, 1975

*This research was supported in part by the National Aeronautics and Space Administration under Grant NSG-3048, and also has been submitted in partial fulfillment of the requirement for the M.S.E.E. degree at the University of Notre Dame.

TABLE OF CONTENTS

	<u>Page</u>
ACKNOWLEDGMENT	ii
LIST OF SYMBOLS	iv
I. INTRODUCTION	1
II. DERIVATION OF SIMULATION MODELS	3
III. SIMULATION AND CONTROL STUDIES OF SEVENTH ORDER SYSTEM	21
IV. SIMULATION AND CONTROL STUDIES OF THIRD ORDER SYSTEM	26
V. CONCLUSION	30
APPENDIX A: SEVENTH ORDER SIMULATION RESULTS	31
APPENDIX B: THIRD ORDER SIMULATION RESULTS	53
APPENDIX C: DETAILS OF SEVENTH ORDER SIMULATION MODEL	68
APPENDIX D: DETAILS OF THIRD ORDER SIMULATION MODEL	75
APPENDIX E: SUMMARY OF REFERENCE [4]	81
REFERENCES	88

LIST OF SYMBOLS

$\dot{\omega}_2$	compressor inlet mass flow, kg/sec
T_2	compressor inlet temperature, K
P_2	compressor inlet pressure, N/m ²
ρ_c	compressor mass density, kg/m ³
P_2'	internal compressor pressure, N/m ²
T_2'	internal compressor temperature, K
$\dot{\omega}_3$	compressor discharge mass flow, kg/sec
T_3	compressor discharge temperature, K
P_3	compressor discharge pressure, N/m ²
V_1	compressor volume, m ³
A_1	compressor area, m ²
l_1	compressor length, m
ρ_B	combustor mass density, kg/m ³
$\dot{\omega}_4$	combustor mass flow, kg/sec
T_4	combustor temperature, K
P_4	combustor pressure, N/m ²
V_4	combustor volume m ³
A_4	combustor area, m ²
l_4	combustor length, m
$\dot{\omega}_f$	fuel flow, kg/sec
$\dot{\omega}_f'$	externally acted upon fuel flow, kg/sec
$\dot{\omega}_5$	turbine mass flow, kg/sec
T_5	turbine temperature, K
P_5	turbine pressure, N/m ²
V_5	turbine volume, m ³
N	rotational speed, rpm

\dot{w}_g	nozzle mass flow, kg/sec
θ	fraction of nozzle area
J	mechanical equivalent of heat, 1-Nm/J
I	rotor inertia, N-m-sec ²
R	universal gas constant, 287 Nm/kgK
γ	ratio of specific heats, 1.4

CHAPTER I

INTRODUCTION

This work represents an attempt to characterize the essential dynamical characteristics of a simple single-spool turbojet engine through simulation of low order system models on an Electronic Associates TR-48 analog computer. The objective is to gain insight into the most important dynamical constraints of such an engine, which can be applied to control studies of more advanced engines. The approach here is to begin with an accurate model which is studied in [1] and reduce system complexity through various linearizations and approximations. References [2] and [3] have been used as guides. Some excellent ideas in [4] have also been used, although this reference became available only after the present simulation was essentially in its final form, and thus certain suggested changes must be postponed for future studies.

This work consists of a derivation of a seventh order simplified simulation model, a derivation of an even simpler third order model, and simulation results from each.

The control problem studied is one of getting from "Windmill" (zero fuel flow equilibrium) to "Design" (a high thrust equilibrium) while taking into account surge margin and turbine inlet temperature constraints. Several control schemes were investigated.

As a matter of terminology, we wish to point out that in this work we consider dynamical system models of the form

$$\dot{x} = f(x,u) \tag{1}$$

with an associated design equilibrium point,

$$u = u_E \quad (2)$$

$$x = x_E$$

such that

$$f(x_E, u_E) = 0 \quad (3)$$

We use normalized variables

$$\hat{u}_i = u_i / u_{E_i} \quad \hat{x}_i = x_i / x_{E_i} \quad (4)$$

so that the normalized equivalent to (1) is

$$\dot{\hat{x}} = F(\hat{x}, \hat{u}) \quad (5)$$

with an equilibrium, corresponding to (2), occurring where components of \hat{x}_E and \hat{u}_E are all unity. It is also convenient to consider linearizations of

the normalized system (5) through

$$\hat{x} = \delta x + \hat{x}_E \quad \hat{u} = \delta u + \hat{u}_E \quad (6)$$

and the standard approximation

$$\dot{\delta x} = A \delta x + B \delta u \quad (7)$$

where

$$A = \frac{\partial F}{\partial \hat{x}} \quad B = \frac{\partial F}{\partial \hat{u}} \quad (8)$$

evaluated at (\hat{x}_E, \hat{u}_E) .

CHAPTER II
DERIVATION OF SIMULATION MODELS

2.1 Introduction

In this section we review the essential details in approximating the accurate simulation model of [1] by a seventh order dynamical system. The principal constraints lie in the limited nonlinear equipment available on the TR-48 analog computer. The main simplifications involved the extensive use of linear approximations, single stage compressor dynamics, a linear compressor map, assumptions of a choked nozzle condition, and certain empirical relations based on design point equilibrium data available in [1]. Additional simplification was achieved by limiting the model to a condition of 20,000 ft. altitude at Mach number .8. We shall term this model used in [1] the "Drone" system.

2.2 The Drone System

A complete description of the Drone system is presented in [1] , with certain details further elucidated in [2] and [4]. A rough simulation diagram is indicated in Figure 1. Throughout the development, P stands for pressure in newtons/meter², T stands for temperature in degrees Kelvin, \dot{w} represents mass flow rate in kilograms/second, and ρ is density in kilograms/meter³. N is rotor speed in revolutions/minute. Using a single stage rather than a four stage compressor model the main dynamical equations are:

Compressor

$$\frac{d\rho_c}{dt} = \frac{1}{V_1} (\dot{\omega}_2 - \dot{\omega}_3) \quad (1)$$

$$\frac{dP_2}{dt} = \frac{RY}{V_1} (T_2 \dot{\omega}_2 - T_2' \dot{\omega}_3) \quad (2)$$

$$\frac{d\dot{\omega}_2}{dt} = \frac{A_1}{I_1} (P_2 - P_2') \quad (3)$$

Burner

$$\frac{d\rho_B}{dt} = \frac{1}{V_4} (\dot{\omega}_4 + \dot{\omega}_f'' - \dot{\omega}_5) \quad (4)$$

$$\frac{dP_4}{dt} = \frac{RY}{V_4} (\dot{\omega}_4 T_3 + (\dot{\omega}_f'' - \dot{\omega}_5) T_4 + \frac{n_4 h_B}{C_{pB}} \dot{\omega}_f''') \quad (5)$$

$$\frac{d\dot{\omega}_4}{dt} = \frac{A_4}{I_4} (P_3 - P_4 - \Delta P_4) \quad (6)$$

$$\frac{d\dot{\omega}_f''}{dt} = \frac{1}{\tau} (\dot{\omega}_f - \dot{\omega}_f'') \quad (7)$$

Turbine

$$\frac{dP_5}{dt} = \frac{RT_5}{V_5} (\dot{\omega}_5 - \dot{\omega}_8) \quad (8)$$

Rotor

$$\frac{dN}{dt} = \left(\frac{30}{\pi}\right)^2 \frac{J}{NI} [C_{pB} (\dot{\omega}_5 T_4 - \dot{\omega}_8 T_5) + C_{pC} (\dot{\omega}_2 T_2 - \dot{\omega}_3 T_3)] \quad (9)$$

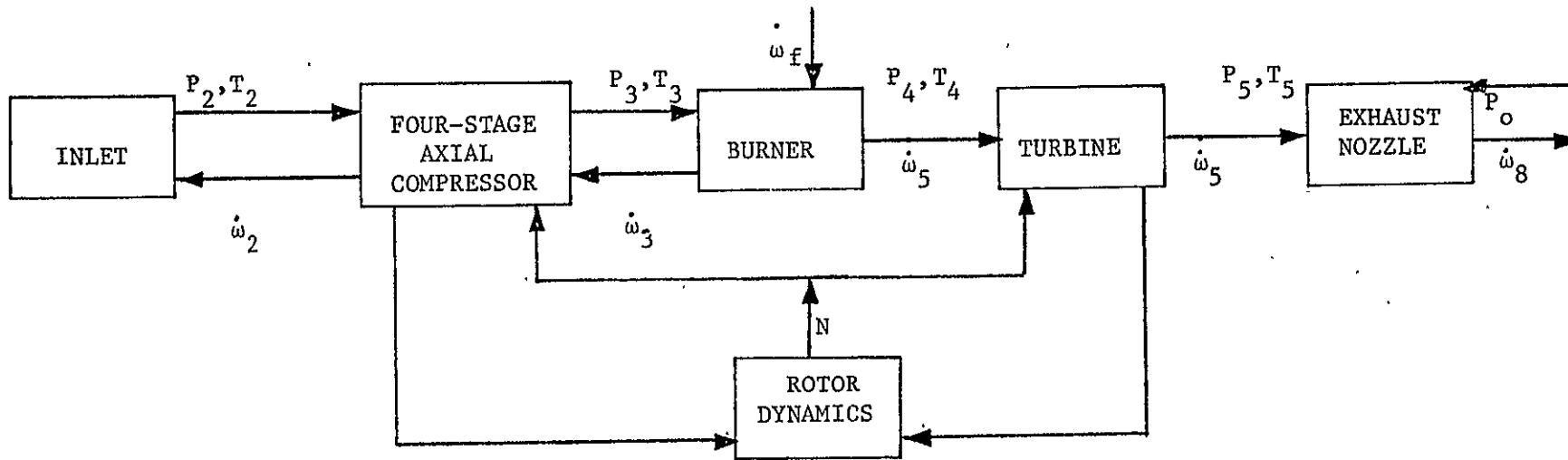


FIGURE 1. ROUGH SIMULATION DIAGRAM FOR DRONE SYSTEM

Auxiliary Relations

$$\begin{aligned}
 P_2' &= R\rho_c T_2' \\
 P_4 &= R\rho_B T_4 \\
 \Delta P_4 &= K_B \dot{\omega}_4^2 / P_3 \\
 \dot{\omega}_3 &= \dot{\omega}_4
 \end{aligned} \tag{10}$$

Non-Linear Functions

Turbine

$$\dot{\omega}_5 = f_1(N, T_4, P_4, P_5) \tag{11}$$

$$T_5 = f_2(T_4, P_4, P_5, N) \tag{12}$$

Nozzle

$$\dot{\omega}_8 = f_3(T_5, P_5) \tag{13}$$

Compressor

$$T_3 = f_4(T_2', N, P_4) \tag{14}$$

$$P_3 = f_5(P_2', T_2', \dot{\omega}_3, \dot{\omega}_2) \tag{15}$$

2.3 Assumptions

We now list the assumptions which were made in order to reduce the required nonlinear function generating equipment. Where appropriate, we point out the corresponding simplifications suggested in [4]. As mentioned earlier, many of the suggested changes were not implemented simply because they were not available by the time the simulations were run. One general comment is also in order with regard to linearizations. Rather than take partial derivatives of theoretical relations, the usual approach here was to take the best linear fits to the numerical data available for the five design points studied in [1].

(a) $T_2 = T_2' = 280.6^\circ\text{K}$. This eliminates the need for state equation (1) involving ρ_c and is consistent with [4].

(b) $\dot{\omega}_f = \dot{\omega}_f^u$ This ignores combustion lags and dead time. This assumption is also made in item (8) of reference [4].

(c) For $\dot{\omega}_5 = f_1(N, T_4, P_4, P_5)$ related to turbine characteristics we have used simply $\dot{\omega}_5 = 12.424 \times 10^{-6} P_4$ based on numerical data fits. This is in contrast to item (13) of [4] which suggests a simplified turbine map to obtain $\dot{\omega}_5$.

(d) For $\dot{\omega}_8 = f_3(T_5, P_5)$ we have used $\dot{\omega}_8 = 0k_8 A_8 P_5 / \sqrt{T_5} \approx 22.835 \times 10^{-6} P_5^\theta$ which amounts to an assumption of choked nozzle condition. This is exactly the same as (15) of [4] except that rather than linearize $1/\sqrt{T_5}$ we finally just use a constant approximation.

(e) For $T_5 = f_2(T_4, P_4, P_5, N)$ we simply use the empirical relation $T_5 = .87694T_4$. This corresponds to item (12) of [4] which suggests linearizing the theoretical relation to obtain an approximation of the form $T_5 = A + BT_4 + CP_5$.

(f) For $T_3 = f_4(T_2', N, P_4)$ we use $T_3 = T_2' + 12.914 \times 10^{-8} N^2$ which is a form suggested by Zucrow [3], but differs with item (4) of [4] which suggest a linearization of the theoretical relation to express $T_3 = A + B P_4$.

(g) For $P_3 = f_5(P_2', \dot{\omega}_3, \dot{\omega}_2)$ which is the compressor map relation we have used essentially the method suggested in item (6) of [4] with the constant speed line function simply a straight line. This results in $P_3 = 5 \times 10^{-4} P_2' N - 2.94104 \times 10^5 \dot{\omega}_3$.

The above assumptions yield a seventh order nonlinear system which will be shown later in this chapter. Additional assumptions made to obtain a third order simplified model are:

(h) Replace equations (2) and (3) by their corresponding equilibrium relations. Thus, we neglect compressor dynamics and bleed losses, corresponding

to items ① and ⑥ of [4].

(i) Replace equation (6) by the corresponding equilibrium condition $P_3 = P_4 + K_B \dot{\omega}_4^2 / P_3$, which relates to item ⑤ of [4] which lets $P_3 = 1.05 P_4$.

(j) Replace equation (8) by the equilibrium condition $\dot{\omega}_5 = \dot{\omega}_8$ which results, with our above assumptions, in the condition $P_4 = (22.835/12.424)P_5\theta$. This assumption is not made in [4], accounting for the fourth order system there and the third order system in this work (We use $0 \leq \theta \leq 1$ as a parameter for nozzle area).

2.4 Thrust Calculation

Here we follow Zucrow [3] to compute net thrust due to internal flow.

We have

$$F = \frac{\dot{\omega}_8}{g} (V_8 - V) + (P_8 - P_o) A_8 \quad (16)$$

or

$$F = F_j - \frac{\dot{\omega}_8}{g} V \quad (17)$$

where

$$F_j = \frac{\dot{\omega}_8 V_j}{g}, \quad V_j = V_8 - \frac{g}{\dot{\omega}_8} (P_8 - P_o) \quad (18)$$

and for the choked nozzle condition

$$F_j = A_8 \left\{ \eta \gamma \left(\frac{2}{\gamma+1} \right)^{\frac{\gamma}{\gamma-1}} + \left(\frac{2}{\gamma+1} \right)^{\frac{\gamma}{\gamma-1}} \right\} P_5 - A_8 P_o \quad (19)$$

Which becomes for $A_8 = .0182\theta$ and $\gamma = 1.4$

$$F_j = \theta \left\{ \eta \frac{13.461}{10^3} + \frac{9.6147}{10^3} \right\} P_5 - .0182 P_o \theta \quad (20)$$

With the Mach .8 at 20,000 ft. condition we get $g = 1$, $V = 252.89$ m/sec,

$\rho_o = 4.66 \times 10^4$. Also we have by assumption (d), $\dot{\omega}_8 = 22.835 \times 10^{-6} P_5 \theta$.

Using an efficiency on $\eta = .9464$ to fit the design data of [1], and equation

(17) we obtain

$$F = \theta \{ .01658 P_5 - 848.12 \} \quad (21)$$

as the approximate expression for thrust.

2.5 Seventh Order Simulation Model

State Equations:

$$\frac{dP_2'}{dt} = \frac{11.2745(10^4)}{V_1} (\dot{\omega}_2 - \dot{\omega}_3) \quad (22)$$

$$\frac{d\dot{\omega}_2}{dt} = \frac{A_1^2}{V_1} (7.09(10^4) - P_2') \quad (23)$$

$$\frac{d\dot{\omega}_3}{dt} = \frac{A_4^2}{V_4} [P_3 - P_4 - \frac{4.108(10^8)}{P_3} \dot{\omega}_3^2] \quad (24)$$

$$\frac{dP_4}{dt} = \frac{401.8}{V_4} [\frac{P_4 \dot{\omega}_f}{287\rho_B} + 36278\dot{\omega}_f + \dot{\omega}_3 T_3 - \frac{4.329}{10^3} \frac{P_4^2}{P_B}] \quad (25)$$

$$\frac{d\rho_B}{dt} = \frac{1}{V_4} [\dot{\omega}_3 + \dot{\omega}_f - \frac{12.424}{10^6} P_4] \quad (26)$$

$$\frac{dP_5}{dt} = \frac{.87694}{10^6 V_5} \frac{P_4}{\rho_B} (12.424 P_4 - 22.835 P_5 \theta) \quad (27)$$

$$\begin{aligned} \frac{dN}{dt} = \frac{1.0616(10^5)}{IN} \left\{ \frac{P_4}{287\rho_B} \left[\frac{12.424}{10^6} P_4 - \frac{20.025}{10^6} P_5 \theta \right] \right. \\ \left. + .8633 [280.6\dot{\omega}_2 - T_3 \dot{\omega}_3] \right\} \quad (28) \end{aligned}$$

Other relations:

$$C_{pB} = 1164.15 \quad C_{pC} = 1005.02 \quad \eta_4 h_B / C_{pB} = 36278 \quad (29)$$

$$T_2 = 280.6 \quad J = 1 \quad K_B = 4.108 \times 10^8 \quad P_2 = 7.09 \times 10^4$$

$$\dot{\omega}_3 = \dot{\omega}_4 \quad P_4 = R \rho_B T_4 \quad A_8 = .0182 \quad R = 287 \quad \gamma = 1.4$$

$$\dot{\omega}_5 = 12.424 \times 10^{-6} P_4 \quad (30)$$

$$\dot{\omega}_8 = 22.835 \times 10^{-6} P_5 \theta \quad (31)$$

$$T_5 = .87694 T_4 \quad (32)$$

$$T_3 = 280.6 + 12.914 \times 10^{-8} N^2 \quad (33)$$

$$P_3 = 5P_2' N \times 10^{-4} - 2.94104 \times 10^5 \dot{\omega}_3 \quad (34)$$

$$F = \theta \{ .01658 P_5 - 848.12 \} \quad (35)$$

2.6 Gains

It was impossible to obtain all the gains determined by the factors: $1/V_1$, A_1^2/V_1 , A_4^2/V_4 , $1/V_4$, $1/V_5$, and $1/I$ in the equations above; although some information given in [4] was useful. To get a range of dynamical characteristics, four gain systems were considered:

System A: Each $V = .1$, each $A = .1$, $I = .00305$

System B: Each $V = .1$, each $A = .1$, $I = .0305$

System C: Each $V = .01$, each $A = .1$, $I = .0305$

System D: Each $V = .01$, each $A = .1$, $I = .305$

Note, in referring back to the model of the previous section, that System A is obtained from System B by multiplying equation (28) by a factor of 10.

System C is derived from B by multiplying equations (22) - (27) by 10 and (28)

by 1. System D is obtained from System B by multiplying (22) - (27) by 10 and (28) by 1/10.

2.7 Normalized Seventh Order Simulation Model

Here we use design point (2) of [1] for the equilibrium values. The associated normalized equations then follow as in the introduction. Gain System B is used here.

State Equations:

$$\frac{d\hat{P}'_2}{dt} = 51.52 (\hat{\omega}_2 - \hat{\omega}_3) \quad (36)$$

$$\frac{d\hat{\omega}_2}{dt} = 2188.27 (1 - \hat{P}'_2) \quad (37)$$

$$\frac{d\hat{\omega}_3}{dt} = 8191.36 [1.05787\hat{P}_3 - \hat{P}_4 - .05787 \frac{\hat{\omega}_3^2}{\hat{P}_3}] \quad (38)$$

$$\frac{d\hat{P}_4}{dt} = .93586 \frac{\hat{P}_4 \hat{\omega}_f}{\hat{\rho}_B} + 31.486\hat{\omega}_f + 21.435\hat{\omega}_3 \hat{T}_3 - 53.86 \frac{\hat{P}_4^2}{\hat{\rho}_B} \quad (39)$$

$$\frac{d\hat{\rho}_B}{dt} = 37.78\hat{\omega}_3 - 38.448 \hat{P}_4 + .66849\hat{\omega}_f \quad (40)$$

$$\frac{d\hat{P}_5}{dt} = 61.97 \frac{\hat{P}_4}{\hat{\rho}_B} [\hat{P}_4 - \hat{P}_5 \hat{\Theta}] \quad (41)$$

$$\begin{aligned} \frac{d\hat{N}}{dt} = \frac{1}{.305\hat{N}} \left\{ \frac{\hat{P}_4}{\hat{\rho}_B} [3.12\hat{P}_4 - 2.7361\hat{P}_5 \hat{\Theta}] \right. \\ \left. + [.688013\hat{\omega}_2 - 1.0715 \hat{T}_3 \hat{\omega}_3] \right\} \quad (42) \end{aligned}$$

Other Relations:

$$\hat{\omega}_3 = \hat{\omega}_4 \quad \hat{P}_4 = \hat{\rho}_B \hat{T}_4 \quad \hat{P}_2 = 1 \quad \hat{T}_2 = \hat{T}'_2 = 1 \quad (43)$$

$$\hat{\dot{\omega}}_5 = \hat{P}_4 \quad (44)$$

$$\hat{\dot{\omega}}_8 = \hat{P}_5 \theta \quad (45)$$

$$\hat{T}_5 = \hat{T}_4 \quad (46)$$

$$\hat{T}_3 = .64212 + .35788\hat{N}^2 \quad (47)$$

$$\hat{P}_3 = 4.394\hat{N} - 3.394\hat{\omega}_3 \quad (48)$$

$$F = \hat{\theta} \{1.5486\hat{P}_5 - .5486\} \quad (49)$$

$$V_1 = V_4 = V_5 = A_1 = A_4 = .1 \quad I = .0305 \quad (50)$$

(this corresponds to Gain System B in 2.6)

2.8 Normalized Third Order Simulation Model

Here we use assumption (h), (i), and (j) of Section 2.3 to eliminate the high frequency terms of the seventh order model. Note that the equilibrium solutions of both systems are identical. Here again we use Gain System B. State equations:

$$\frac{d\hat{P}_4}{dt} = \hat{\omega}_F (.93586\hat{P}_4/\hat{\rho}_B + 31.486) + 21.435\hat{\omega}_3\hat{T}_3 - 53.86\hat{P}_4^2/\hat{\rho}_B \quad (51)$$

$$\frac{d\hat{\rho}_B}{dt} = 37.78\hat{\omega}_3 - 38.448\hat{P}_4 + .66849\hat{\omega}_F \quad (52)$$

$$\frac{d\hat{N}}{dt} = \frac{1.258}{\hat{N}} (\hat{P}_4^2/\hat{\rho}_B - \hat{\omega}_3\hat{N}^2) \quad (53)$$

Other Relations:

All relations equations (43) to (50) in the previous seventh order model are valid, plus

$$\hat{P}_2 = 1 \quad \hat{\omega}_2 = \hat{\omega}_3 \quad \hat{P}_4 = \hat{P}_5 \hat{\theta} \quad (54)$$

$$\hat{\omega}_3 = 1.3009\hat{N} - .13982(\hat{P}_4 - \sqrt{\hat{P}_4^2 + .41688\hat{N}^2 - .0899\hat{P}_4\hat{N}}) \quad (55)$$

2.9 Equilibrium Conditions

Equilibrium conditions for the normalized seventh order and third order models are the same, and independent of whether Gain Systems A, B, C, or D are used. The "Design" equilibrium occurs when all normalized state variables are unity, and this corresponds to the design point (2) of Mach .8 and 20000 ft. in [1]. Other equilibrium points must be calculated using a successive approximation procedure to solve the nonlinear equations which result by setting all derivatives zero. In particular, we define "Windmill" as the equilibrium which occurs when fuel flow $\hat{\omega}_f = 0$ and nozzle area $\hat{\theta} = 1$.

The algorithm used to calculate equilibrium conditions is as follows.

1. Set values of $\hat{\omega}_f$ and θ (the controls.)
2. As initial estimates, set

$$\hat{P}_2 = 1, \hat{N} = \hat{P}_4 = .5(\hat{\omega}_f + 1)$$

3. Set in order

$$\hat{\omega}_3 = 1.3009\hat{N} - .13982(\hat{P}_4 - \sqrt{\hat{P}_4^2 + .41688\hat{N}^2 - .0899\hat{P}_4\hat{N}})$$

$$\hat{T}_3 = .64212 + .35788\hat{N}^2$$

$$\hat{P}_3 = 4.394\hat{N} - 3.394\hat{\omega}_3$$

$$\hat{P}_4 = (\hat{\omega}_f + 56.515\hat{\omega}_3)/57.515$$

$$\hat{\rho}_B = (53.86\hat{P}_4^2 - .93586\hat{P}_4\hat{\omega}_F) / (21.435\hat{\omega}_3\hat{T}_3 + 31.486\hat{\omega}_F)$$

$$\hat{T}_4 = \hat{P}_4 / \hat{\rho}_B$$

$$\hat{P}_5 = \hat{P}_4 / \hat{\Theta}$$

4. Set

$$\hat{N} = \sqrt{\hat{P}_4^2 / \hat{\rho}_B \hat{\omega}_3}$$

and return to 3. until convergence is achieved.

This algorithm gave five place convergence in twenty iterations and showed a very nearly linear operating line relation of approximately

$$\hat{P}_3 \cong 1.0263\hat{\omega}_3 - .0263 \quad (56)$$

or equivalently (using the linear compressor relation $\hat{P}_3 = 4.394\hat{N} - 3.394\hat{\omega}_3$)

$$\hat{\omega}_3 \cong .99405\hat{N} - .00595 \quad (57)$$

Some values of interest are tabulated in Table I for $\hat{\Theta} = 1$.

2.10 Compressor Map and Surge Lines

The equation used to approximate the compressor map of Figure 3. in [1] is

$$P_3/P_2' = 5N/10^4 - 2.94215\omega_3\sqrt{\Theta_2}/\delta_2 \quad (58)$$

where

$$\begin{aligned} \Theta_2 &= T_2/288.3 = 280.6/288.3 = .97329 \\ \delta_2 &= P_2/10.1325 \times 10^4 \end{aligned} \quad (59)$$

Using these relations and the equilibrium values

$$\begin{aligned} P_{3E} &= 28.076 \times 10^4 \\ P_{2E} &= 7.09 \times 10^4 \\ \omega_{3E} &= 3.24 \end{aligned} \quad (60)$$

TABLE I
 SAMPLE EQUILIBRIUM VALUES

$\hat{\epsilon}_F$	\hat{P}_4	\hat{N}	$\hat{\rho}_B$	\hat{T}_4	$\hat{\omega}_3$	\hat{P}_3	\hat{T}_3
0.00	.53831	.54589	1.77504	.30326	.54783	.53931	.74876 (Windmill)
0.25	.72430	.73097	1.34002	.54051	.73269	.72513	.83334
0.50	.83809	.84284	1.17141	.71545	.84407	.83867	.89635
0.75	.92614	.92861	1.07041	.86522	.92926	.92640	.95073
1.00	.99998	.99997	1.00004	.99994	.99998	.99994	.99998 (Design)

REPRODUCIBILITY OF 1.
 ORIGINAL PAGE IS PO...

we obtain

$$\hat{P}_3 = 4.394\hat{P}_2' - 3.394\hat{\omega}_3 \quad (61)$$

This relation is graphed in Figure 2. for $\hat{P}_2' = 1$ along with the operating line of equilibrium points calculated in the previous section. It would be natural to map a linear approximation of the surge line of Figure 3 in [1] on to Figure 2, except that our Windmill equilibrium, unfortunately, does not match the image of the windmill equilibrium in [1]. This is due to the many approximations made in section 2.3.

We have thus chosen to define the surge line as a line running parallel to and above the operating line. This is rather arbitrary, but preserves the qualitative nature of the problem of getting from Windmill to Design without transgressing on the surge characteristic. Indicated on Figure 2. is a surge line specified by the relation

$$\hat{P}_3 = 1.0263\hat{\omega}_3 + .24105 \quad (62)$$

2.11 Linear Normalized Systems

In order to estimate the dynamical modes of the various models, and to provide models for linear control studies, linear representations of the form

$$\frac{d\hat{\delta x}}{dt} = A\hat{\delta x} + B\hat{\delta u} \quad (63)$$

were determined, where $A = \frac{\partial f}{\partial \hat{x}}$ and $B = \frac{\partial f}{\partial \hat{u}}$. Using the seventh order normalized equations of section 2.7, with Gain System B and linearizing about the design equilibrium

$$\hat{x}_E = (1, 1, 1, 1, 1, 1, 1)$$

we have

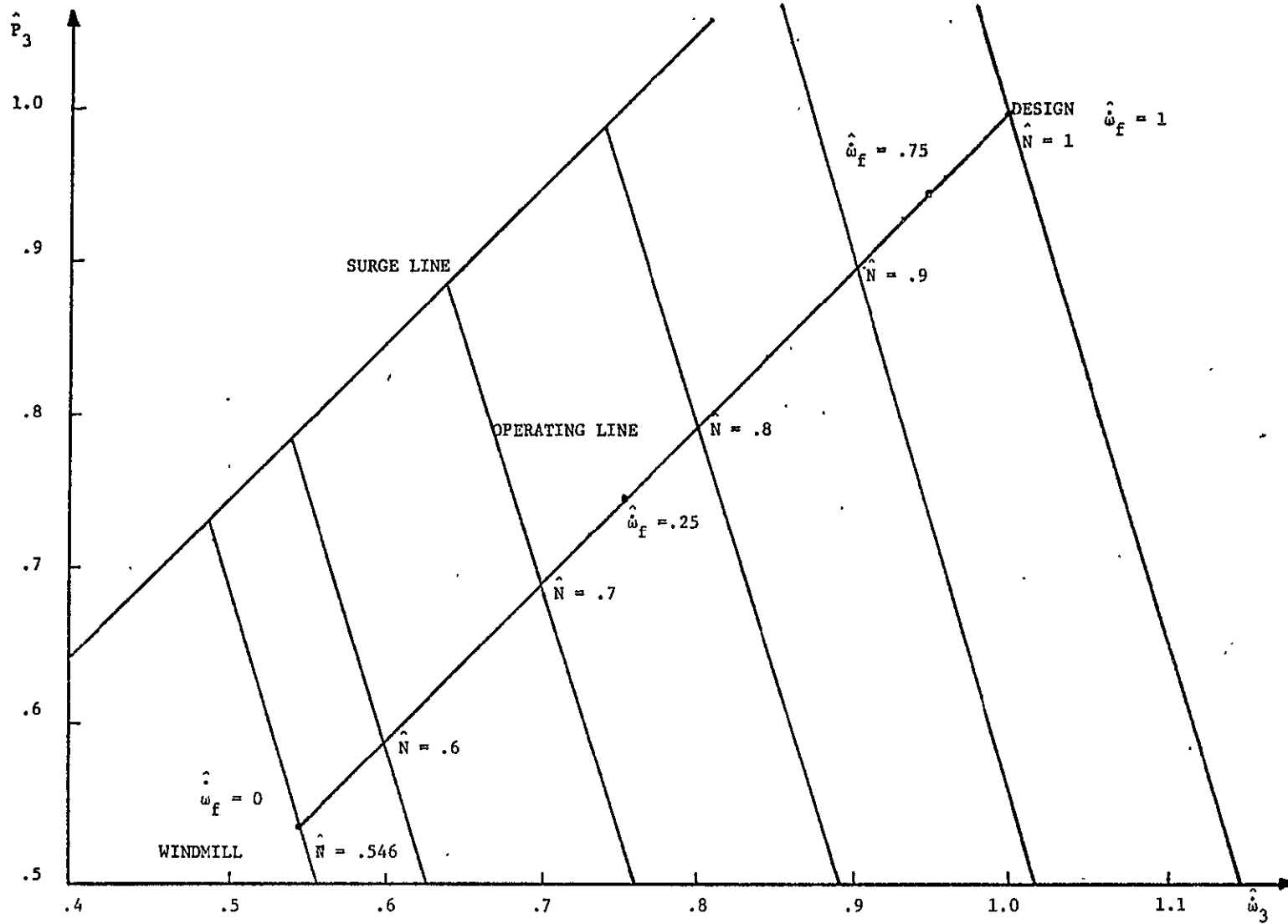


Figure 2. Linearized Compressor Map in Terms of Normalized Variables.

$$A = \begin{matrix} & \hat{P}_2 & \hat{\omega}_2 & \hat{\omega}_3 & \hat{P}_4 & \hat{\rho}_B & \hat{P}_5 & \hat{N} \\ \hat{P}_2 & 0 & 51.52 & -51.52 & 0 & 0 & 0 & 0 \\ \hat{\omega}_2 & -2188.3 & 0 & 0 & 0 & 0 & 0 & 0 \\ \hat{\omega}_3 & 40159 & 0 & -31967 & -8191.4 & 0 & 0 & 40159 \\ \hat{P}_4 & 0 & 0 & 21.436 & -106.72 & 52.893 & 0 & 15.343 \\ \hat{\rho}_B & 0 & 0 & 37.78 & -38.448 & 0 & 0 & 0 \\ \hat{P}_5 & 0 & 0 & 0 & 61.97 & 0 & 61.97 & 0 \\ \hat{N} & 0 & 2.2558 & -3.5131 & 11.488 & -1.2587 & -8.9708 & -2.5146 \end{matrix} \quad (64)$$

$$B = \begin{matrix} & \hat{\omega}_F & \hat{\theta} \\ \hat{P}_2 & 0 & 0 \\ \hat{\omega}_2 & 0 & 0 \\ \hat{\omega}_3 & 0 & 0 \\ \hat{P}_4 & 32.4219 & 0 \\ \hat{\rho}_B & .66849 & 0 \\ \hat{P}_5 & 0 & -61.97 \\ \hat{N} & 0 & -8.9708 \end{matrix} \quad (65)$$

The corresponding Gain System B third order normalized linearizations are

$$A = \begin{array}{c} \hat{P}_4 \\ \hat{\rho}_B \\ \hat{N} \end{array} \begin{array}{c} \hat{P}_4 \\ \hat{\rho}_B \\ \hat{N} \end{array} \begin{bmatrix} -112.27 & 52.924 & 42.26 \\ -48.12 & 0 & 47.444 \\ 2.8377 & -1.258 & -4.096 \end{bmatrix} \quad (66)$$

$$B = \begin{array}{c} \hat{P}_4 \\ \hat{\rho}_B \\ \hat{N} \end{array} \begin{array}{c} \hat{\omega}_F \\ \hat{\omega}_F \\ \hat{\omega}_F \end{array} \begin{bmatrix} 32.4219 \\ .66849 \\ 0 \end{bmatrix} \quad (67)$$

With this A matrix we were able to determine the A matrix of the other Gain Systems rather easily. We were also able to calculate the eigenvalues of these matrices with the aid of a digital computer program. These results are presented below.

Gain System A. ($V = .1$, $A = .1$, $I = .00305$) to obtain A and B matrices, multiply bottom rows of all matrices by 10.

7th order eigenvalues: -31852 , -141.43 , -60.278
 $(\tau \approx .0425)$ $-44.907 \pm j329.24$
 $-8.5923 \pm j21.913$

3rd order eigenvalues: -89.288 , -45.638 , -18.304
 $(\tau \approx .0546)$

Gain System B. ($V = .1$, $A = .1$, $I = .0305$) A and B matrices exactly as shown

in equations (64)- (67).

7th order eigenvalues: -31892, -88.732, -61.218
 $(\tau \approx .296)$ -25.204, -3.3818
 -33.738 $\pm j333.68$

3rd order eigenvalues: -81.219, -32.309, -2.8386
 $(\tau \approx .352)$

Gain System C. (V = .01, A = .1, I = .0305) to obtain A and B matrices

multiply all rows except the bottom one by 10.

7th order eigenvalues: -318962, -814.82, -618.54
 $(\tau \approx .339)$ -310.44, -2.9529
 -325.38 $\pm j3339.7$

3rd order eigenvalues: -807.68, -316.2, -2.9166
 $(\tau \approx .343)$

Gain System D. (V = .01, A = .1, I = .305) to obtain A and B matrices multiply

all upper rows by 10 and the bottom one by 1/10.

7th order eigenvalues: -318966, -806.7, -619.58
 $(\tau \approx 3.423)$ -316.34, -.29218
 -324.17 $\pm j3340$

3rd order eigenvalues: -807.25, -315.57, -.2924
 $(\tau \approx 3.420)$

CHAPTER III

SIMULATION AND CONTROL STUDIES OF THE SEVENTH ORDER SYSTEM

3.1 Introduction

This chapter presents the analog simulation study of the seventh order Drone engine dynamics of section 2.5. The purpose of the simulation was to develop a low order realistic representation of a turbojet engine which would coincide with the data of reference [1]. With this model, we were able to gain further insight into the equations which govern engine operations, as well as investigate various fuel controls. Gain Systems B and C were considered. (Recall the discussion of section 2.6.) Four different fuel controls were examined, and the results appear in the form of trajectories plotted on the outline of an approximate compressor map and time response curves. These figures are located in Appendix A.

3.2 Simulation

The actual simulation was conducted at the University of Notre Dame's Analog Computer Laboratory. An Electronic Associates TR-48, and a few small TR-20 and TR-10 analog computers were used. Patching diagrams were obtained with the aid of ANSIR 3, a digital computer program which generates all pertinent analog simulation information, given the differential equations. Details of the simulation are given in Appendix C.

A preliminary check of the seventh order system was conducted to verify its consistency with theoretical equilibrium values. The ratio of Windmill condition to Design point values of the state variables was calculated. The same ratio was also computed from experimental data. Table II, illustrates

these findings. Discrepancies between the two sets of ratios arise from the inaccuracies in the equipment used, especially the nonlinear function generators.

TABLE II
SEVENTH ORDER SYSTEM CHECK

VARIABLE	CALCULATED RATIO	EXPERIMENTAL RATIO
P_2'	1.000	1.000
$\dot{\omega}_2$.5478	.5752
$\dot{\omega}_3$.5478	.6000
ρ_B	1.774	1.655
P_4	.5383	.5854
P_5	.5388	.5237
N	.5459	.5831

3.3 Control Problem

As stated earlier, the control problem is to schedule fuel in order to accelerate the engine operating state from Windmill to Design equilibrium conditions. However, maximum acceleration potential is limited by compressor surge or stall. As fuel is increased to accelerate the engine, pressure ratio, P_3/P_2' , increases and airflow, $\dot{\omega}_2$, decreases. When stall is reached the pressure will drop and will cause a similar decrease in compressor efficiency. It is desirable to design controls which will cause the compressor to approach the stall line however, since these controls tend to give a faster engine response. Trajectories were plotted on the outline of an approximate compressor

map to provide an illustrative look at surge margin constraint. Since this thesis is only an introductory study of the Drone engine, the surge line was considered arbitrary. Although, the underlying thought in this investigation was to regard the stall line as minimal.

Several coordinate systems were tried to observe the effect of the control on surge margin. These curves were determined using Gain System B and open loop control. The first natural choice was to use the pressure ratio versus airflow as shown in Figure 3(a). Figure 3(b) follows from the assumption that compressor inlet airflow equals outlet airflow ($\dot{\omega}_2 = \dot{\omega}_3$). Time response curves of P_2' indicate that it remains constant except for slight oscillations at the outset of the transient. By assuming P_2' constant, we obtain the plots in Figures 3(c) and 3(d). We also chose to make a graph with P_4 and N as the coordinate axis in Figure 4. This was done so that surge margin studies of the third order model could be carried out using state variables. We chose P_3 versus $\dot{\omega}_3$ and P_4 versus N as our representative coordinate systems.

3.4 Fuel Controls

Four different fuel control concepts were investigated on the simulation with Gain System B and C. They consist of an open loop control, linear feedback design, and two nonlinear controls developed by empirical methods. Their effects on engine performance and surge constraint are indicated by time response curves and trajectory plots in Appendix A. Two equations for each control are given. The first equation being the control used for the dynamic equations of 2.5 and the second pertaining to normalized equations of 2.7. The value of $\hat{\omega}_f$ at the design point is one.

Control 1 - Here we use the term open loop to refer to this control. It simply involves letting

$$\dot{\omega}_f = .057353 \text{ kg/sec} \quad (1)$$

or

$$\hat{\dot{\omega}}_f = 1 \quad (2)$$

This corresponds to the value of $\hat{\dot{\omega}}_f$ at design equilibrium. State variable time response graphs for System B are in Figures 5 and 6 and System C graphs in Figures 7 and 8.

Control 2 - Control 2 fuel scheduling is analogous to Case B control of [1]. It is a linear combination of compressor and turbine pressures given by

$$\dot{\omega}_f = 2.02954 \times 10^{-7} (P_3 + .032047P_2') \text{ kg/sec} \quad (3)$$

$$\hat{\dot{\omega}}_f = .99392 \hat{P}_3 + .00608 \hat{P}_2' \quad (4)$$

This control provided another means of comparing our simulation results to the data of reference [1]. System B acceleration transients for this control are in Figures 9 and 10 while System C curves are in Figures 11 and 12.

Control 3 - This control is the product of compressor airflow and rotor speed. It is defined as

$$\dot{\omega}_f = 5.0867 \times 10^{-7} (\dot{\omega}_3 N) \text{ kg/sec} \quad (5)$$

$$\hat{\dot{\omega}}_f = \hat{\dot{\omega}}_3 \hat{N} \quad (6)$$

Figures 13 and 14 give time plots of Gain System B and Figures 15 and 16 are of System C.

Control 4 - Figures 17, 18, 19, and 20 show engine dynamic time response for this nonlinear control given by

$$\dot{\omega}_f = 6.982 \times 10^{-13} (P_4^2 / \rho_B) \text{ kg/sec} \quad (7)$$

$$\hat{\dot{\omega}}_f = \hat{P}_4^2 / \hat{\rho}_B \quad (8)$$

3.5 Results

Relative time responses for each system and control are presented in Table III. The time constants were determined from the response of the rotor speed.

TABLE III
TIME CONSTANTS (sec)

FUEL CONTROL	SYSTEM B	SYSTEM C
1	.196	.266
2	.226	.432
3	.500	.633
4	.426	.533

These agree fairly well with the linearized results of section 2.11. A comparison to the Case B acceleration transients of [1] to our corresponding control 2 and System C. System C was chosen since it most closely represents the engine described in [1] and [4]. Our time constants are approximately .432 sec for N and .456 sec for $\dot{\omega}_3$. Whereas the results in [1] indicate response times of .5 sec for N and .565 sec for $\dot{\omega}_3$.

Analysis of these four controls on compressor surge indicate that Control 1 and 2 allow for approximately the same surge margin with 1 yielding a slightly higher compressor surge. Controls 3 and 4, however, would tolerate a stall line much less than the one required by 1 and 2 to insure efficient compressor operation. This is particularly evident in System B, Figure 21 where we were able to plot the trajectories of all four controls on the same graph without confusion. System C yields the same results as shown in Figures 22 and 23.

We note that although controls 3 and 4 tolerate lower stall lines, they also require more time to accelerate the engine from Windmill to Design.

3.6 Comment

Analog computer results seem to suggest that the seventh order model is a good representation of the Drone engine. The major difference between Gain Systems B and C is in the response time, with System B yielding a faster acceleration time. However, it appears that System C most closely approximates the theoretical engine design in [1] necessary for further control studies.

CHAPTER IV

SIMULATION AND CONTROL STUDIES OF THE THIRD ORDER SYSTEM

4.1 Introduction

The third order Drone engine simulation results are contained in this chapter. The purpose in developing this model was to examine the possibility of achieving an even simpler representation of a turbojet engine and still retain the essential characteristics of engine dynamics. Gain Systems A, C, and D were used in this study. The four controls discussed in section 3.4 were also implemented on this simulation. Slight modifications were necessary in the control schemes to be consistent with the third order simplifications. Also the effect of a linear combination of Controls 1 and 4 was investigated on surge margin constraint. The normalized equations of 2.8 were simulated and details of the actual simulation are in Appendix D.

4.2 Simulation Check

A check of the third order model where ratios of Windmill to Design point equilibrium values were calculated, reveals that the third order system more closely approximates the theoretical values. The major discrepancy in $\dot{\omega}_3$ is probably caused by the dynamical equation characterizing its behavior. The airflow is given as an equality rather than a differential equation. Also, the numerous simplifications needed to reduce the seventh order model undoubtedly had a significant effect. The results of this check are shown in Table IV.

TABLE IV
THIRD ORDER SYSTEM CHECK

VARIABLE	CALCULATED RATIO	EXPERIMENTAL RATIO
$\hat{\omega}_3$.5478	.4348
$\hat{\rho}_B$	1.774	1.852
\hat{P}_4	.5383	.5324
\hat{N}	.5459	.5472

4.3 Fuel Controls

The four controls studied were basically the same as in 3.4 the only change occurring in Control 2. With the simplifications necessary to derive the third order model, Control 2 reduces to

$$\hat{\omega}_f = \hat{P}_4 \quad (1)$$

The third order normalized fuel controls each have equilibrium values of 1 and are given by

$$\begin{array}{ll} \text{Control 1} & \hat{\omega}_f = 1 \\ \text{Control 2} & \hat{\omega}_f = \hat{P}_4 \end{array} \quad (2)$$

$$\text{Control 3} \quad \hat{\omega}_f = \hat{\omega}_3 \hat{N} \quad (3)$$

$$\text{Control 4} \quad \hat{\omega}_f = \hat{P}_4^2 / \hat{\rho}_B \quad (4)$$

4.4 Results

Time response curves for Control 1 are shown in Figures 24 and 25; Control 2 in Figures 26 and 27; Control 3 in Figures 28 and 29; and Control 4 in Figures 30 and 31. The first figure number for each control refers to System A response and the second to System C. Time Constants measured on these plots are given in Table V.

TABLE V
TIME CONSTANTS (sec)

FUEL CONTROL	SYSTEM A	SYSTEM C
1	.049	.299
2	.059	.466
3	.119	.799
4	.153	.633

Time constants determined from the linearized model of .0546 sec. for System A and .343 sec. for System C agree fairly well with the experimental time constants of .049 sec and .299 sec.

Surge margin studies of Systems C and D yield the same conclusions as in the previous Chapter. Controls 1 and 2 would be preferable if the stall line was sufficiently distant from the operating line. As the surge line approaches the operating line Controls 3 and 4 would tend to give better engine efficiency. These plots are shown in Figures 32, 33, 34, and 35. Gain System A, however, demonstrates the necessity for improvements to be made in the simulation model. While System A still preserves the same qualitative results, we see that Control 4 would allow for a slightly smaller stall line than Control 3 as shown in Figure 36. This is contrary to what we have observed from the other Gain Systems. The reason being the large gain on the rotor dynamics, equation causing $\hat{\omega}_f = \hat{\omega}_3 \hat{N}$ to respond faster, which in turn gives rise to a somewhat larger pressure surge at the outset of engine acceleration.

4.5 Linear Combination Control

From trajectory plots that were determined from the simulation, it was decided to test a linear combination of Controls 1 and 4. The intuitive idea was to design a control which would be time optimal (Control 1) with a control which would tolerate the greatest surge margin. The form of the control is

$$\hat{\omega}_F = K_1(1) + K_2 (\hat{P}_4^2 / \hat{\rho}_B) \quad (5)$$

where K_1 and K_2 were varied between zero and one; and $K_1 + K_2 = 1$.

Representative trajectories shown in Figure 37 were obtained using Gain System A. This controller is pleasing in the sense that almost regardless of the location of the surge line, a control of the form of equation (5) could be designed so that compressor stall would not occur. The lower limit on the surge line constraint and still have this control avoid engine stall is the case where $K_1 = 0$ and equation (5) reduces to equation (4). We also might note that the time to accelerate from Windmill to Design increases as K_2 increases.

4.6 Comments

It should be pointed out that the equations which characterize rotor dynamics (42) for the seventh order model and (53) for the third order system) both involve a division by N . Due to the lack of available nonlinear equipment for the seventh order model, this was set equal to the constant value of N at Windmill condition. The third order model allowed for the division of to be carried out. The effect of the approximation made on the seventh order model is not really certain, although the results seem to indicate a valid assumption.

The third order model results lead us to believe that our simulator is a good representation of the Drone engine. We were able to reduce the number of nonlinear elements such that the entire simulation could be conducted on the TR-48 and on TR-20 analog computer. This reduces the inaccuracies often times encountered in large simulations without significant effect on the results. This model will provide a quick, easy, and inexpensive method of developing and testing time optimal controls before they are attempted on a digital computer.

CHAPTER V
CONCLUSION

This thesis represents an introductory study into the Drone engine. As such, the results seem good. It is unfortunate that all suggestions of reference [4] could not be implemented in this study, since the simulation was well underway before this information became available.

Suggested further research regarding the simulation is to pinpoint exact values of volumes, areas, and lengths which geometrically describe the engine under consideration. Also the rotor inertia should be determined since there was an inconsistency in [4]. Placement of surge line and constraints on turbine inlet temperatures should be defined in order to determine an efficient control.

Control design studies to be conducted in the future involve developing a time optimal control. This design will center around Dynamic Programming solutions to the Hamilton Jacobi-equation and Fletcher-Reeves Conjugate Gradient method for solving the Hamilton-Jacobi Canonical equations. With these digital computer results, a control can be tested on the third order model and hopefully provide a control for more advanced turbojet engines.

REPRODUCIBILITY OF THE
ORIGINAL PAGE IS POOR

APPENDIX A

SEVENTH ORDER SIMULATION ACCELERATION PLOTS

The following pages illustrate the acceleration transients of the seventh order system as well as graphs relating to surge margin studies.

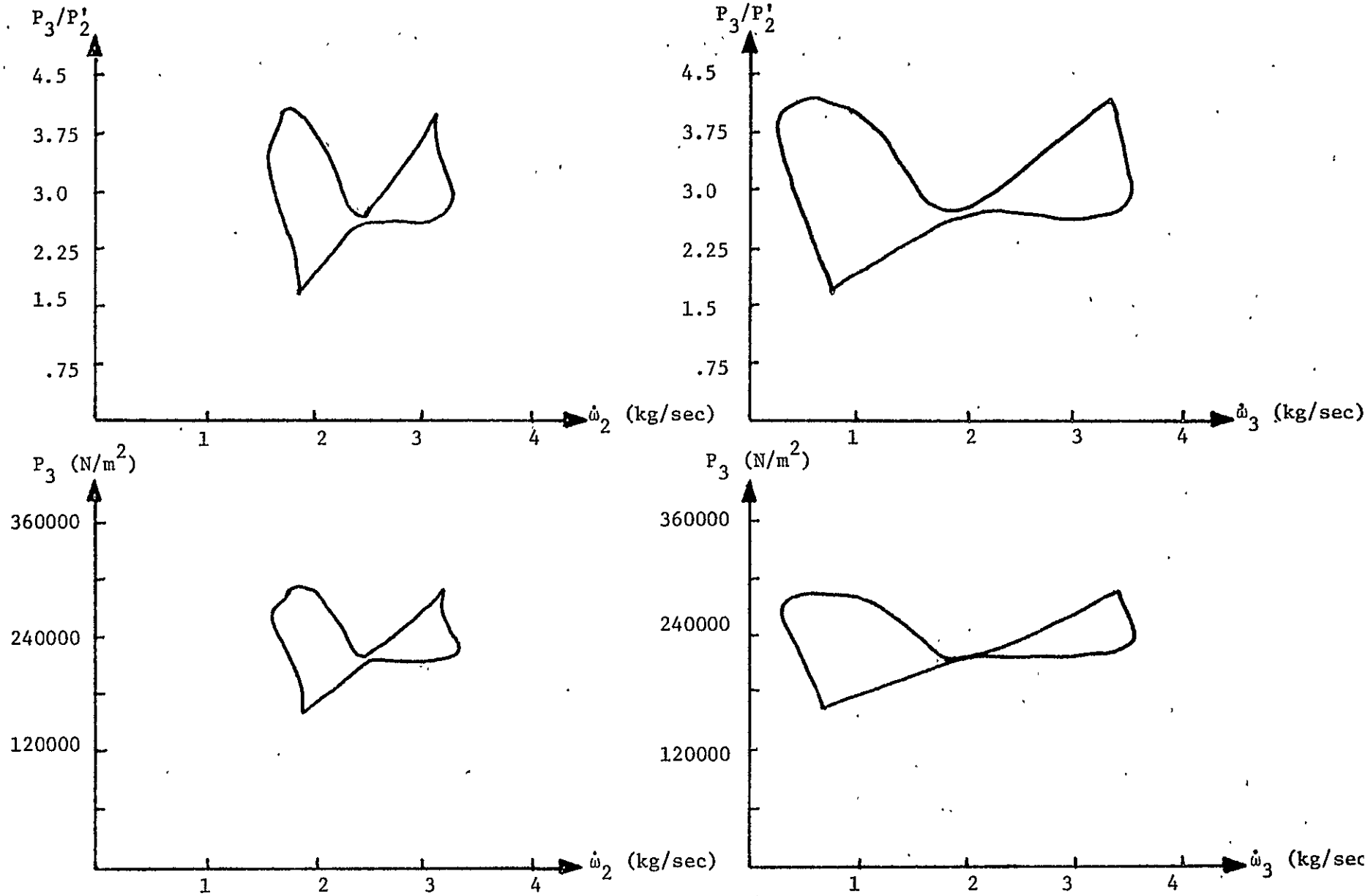


FIGURE 3. Examples of various coordinate systems used in surge margin study.

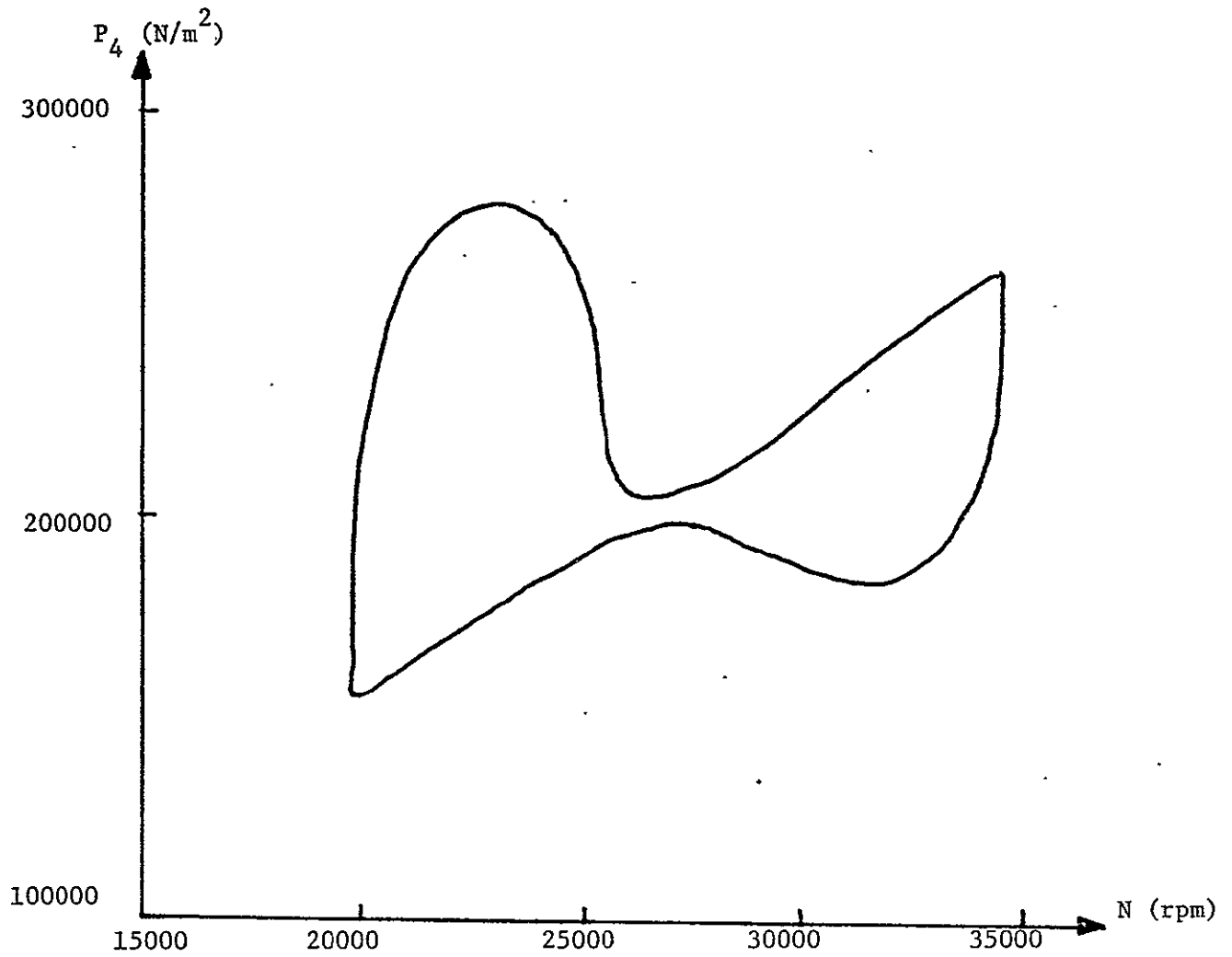


FIGURE 4. Example of surge margin study using P_4 and N as coordinate axis.

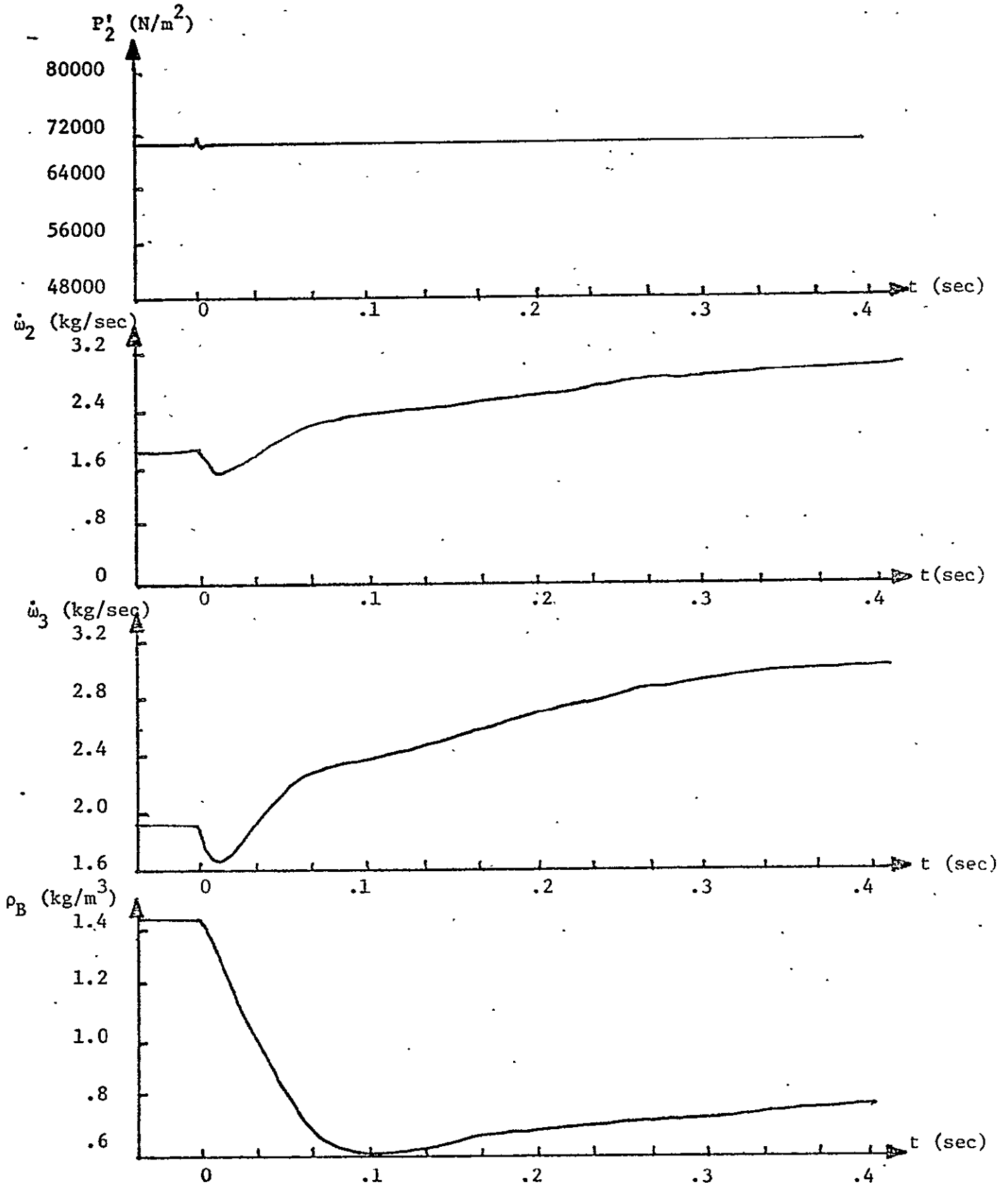


FIGURE 5. Acceleration transients, System B, Control 1.

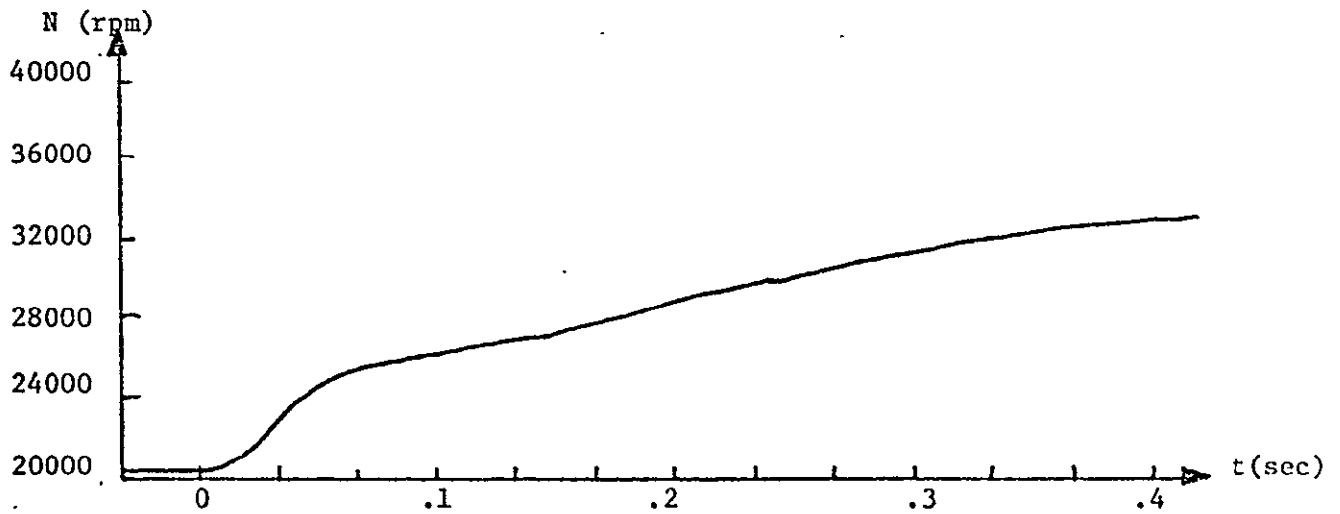
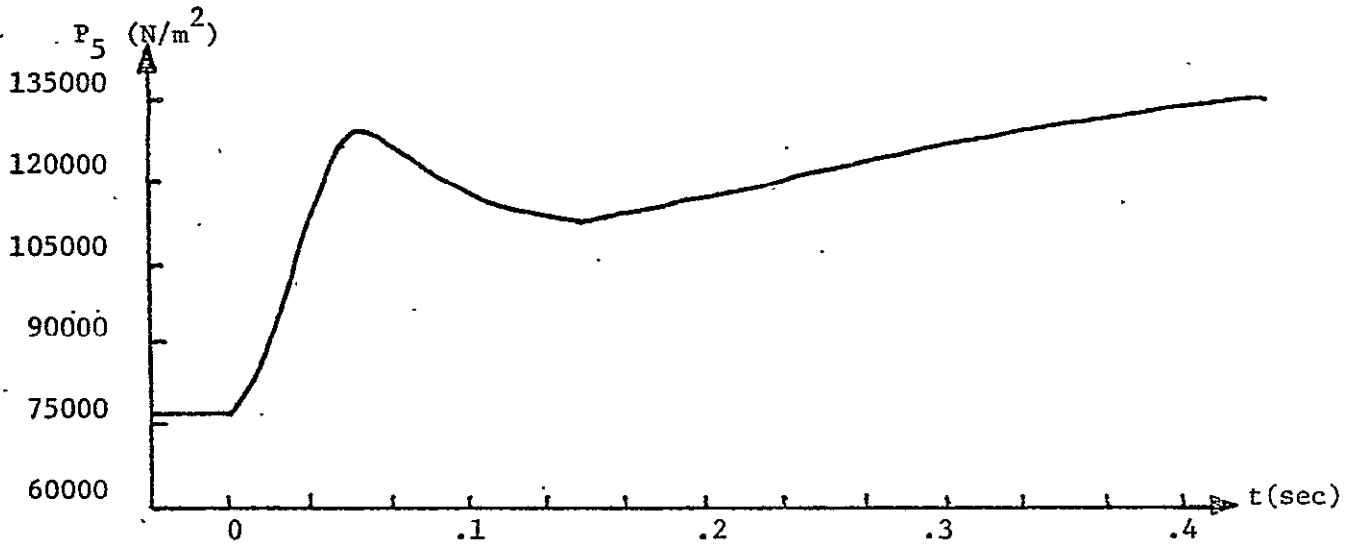
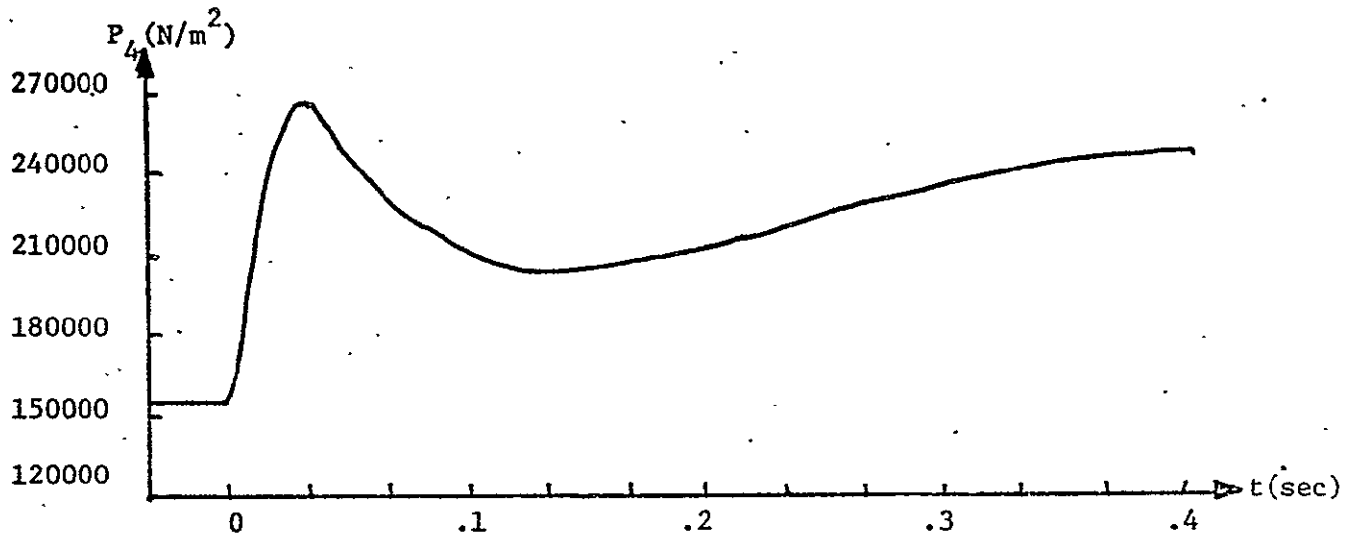


FIGURE 6. Acceleration transients, System B, Control 1.

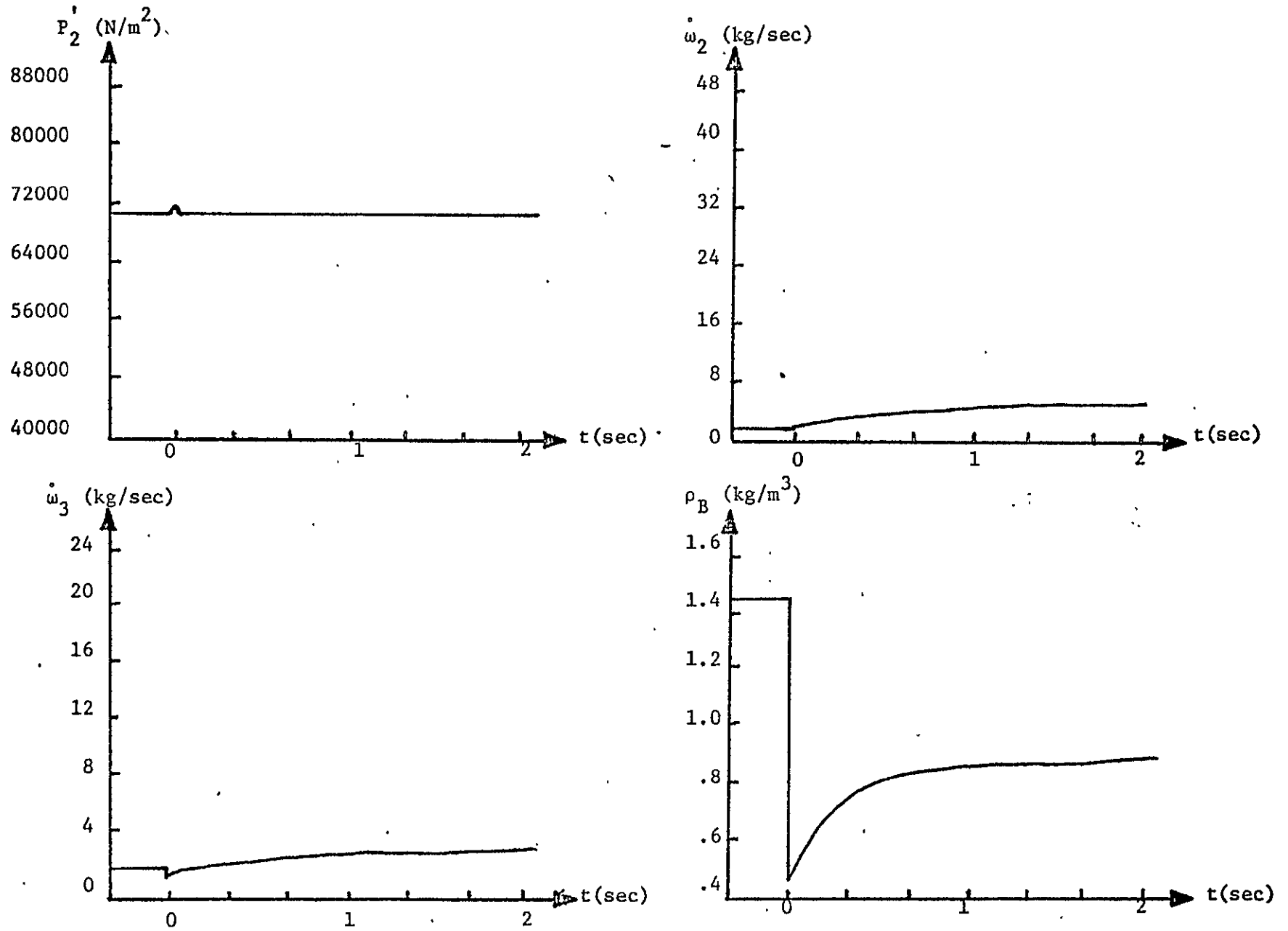


FIGURE 7. Acceleration transients, System C, Control 1.

REPRODUCIBILITY OF
ORIGINAL PAGE IS POOR

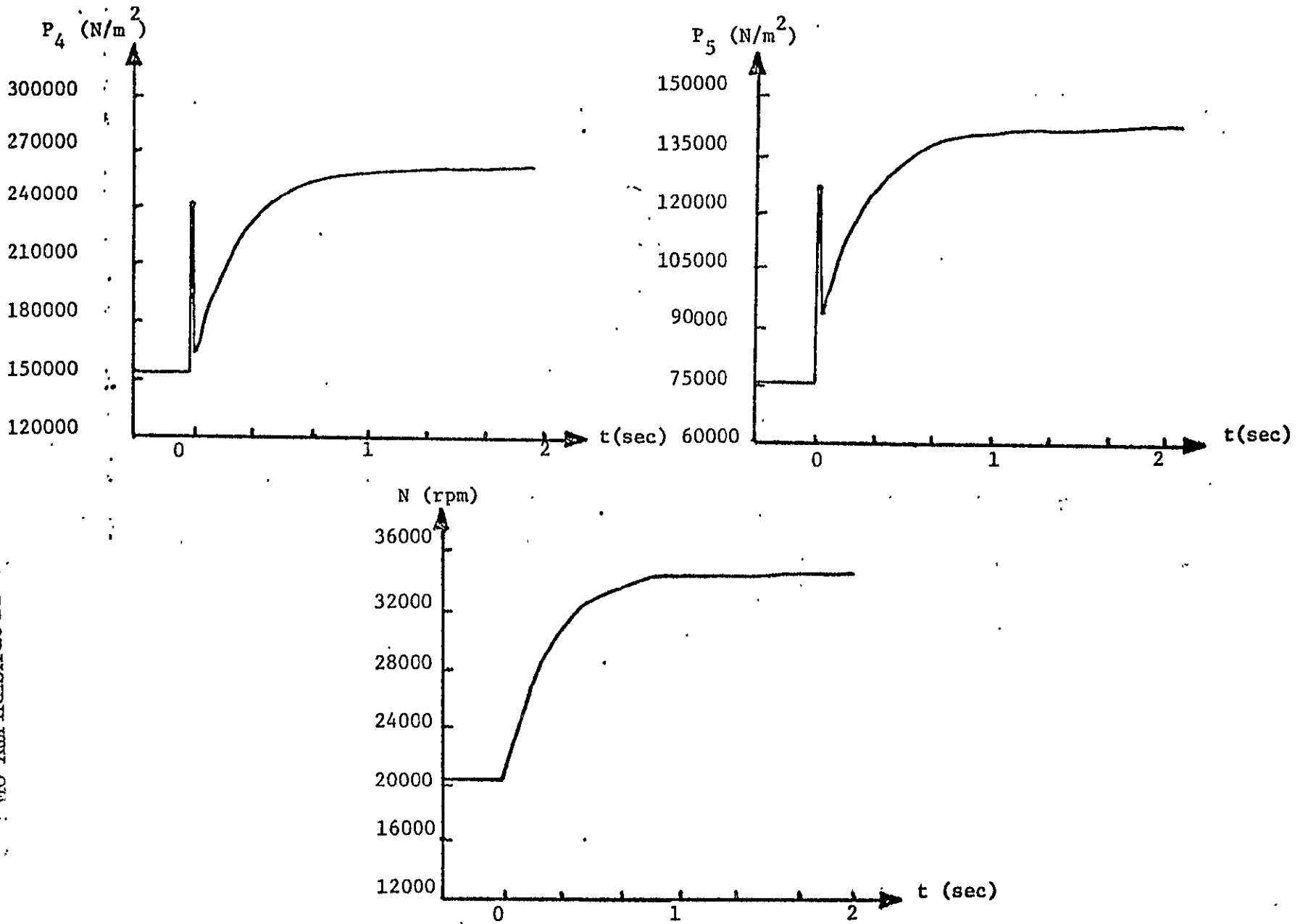


FIGURE 8. Acceleration transients, System C, Control 1.

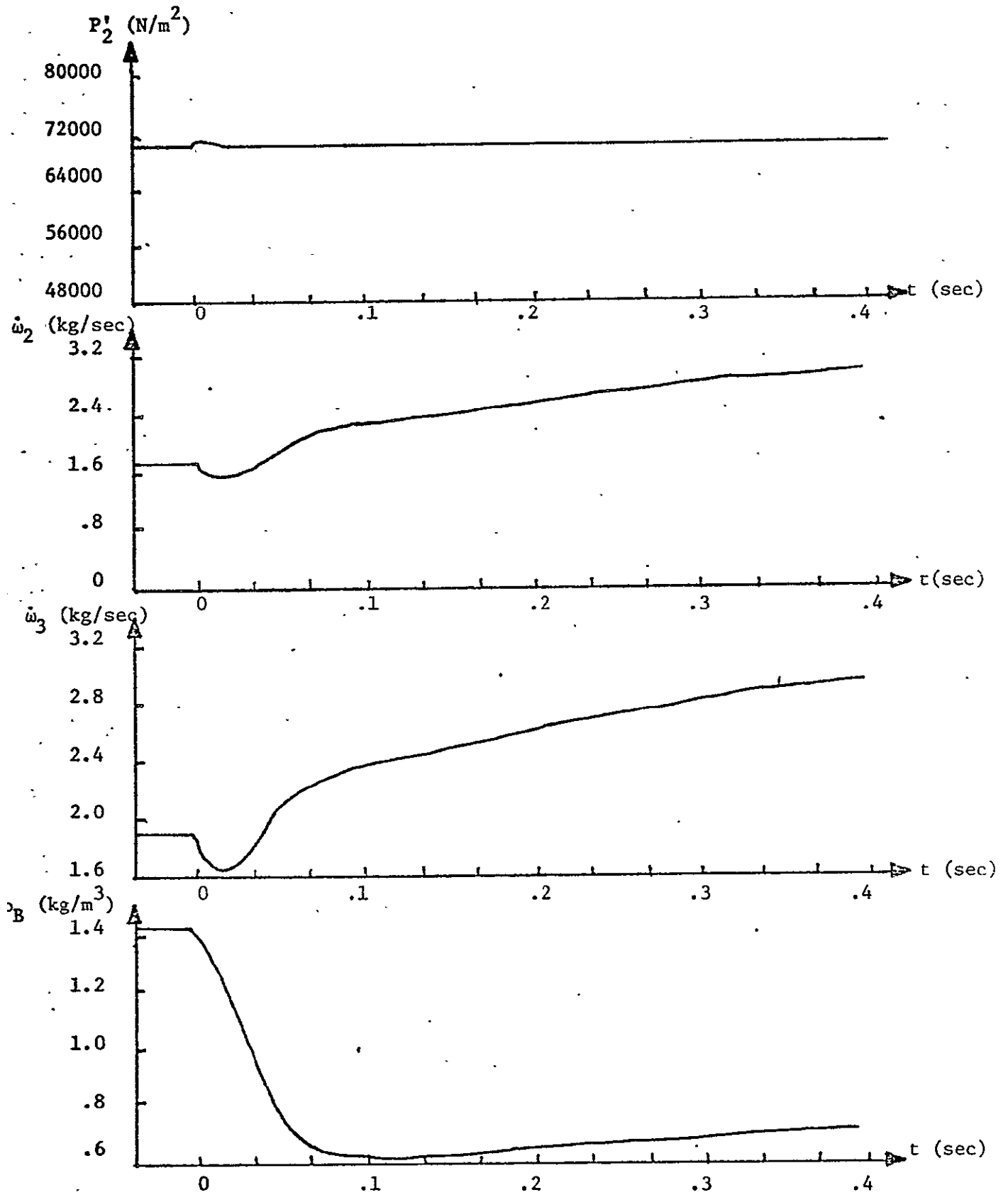


FIGURE 9. Acceleration transients, System B, Control 2.

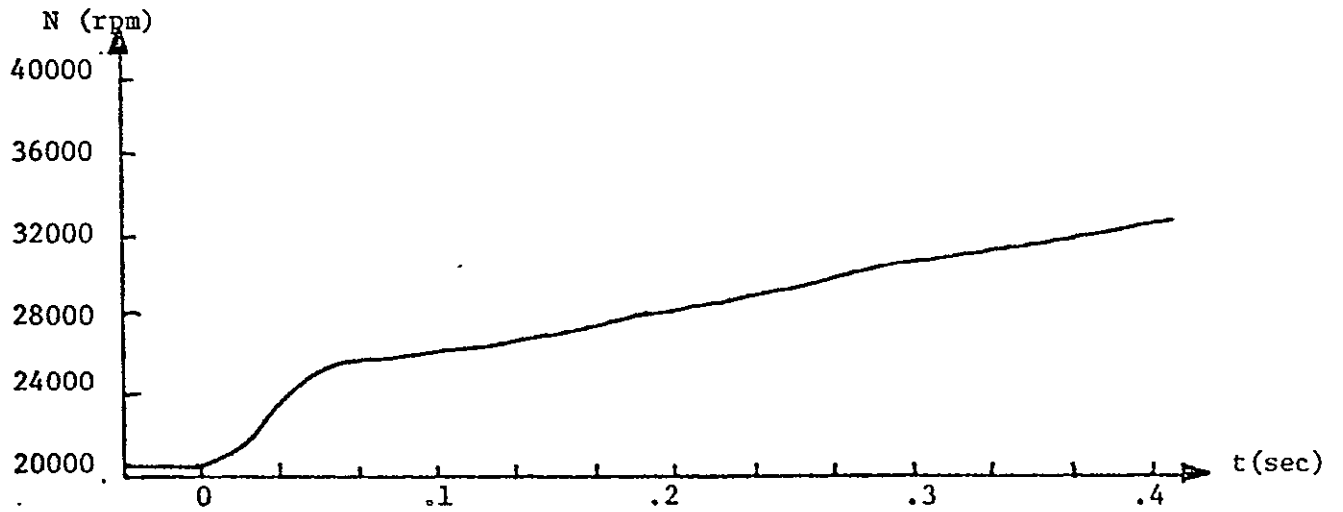
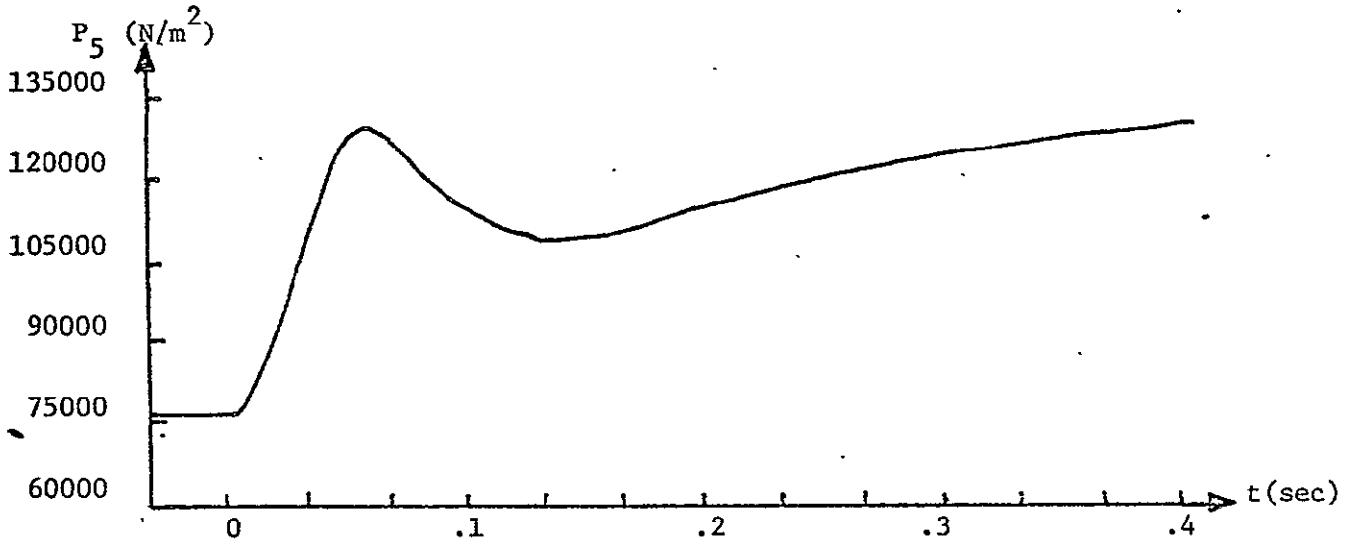
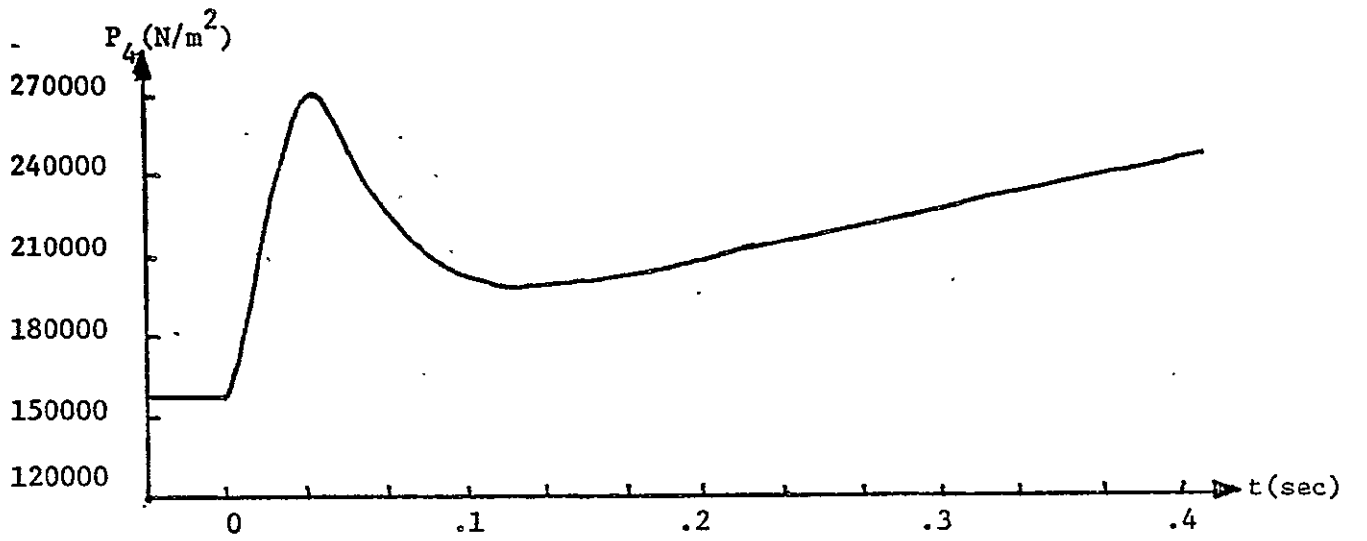
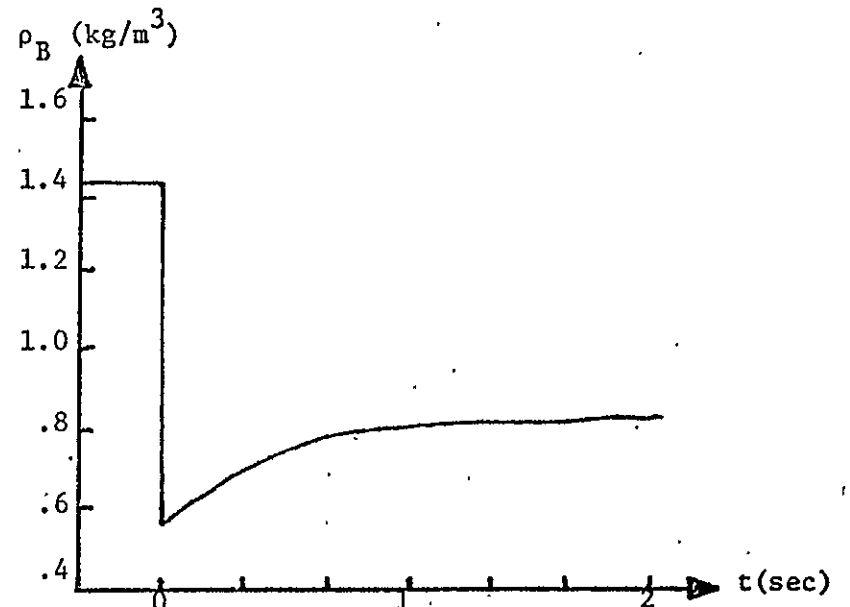
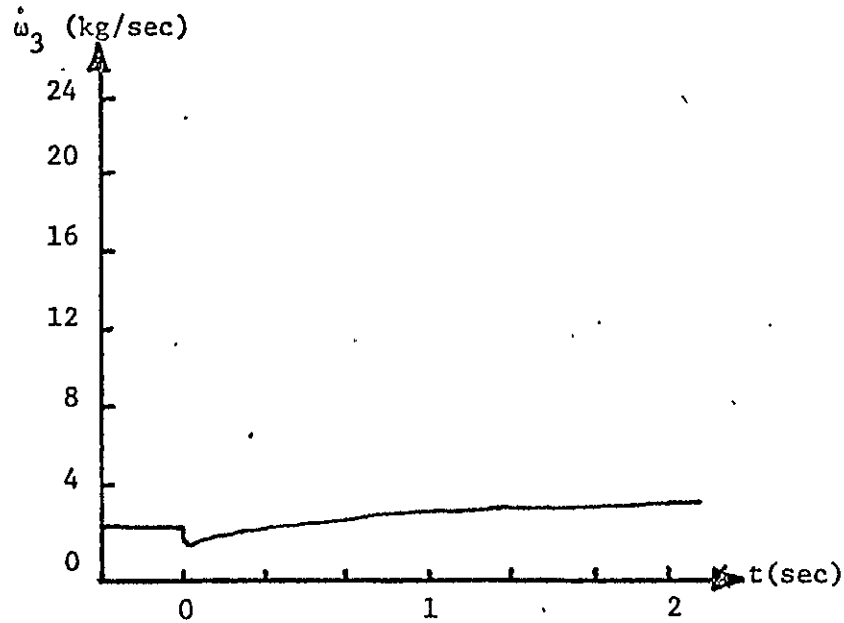
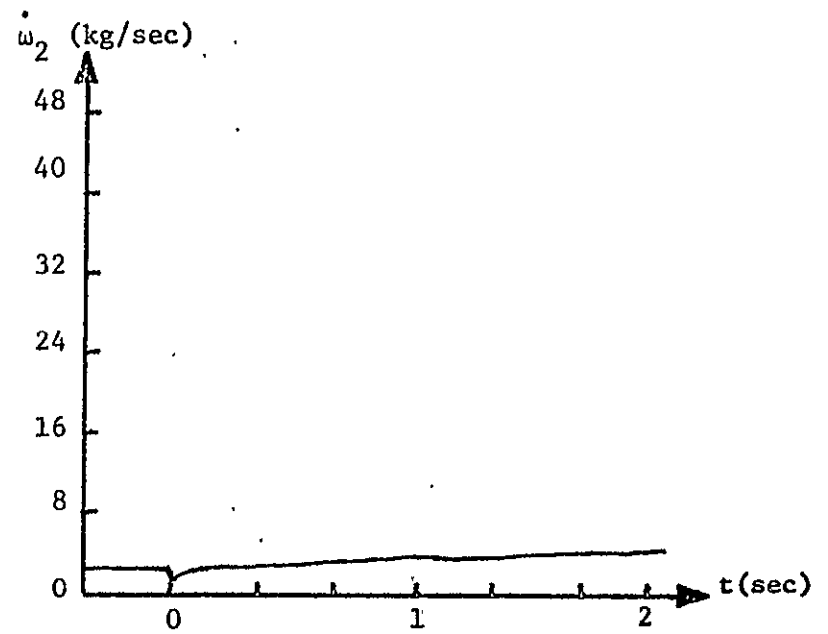
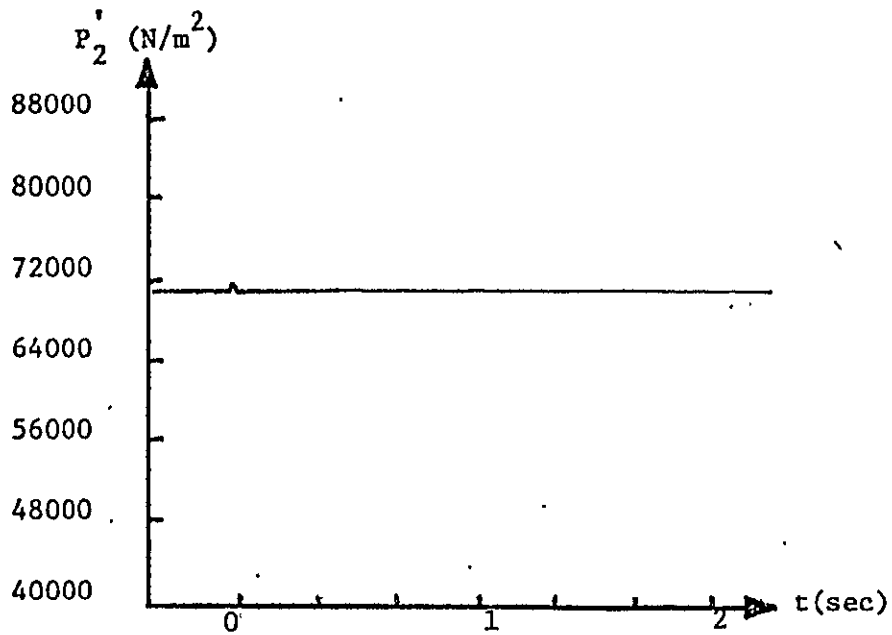


FIGURE 10. Acceleration transients, System B, Control 2.



REPRODUCIBILITY OF THE ORIGINAL DATA IS NOT GUARANTEED

FIGURE 11. Acceleration transients, System C, Control 2.

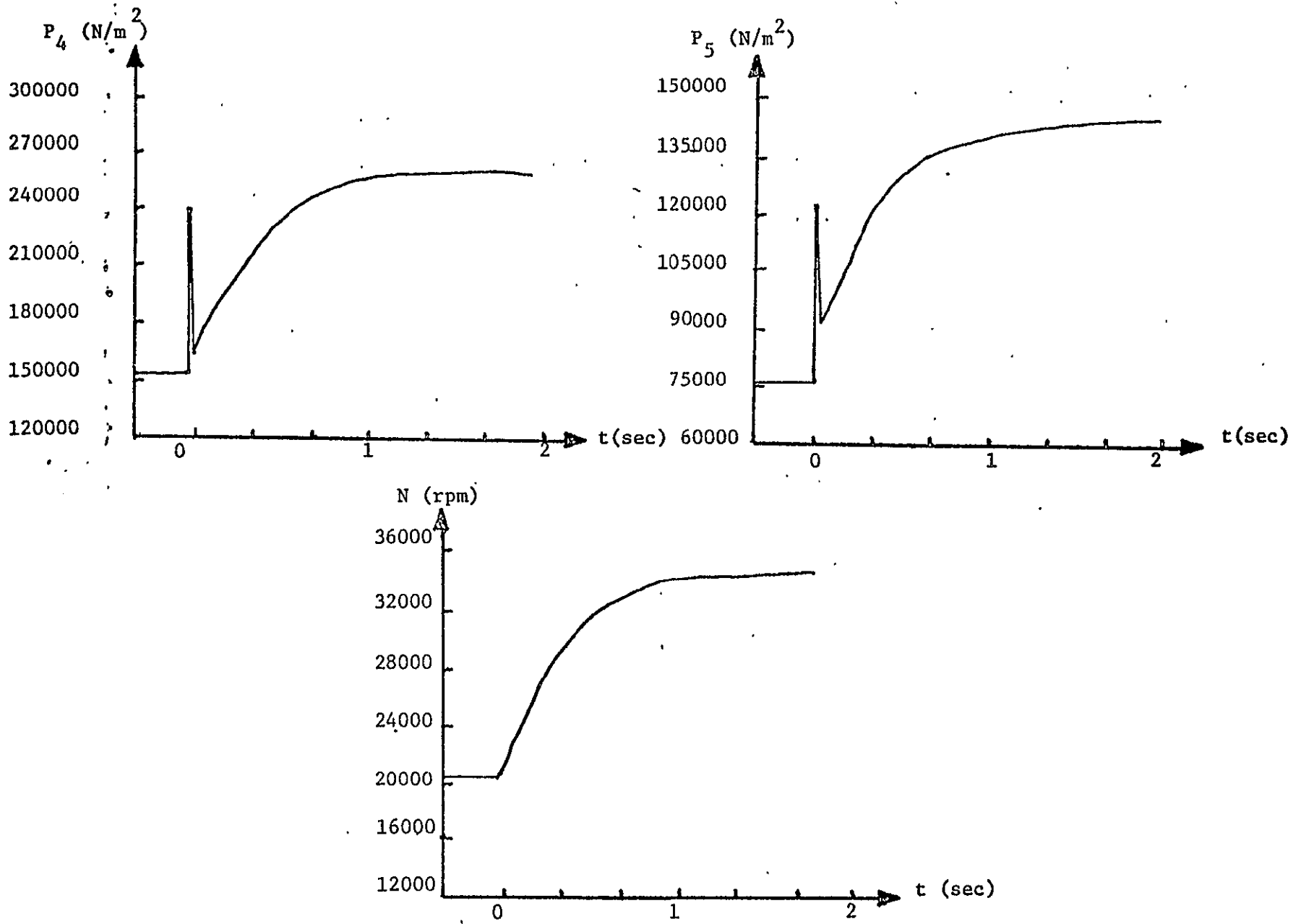


FIGURE 12. Acceleration transients, System C, Control 2.

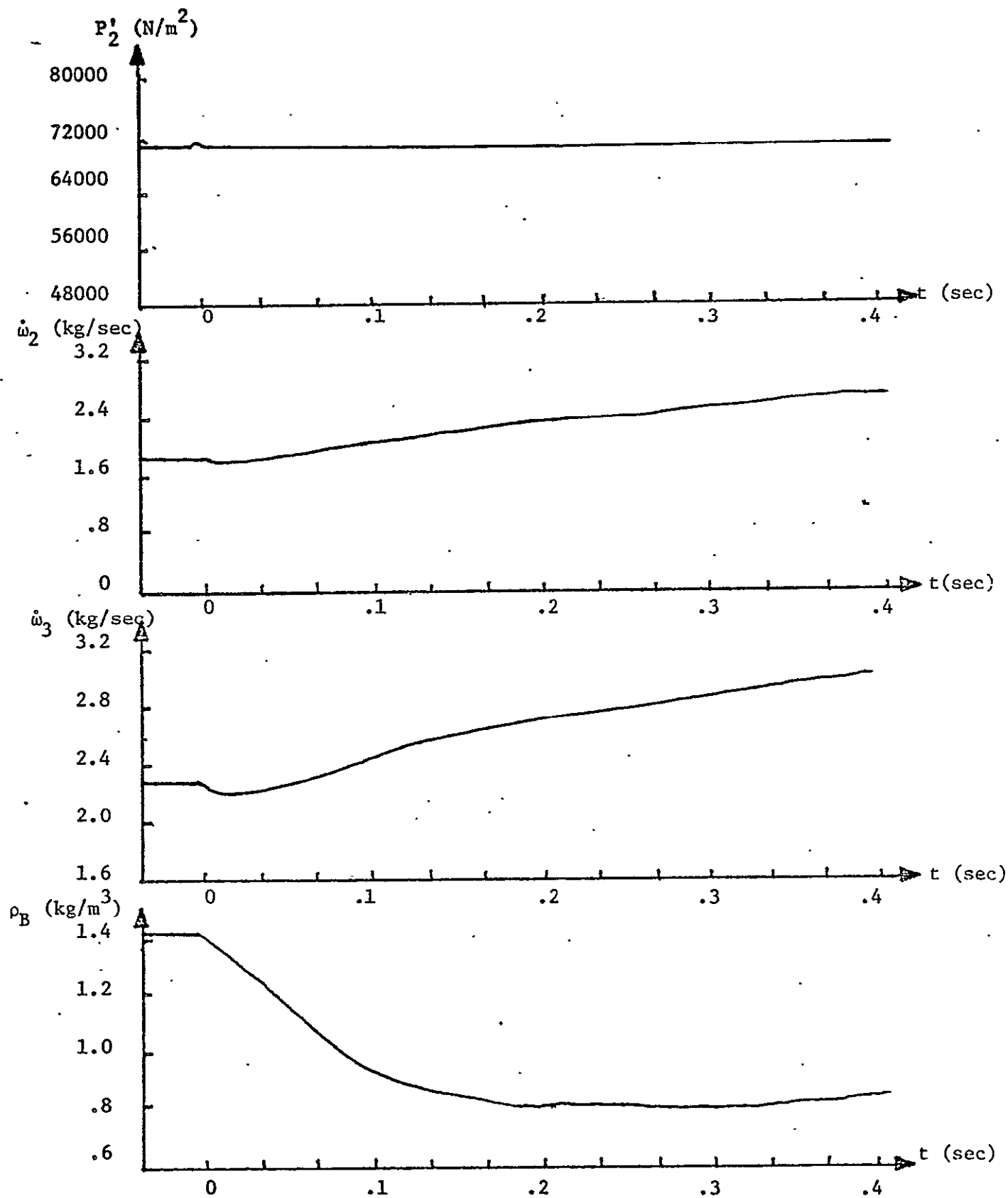


FIGURE 13. Acceleration transients, System B, Control 3.

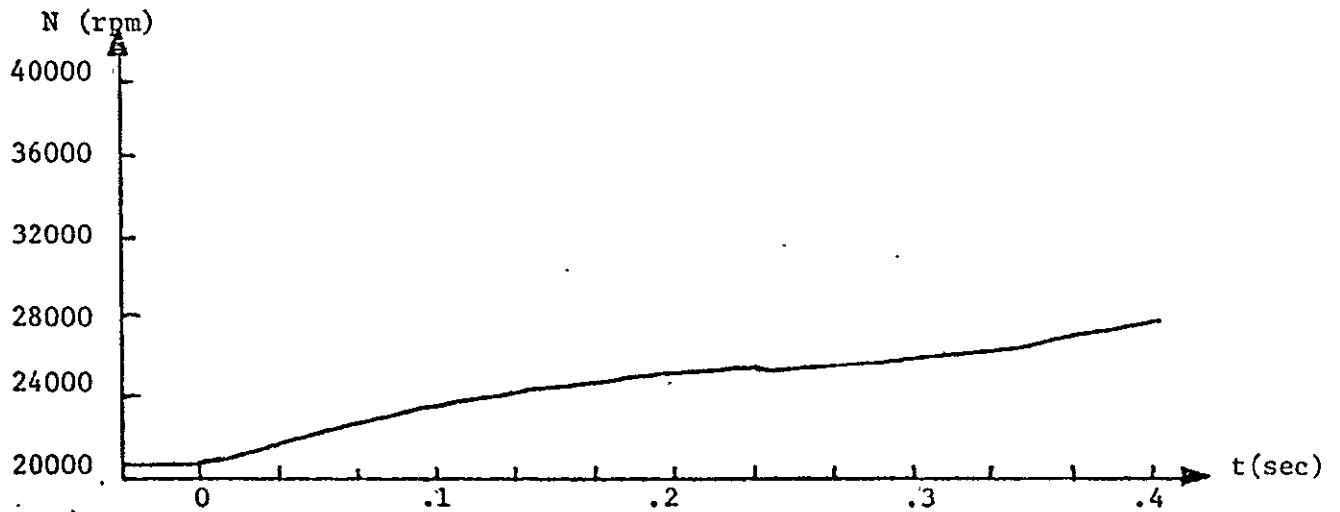
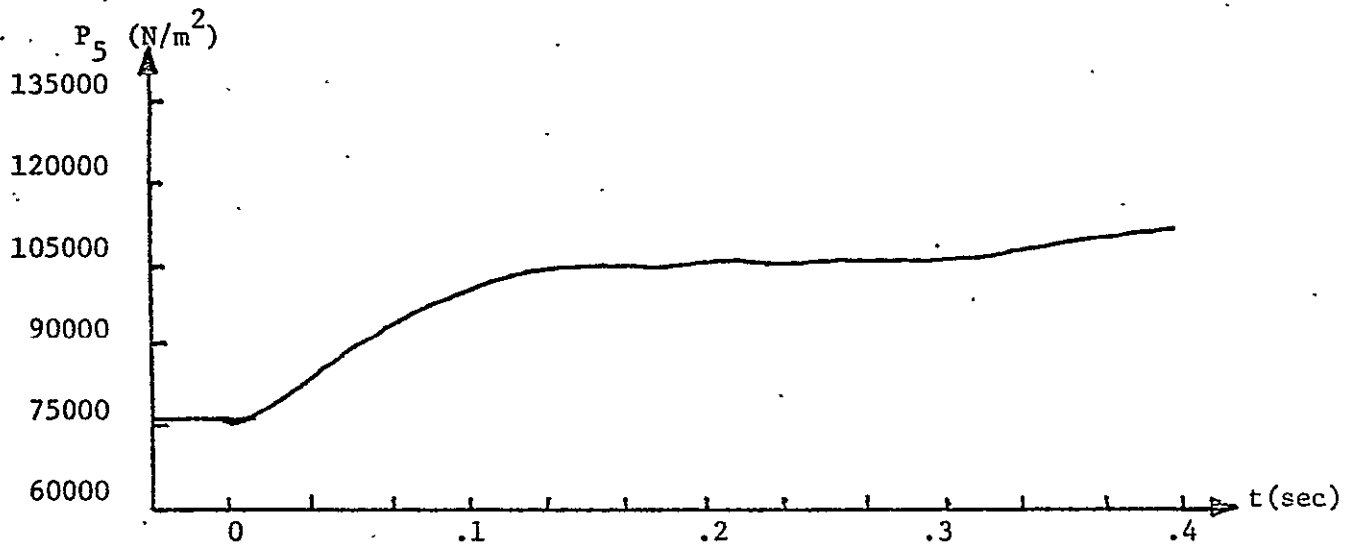
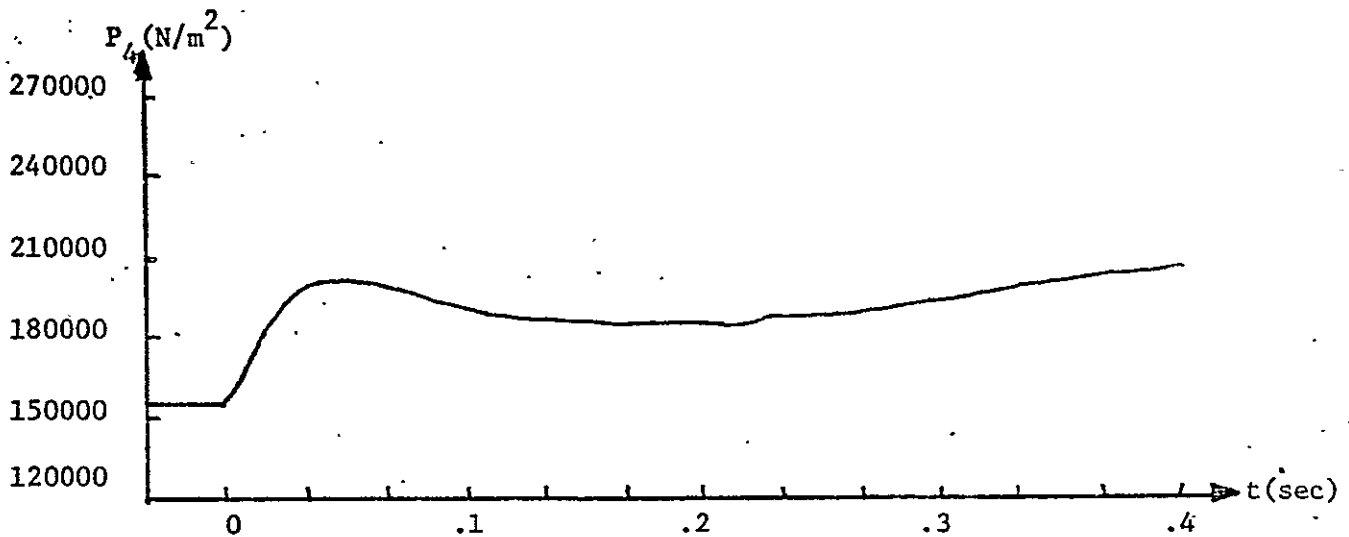


FIGURE 14. Acceleration transients, System B, Control 3.

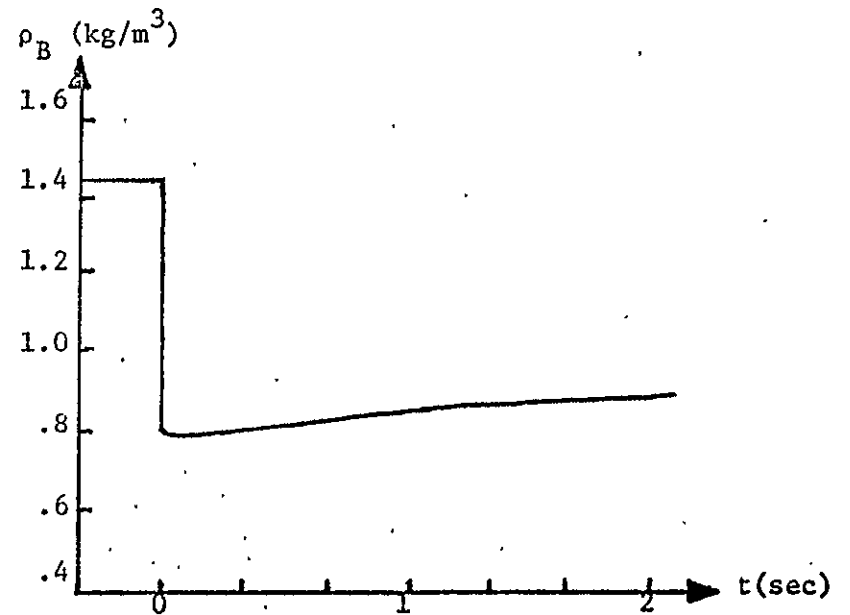
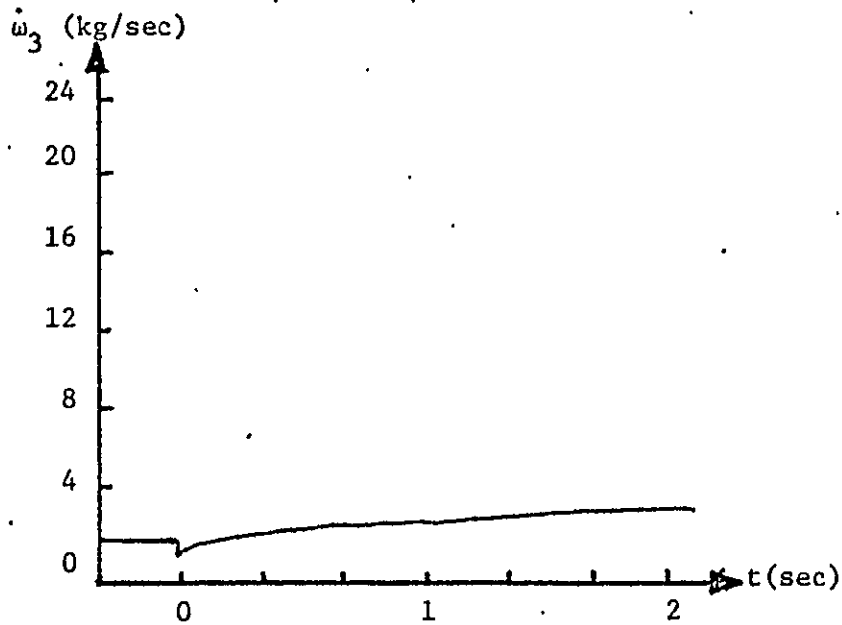
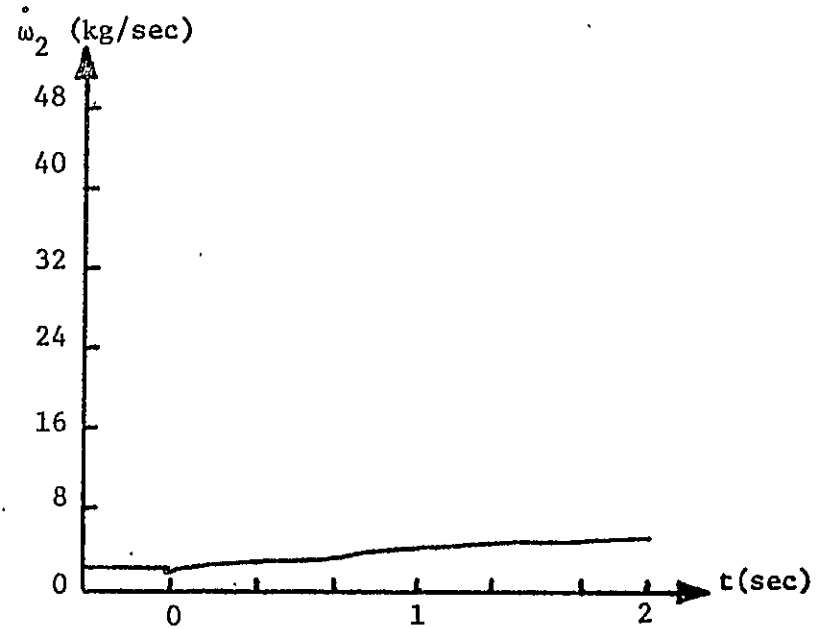
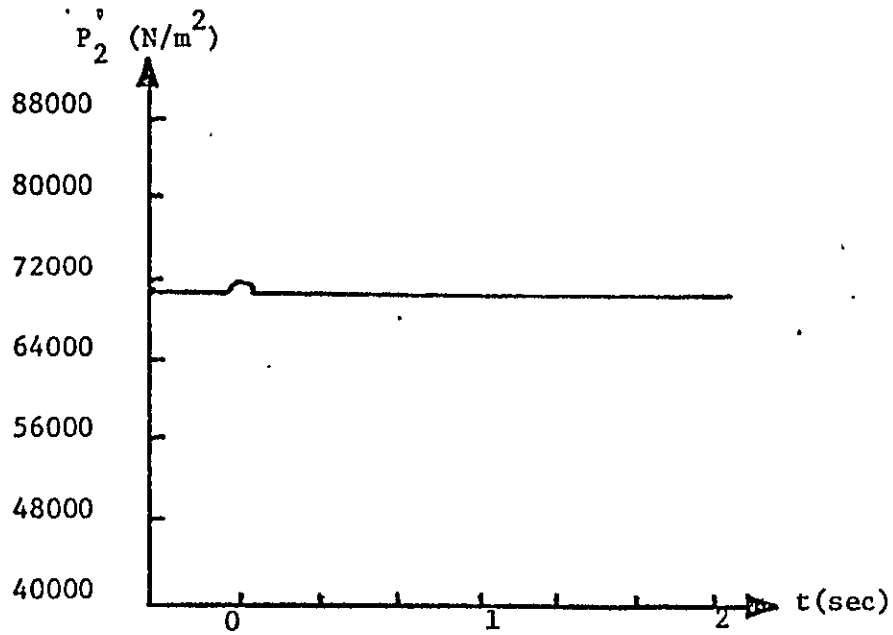
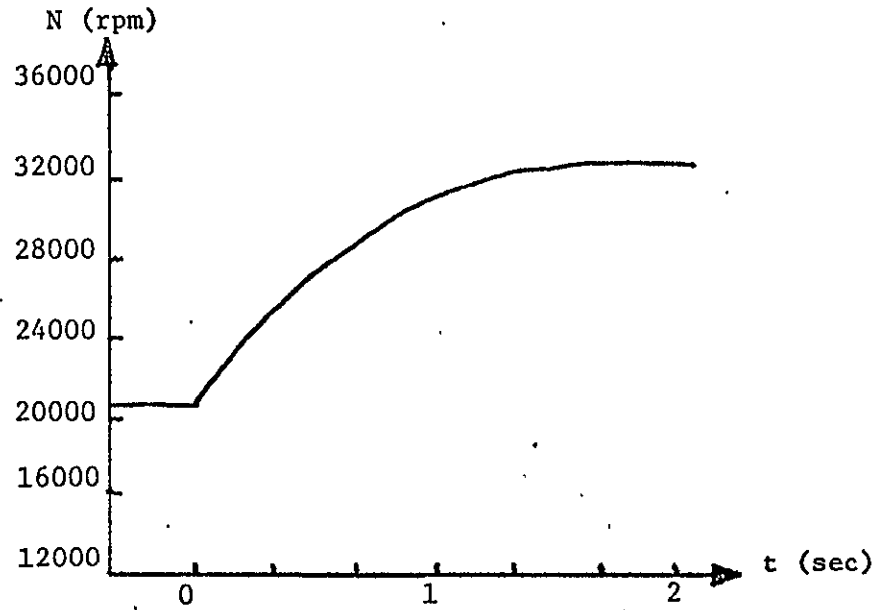
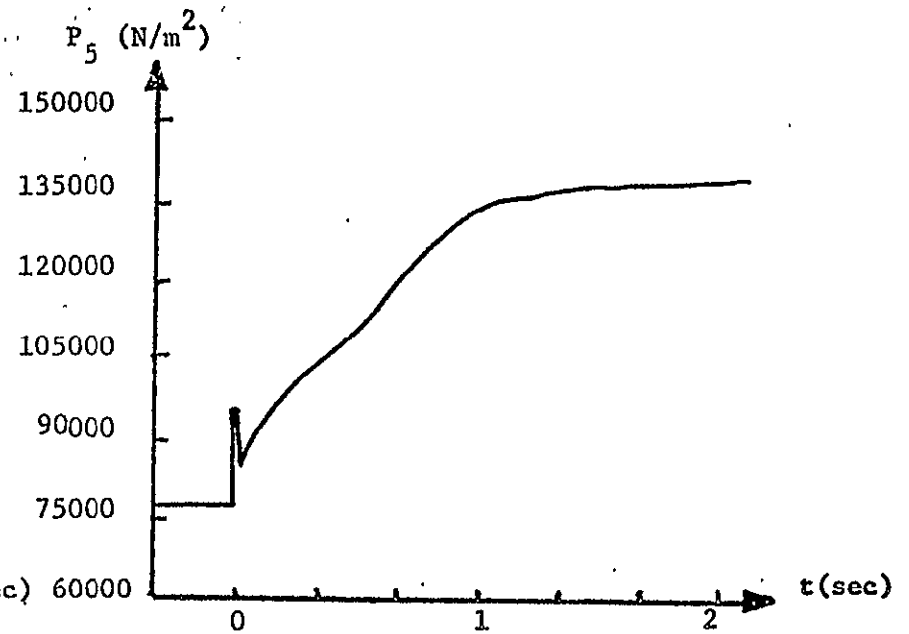
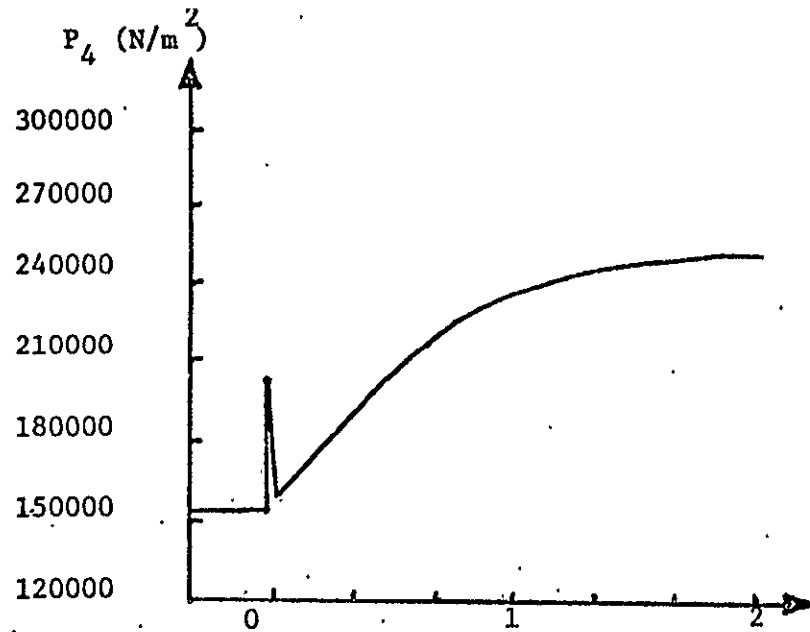


FIGURE 15. Acceleration transients, System C, Control 3.



REPRODUCIBILITY OF THIS
 ORIGINAL PAGE IS POOR

FIGURE 16. Acceleration transients, System C, Control 3.

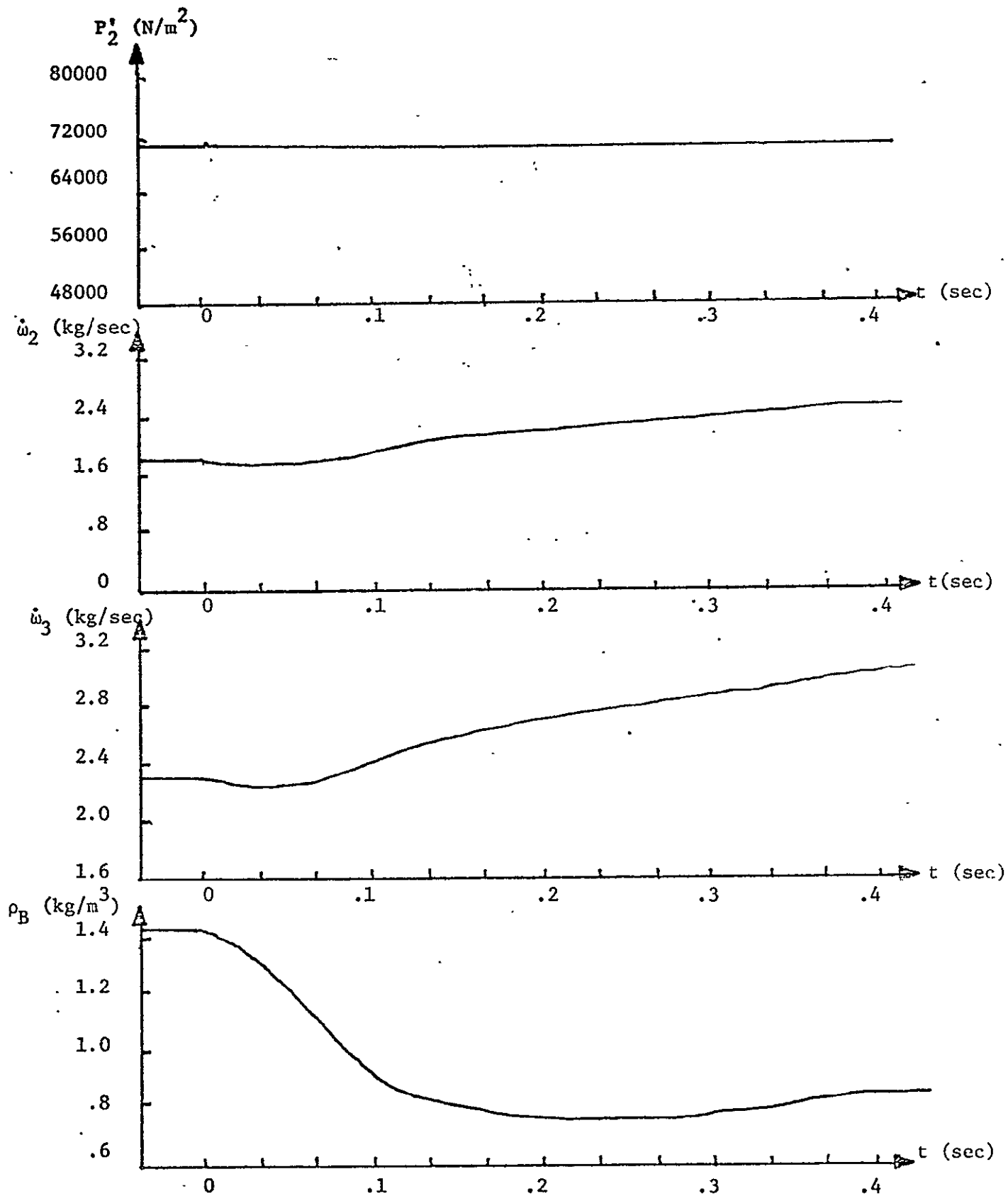


FIGURE 17. Acceleration transients, System B, Control 4.

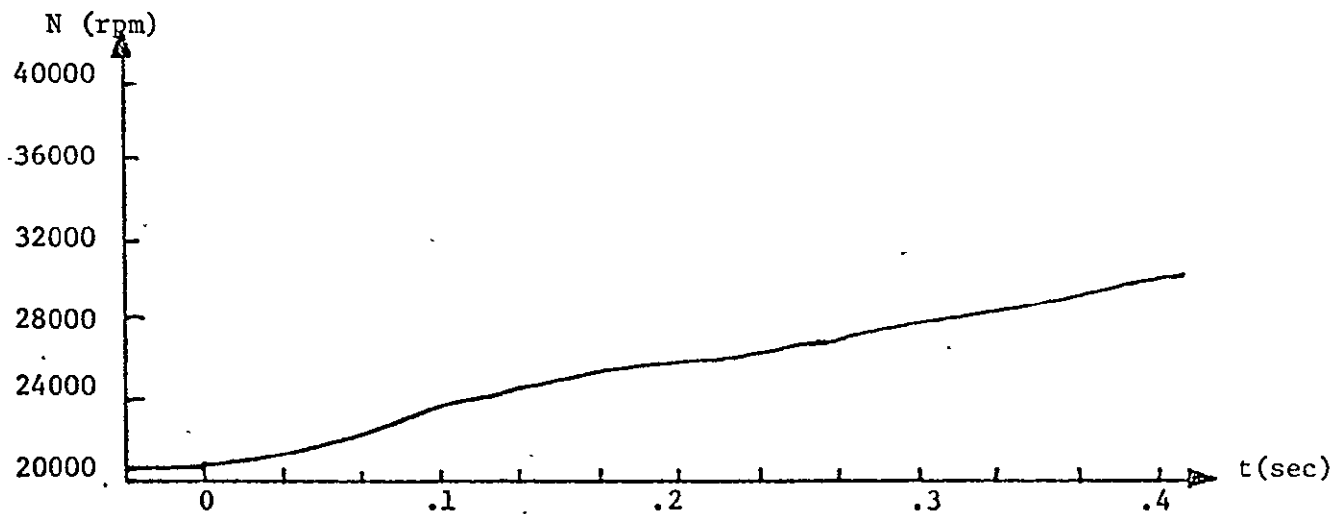
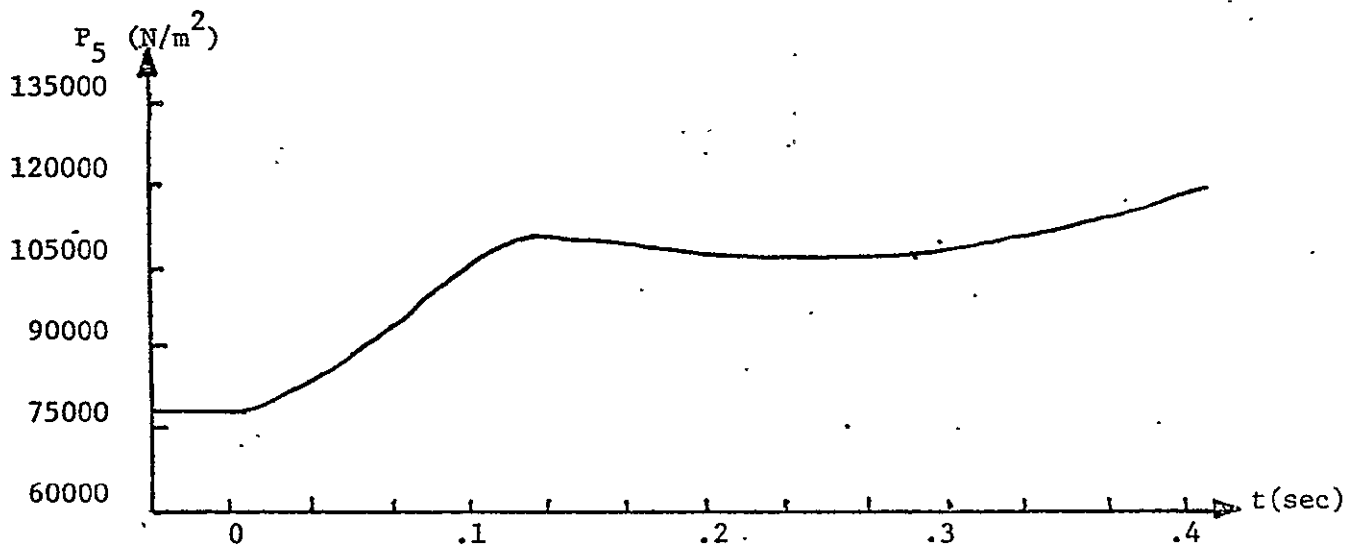
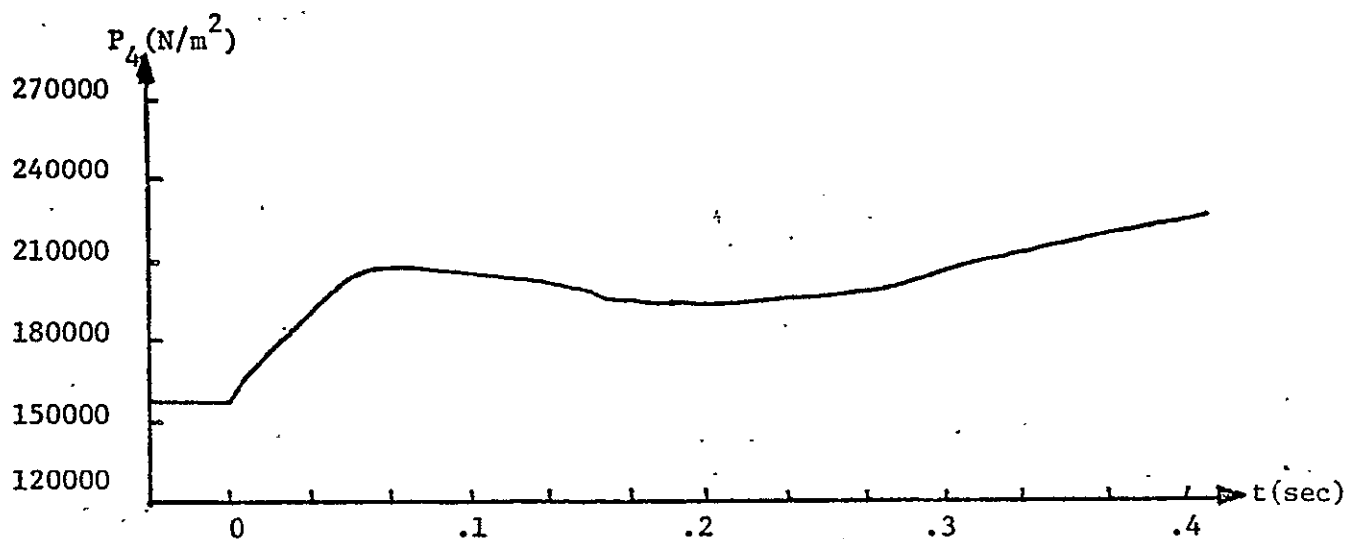
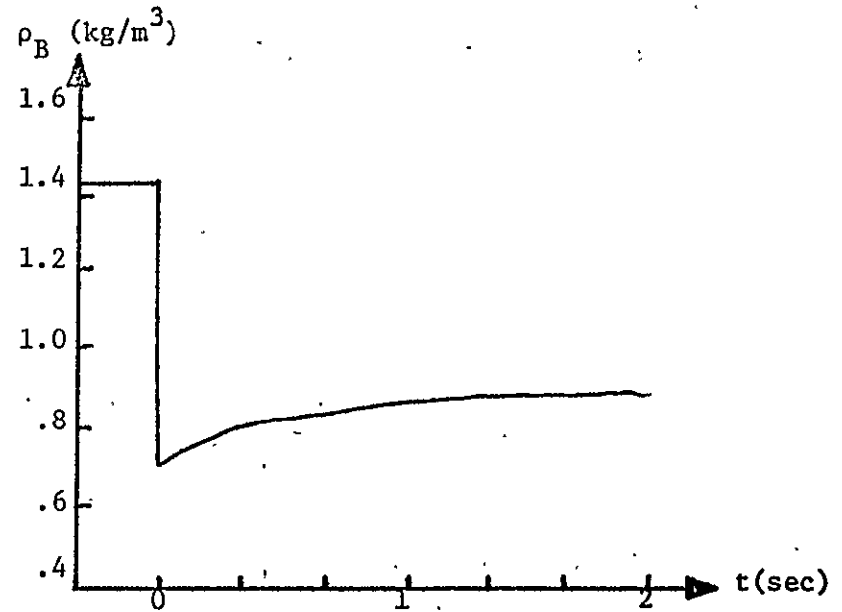
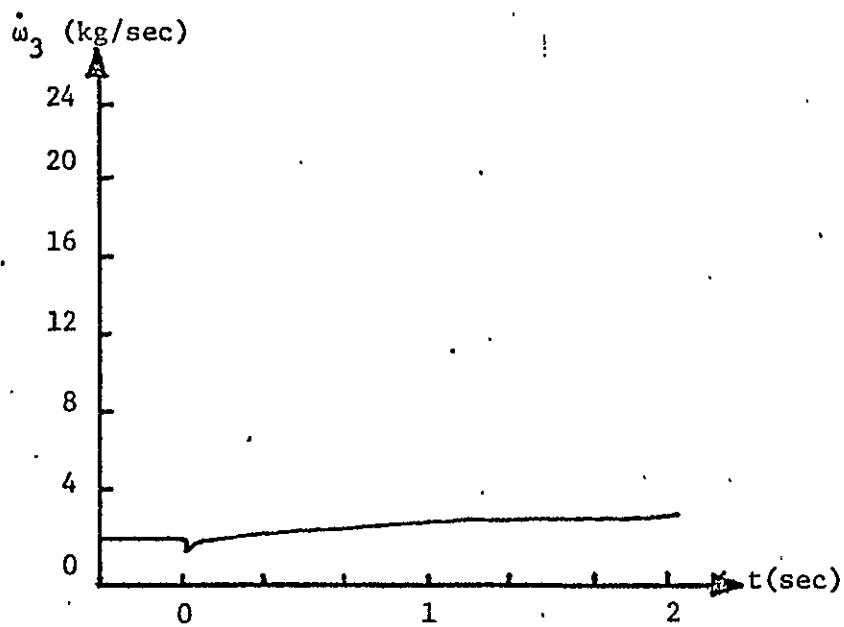
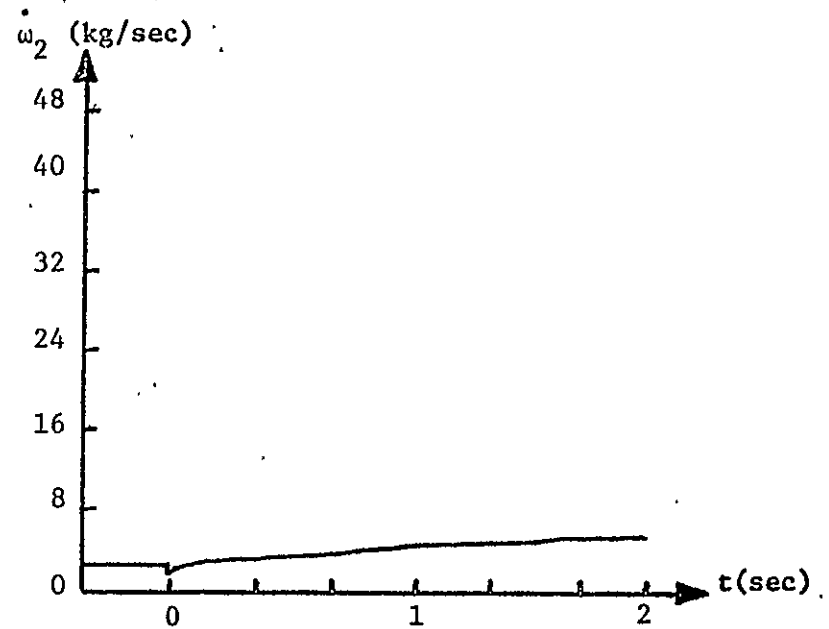
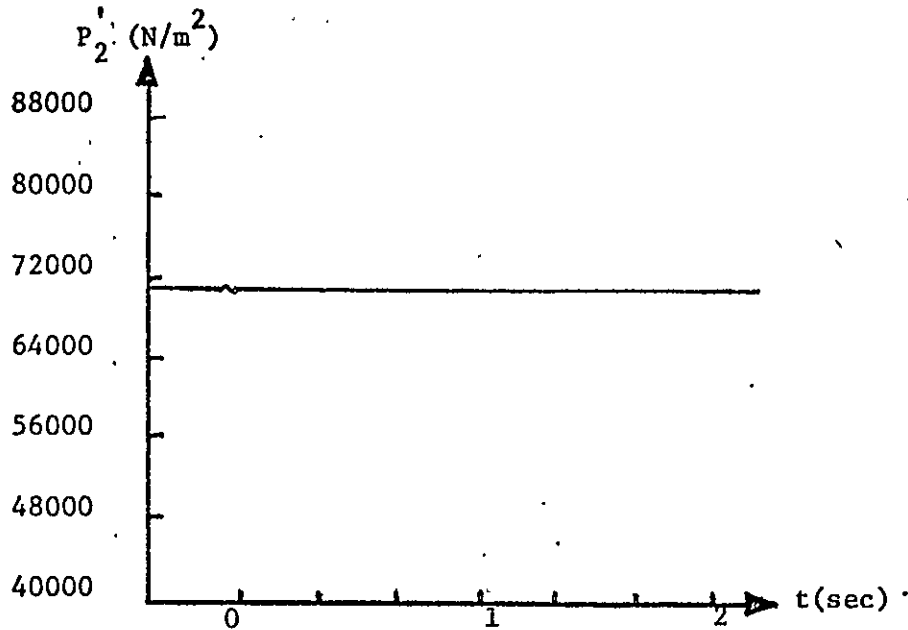


FIGURE 18. Acceleration transients, System B, Control 4.



REPRODUCIBILITY OF ORIGINAL PAGE IS POOR.

FIGURE 19. Acceleration transients, System C, Control 4.

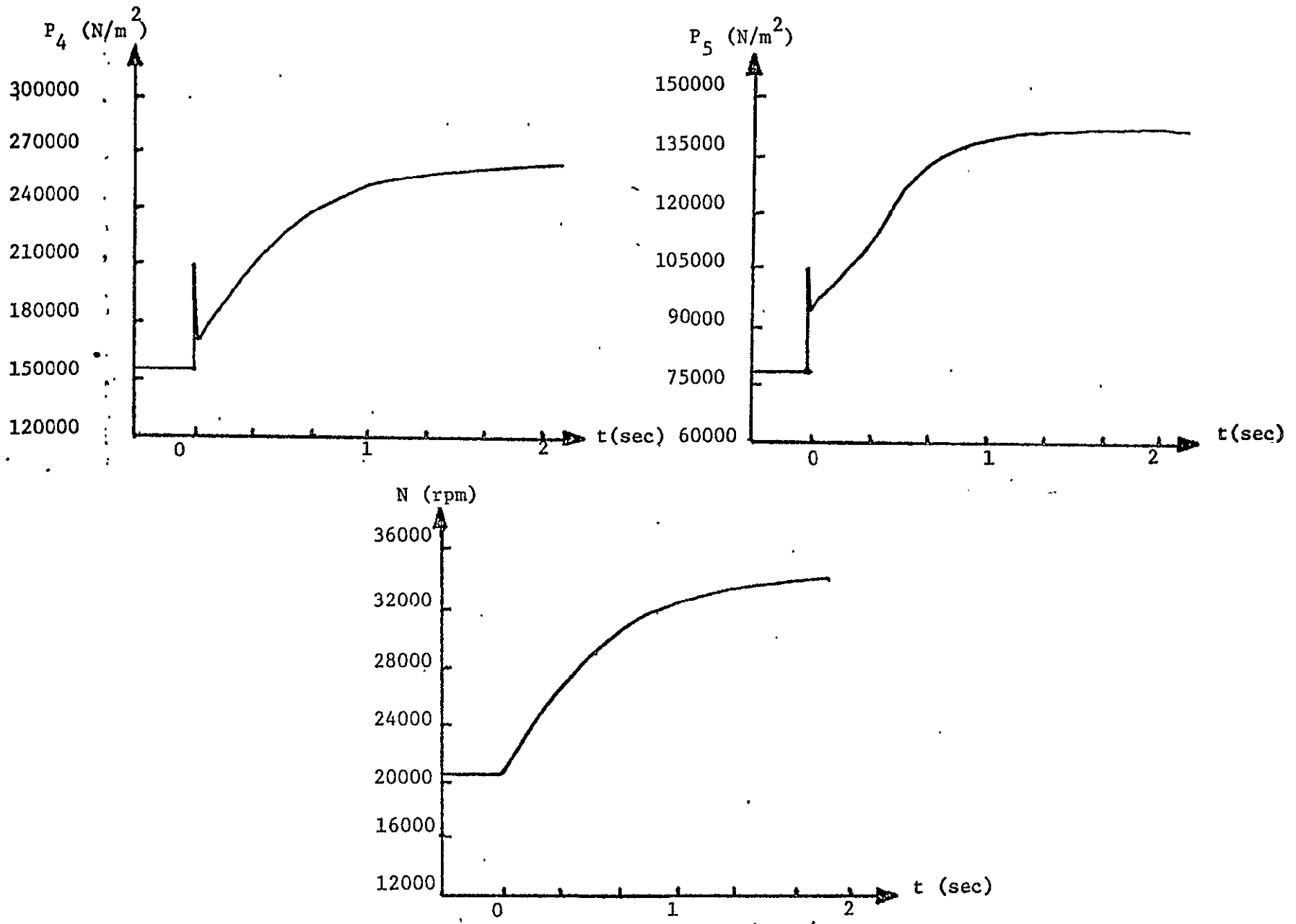


FIGURE 20. Acceleration transients, System C, Control 4.

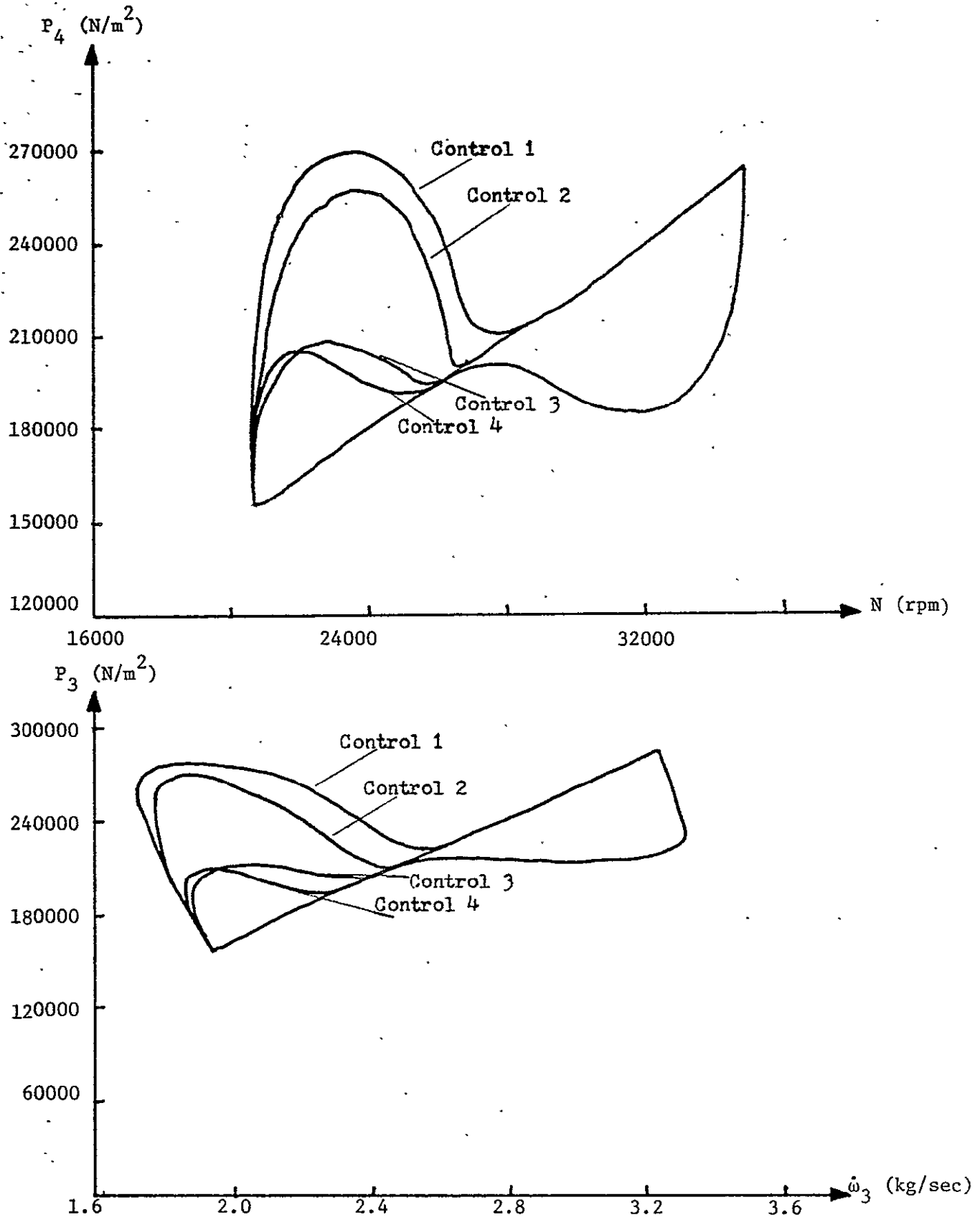


FIGURE 21. Graphs of surge margin studies for all four controls using System B.

REPRODUCIBILITY OF THIS
ORIGINAL PAGE IS POOR.

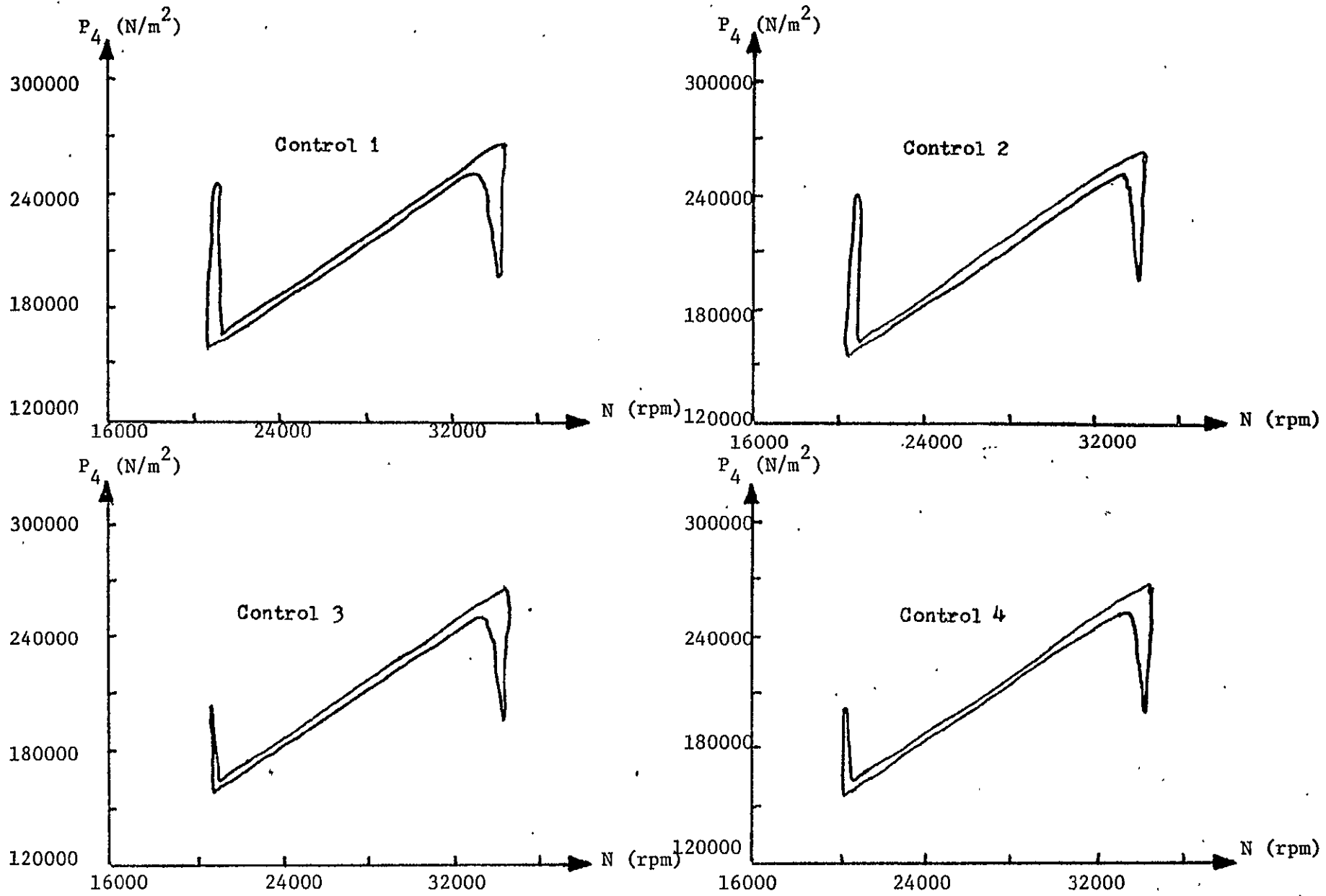


FIGURE 22. P_4 vs N coordinate system plots of surge margin studies using System C.

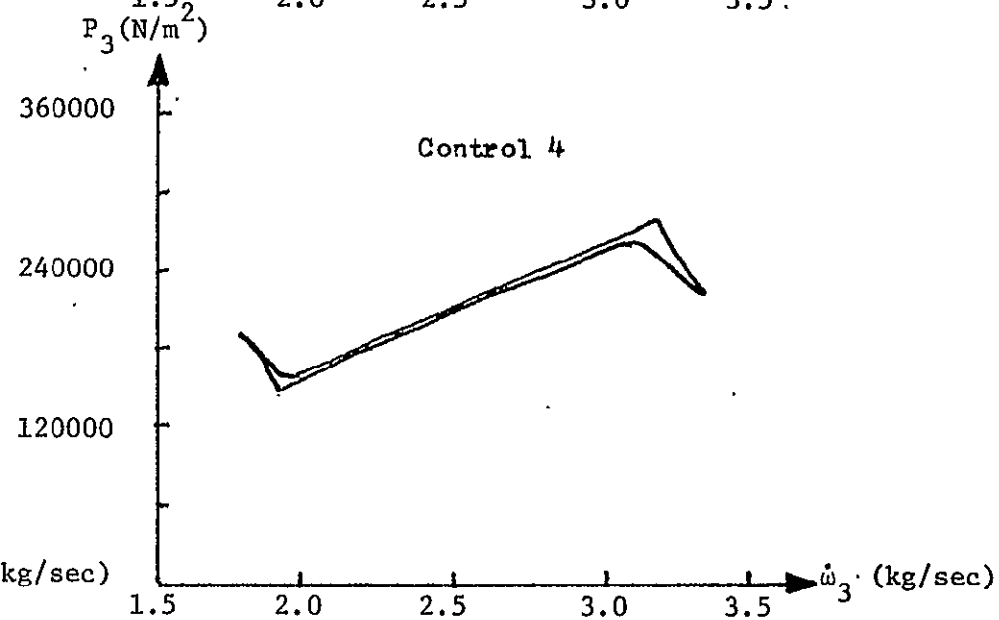
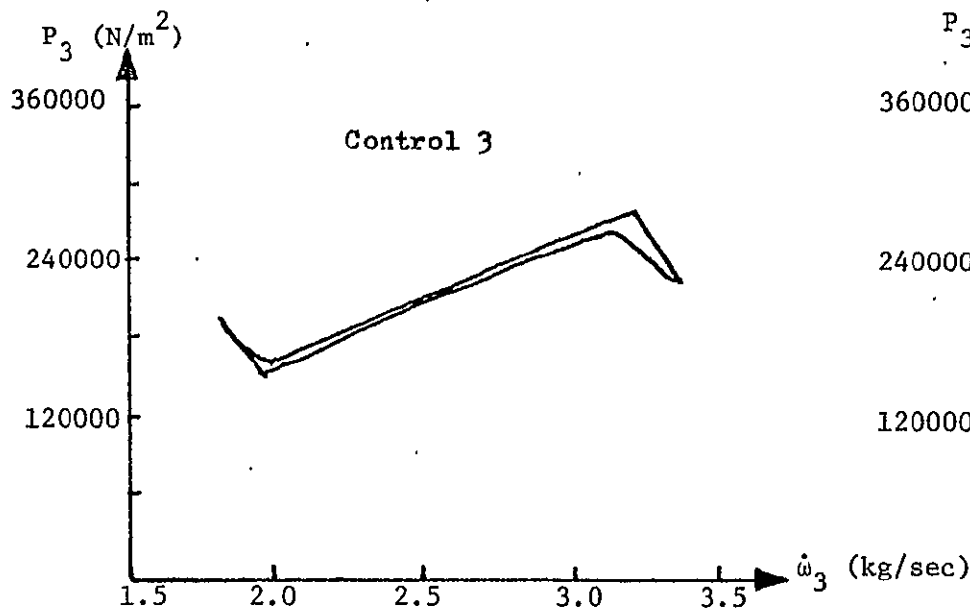
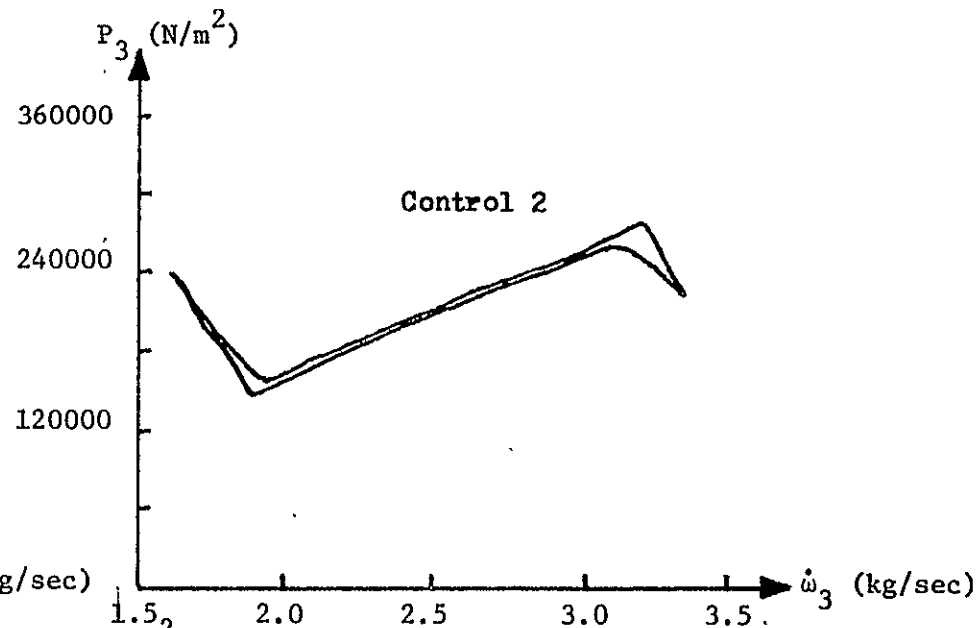
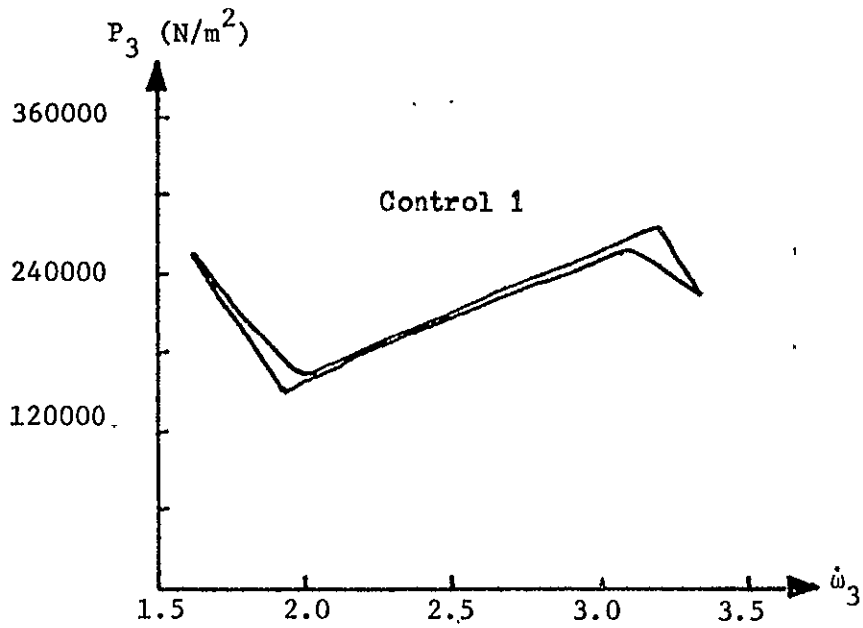


FIGURE 23. P_3 vs \dot{w}_3 coordinate system plots of surge margin studies using System C.

APPENDIX B

THIRD ORDER SIMULATION ACCELERATION PLOTS

The third order simulation acceleration transients and surge margin studies are illustrated in the following pages.

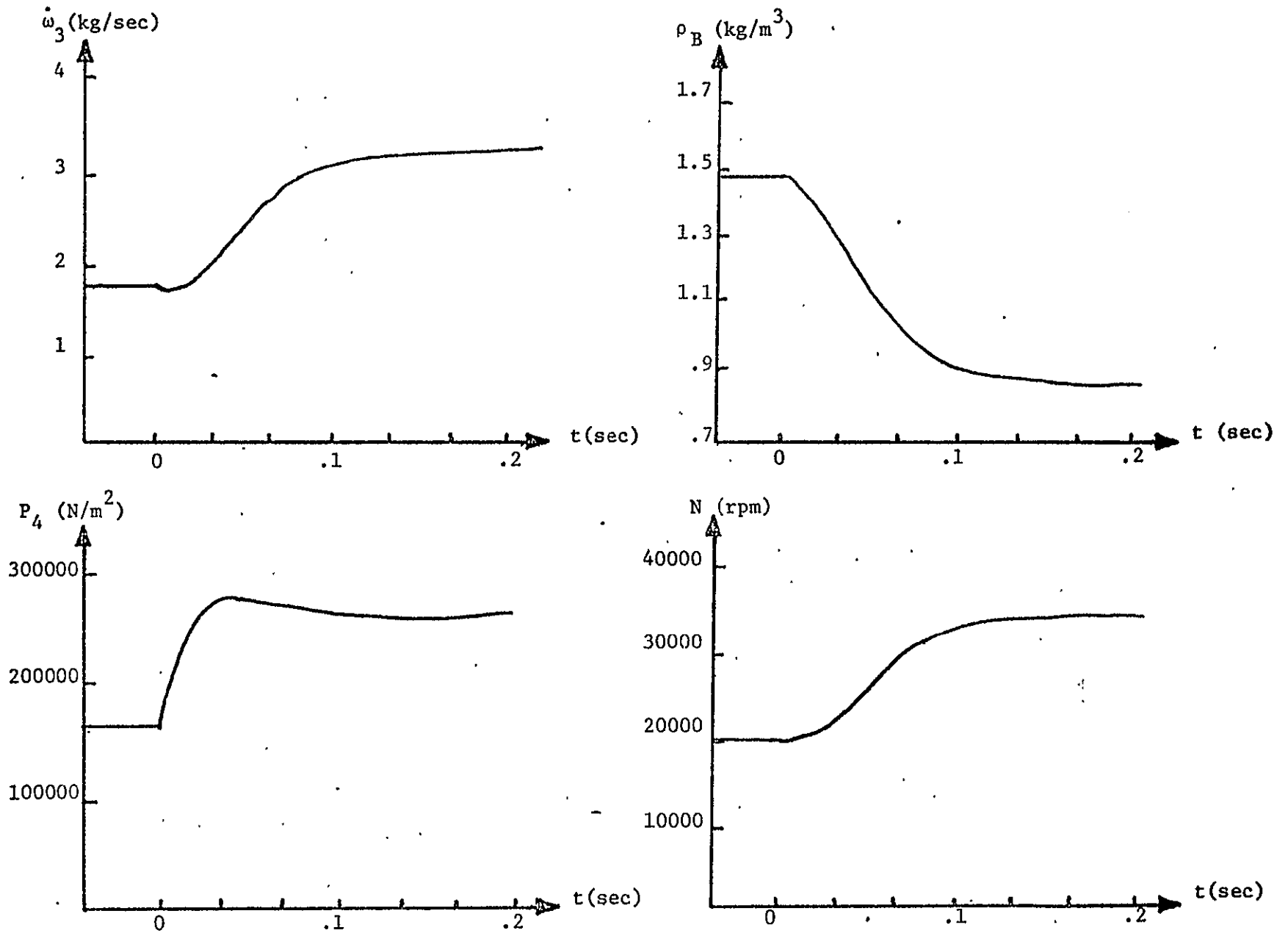


FIGURE 24. Acceleration transients, System A, Control 1.

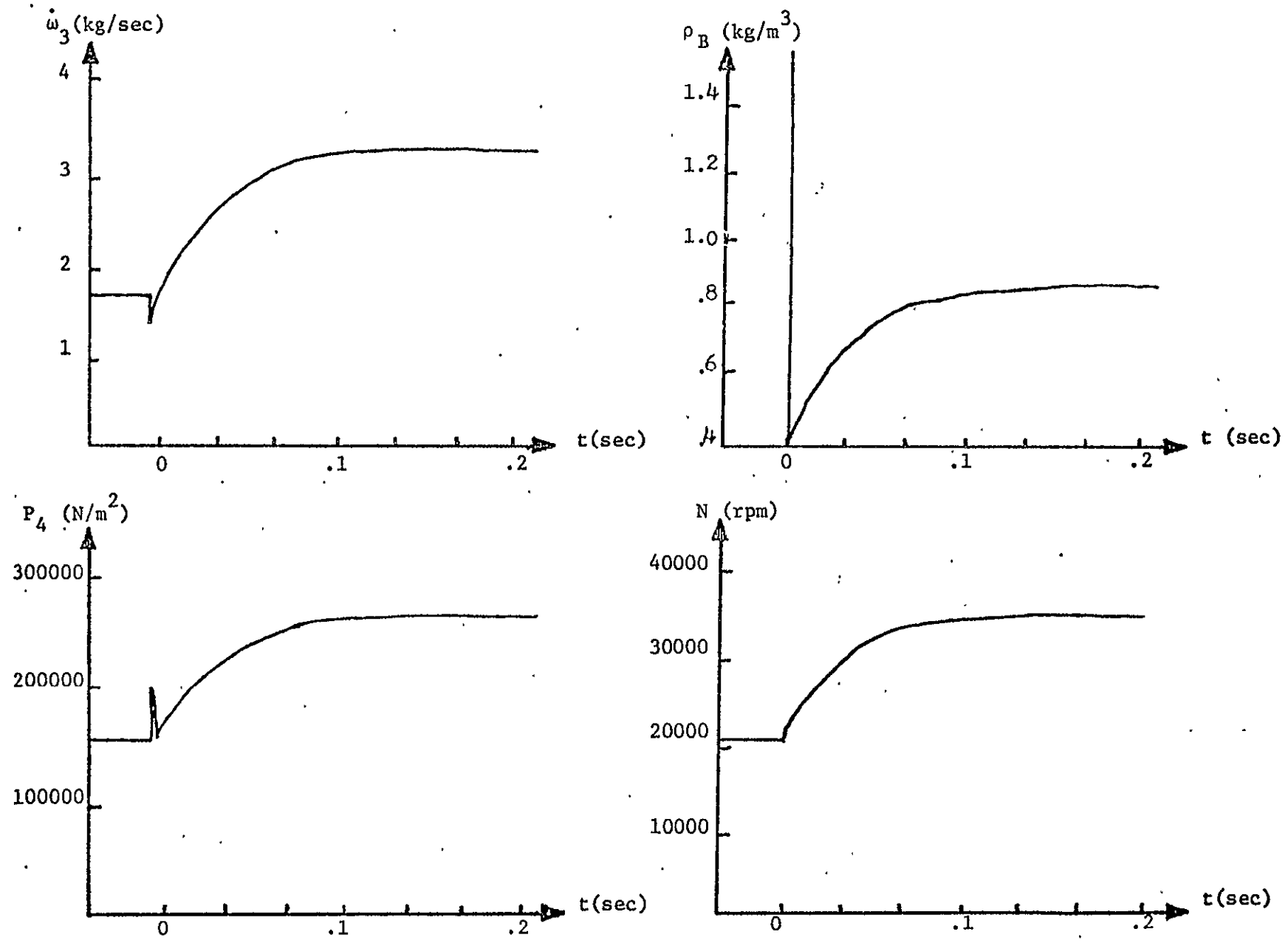


FIGURE 25. Acceleration transients, System C, Control 1.

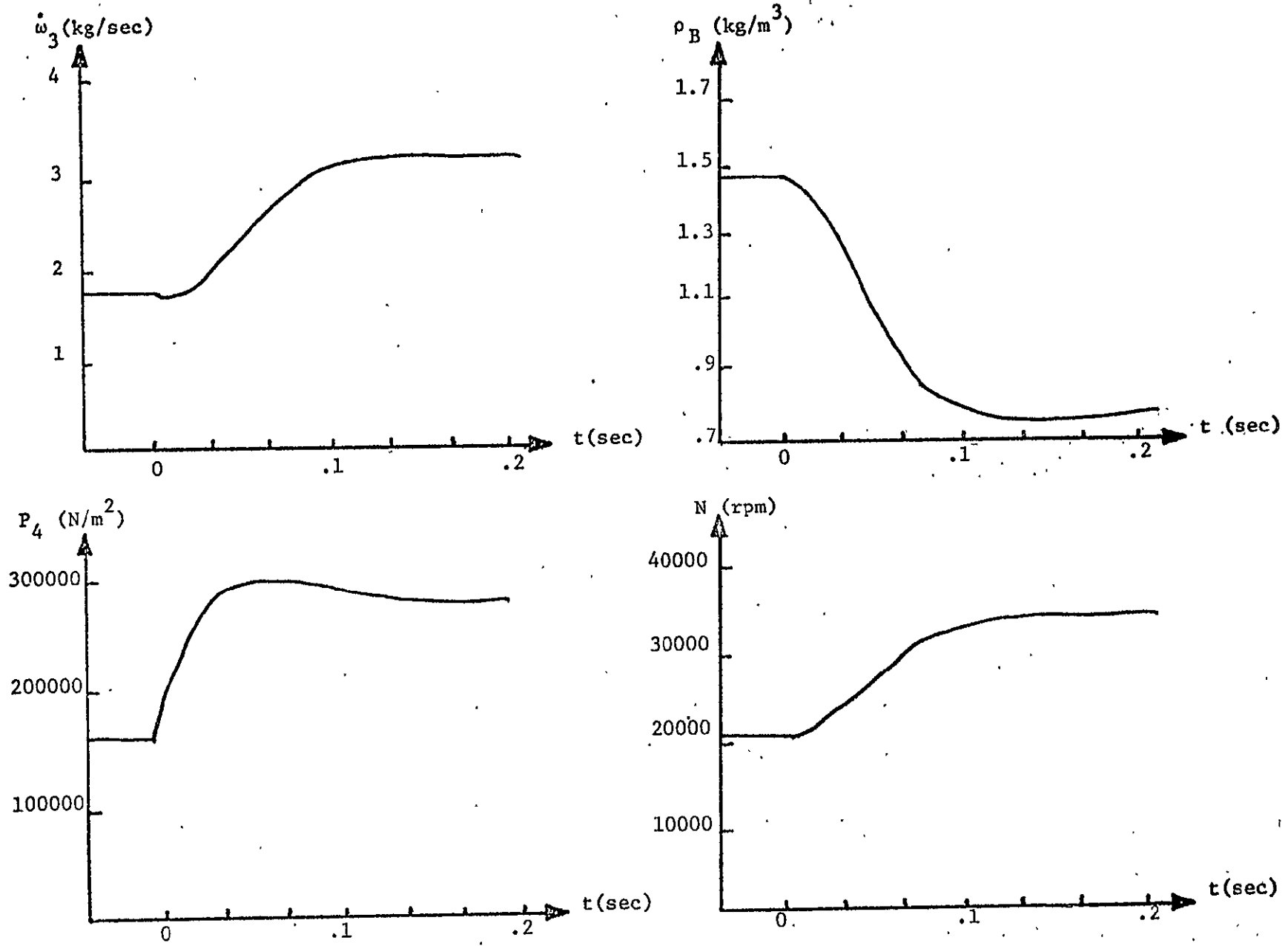


FIGURE 26. Acceleration transients, System A, Control 2.

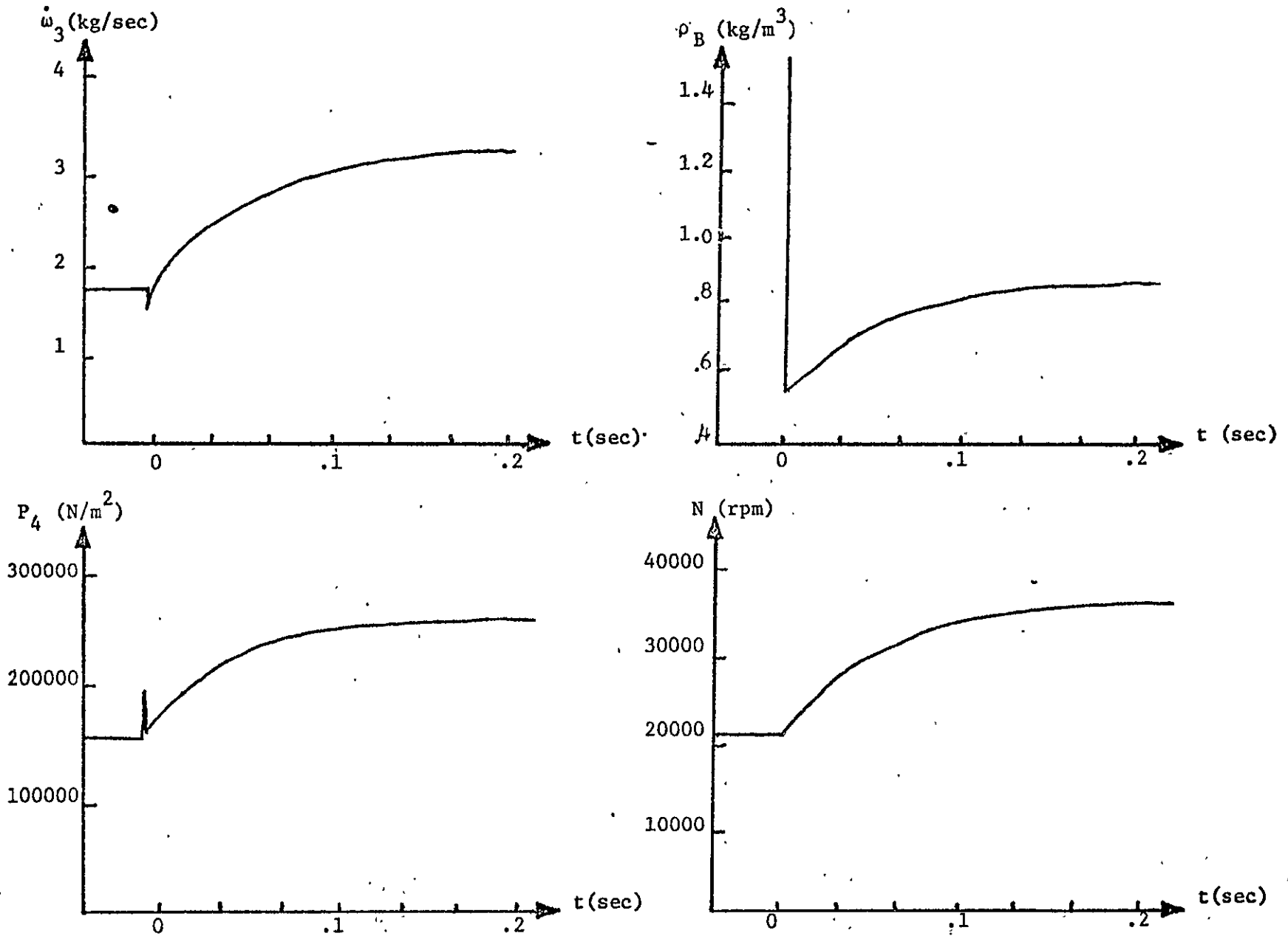
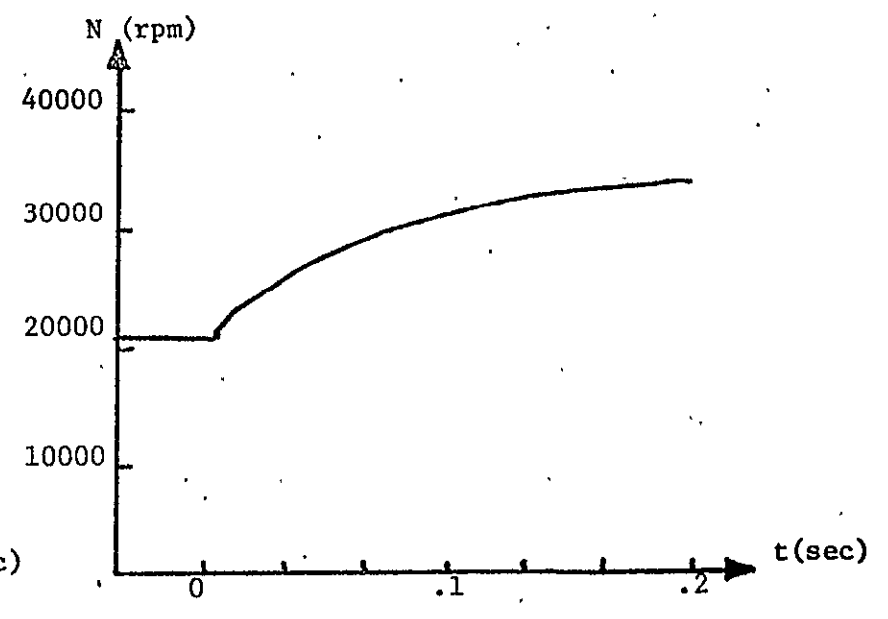
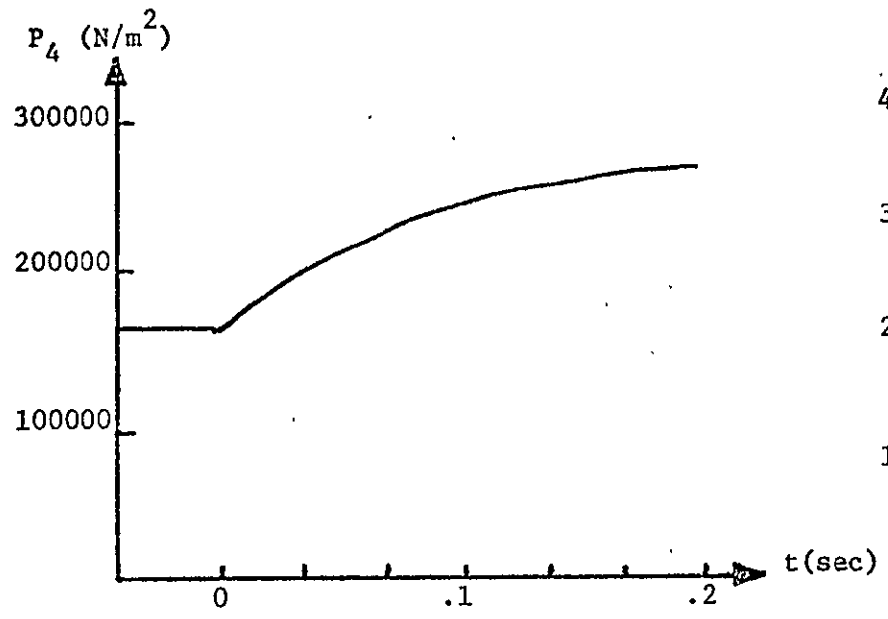
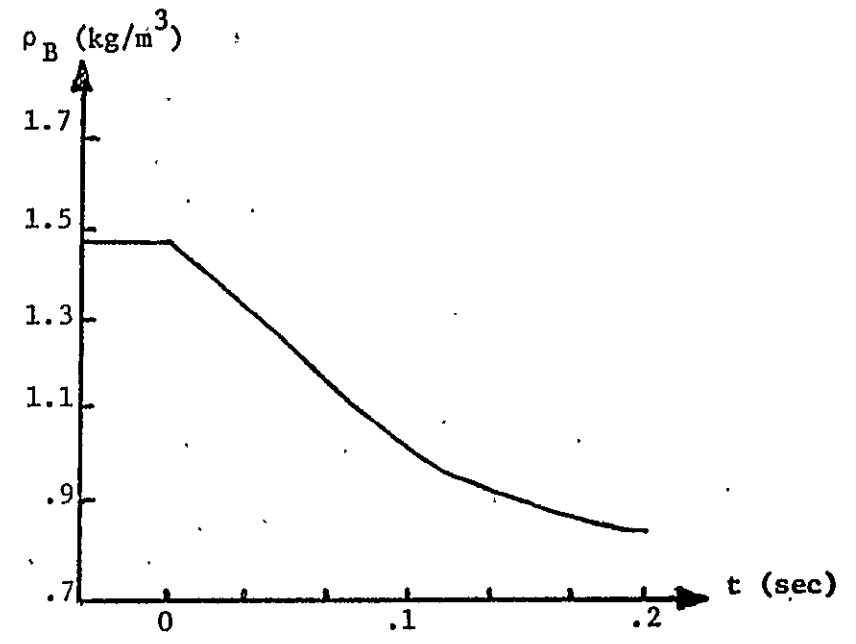
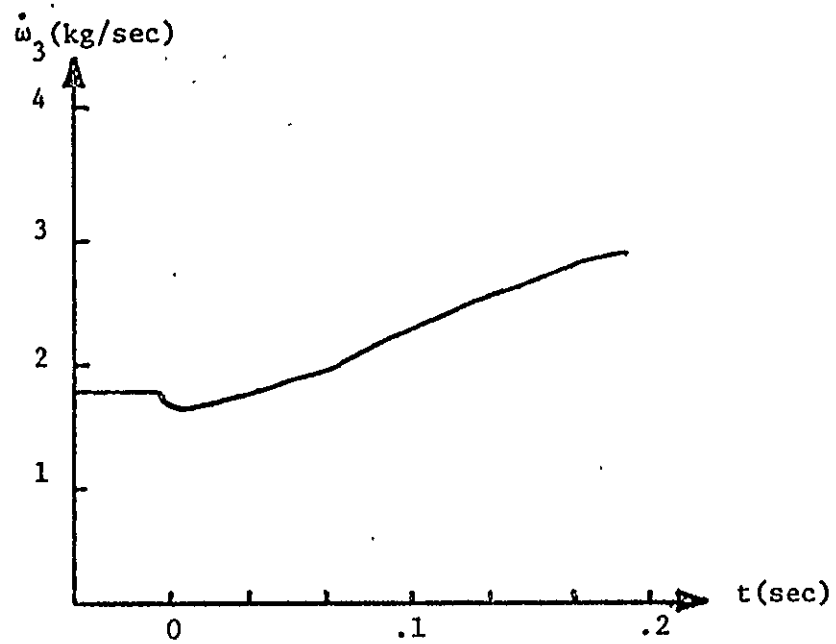


FIGURE 27. Acceleration transients, System C, Control 2.



REPRODUCIBILITY OF THIS ORIGINAL PAGE IS POOR

FIGURE 28. Acceleration transients, System A, Control 3.

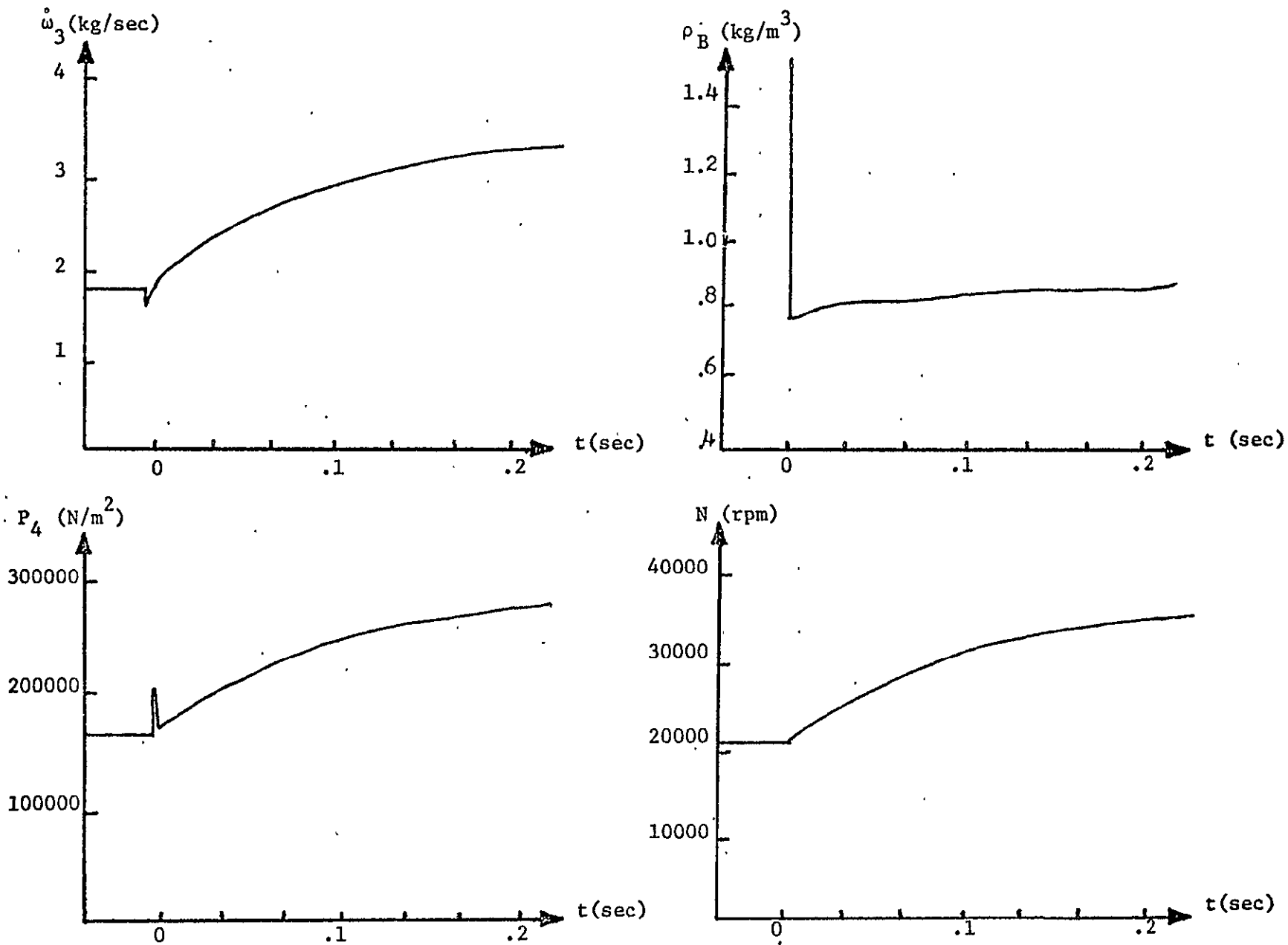


FIGURE 29. Acceleration transients, System C, Control 3.

REPRODUCIBILITY OF THIS
ORIGINAL PAGE IS POOR

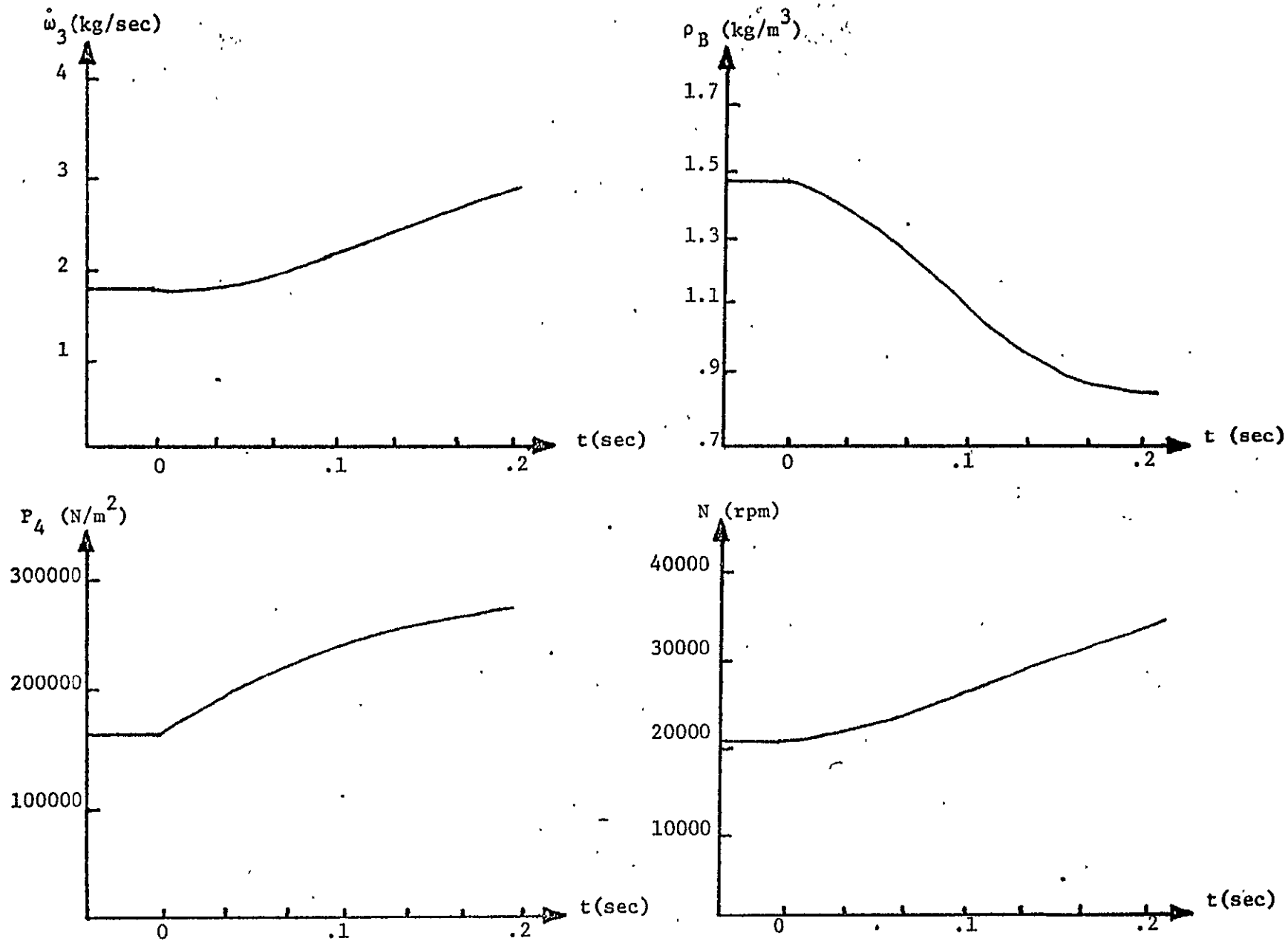


FIGURE 30. Acceleration transients, System A, Control 4.

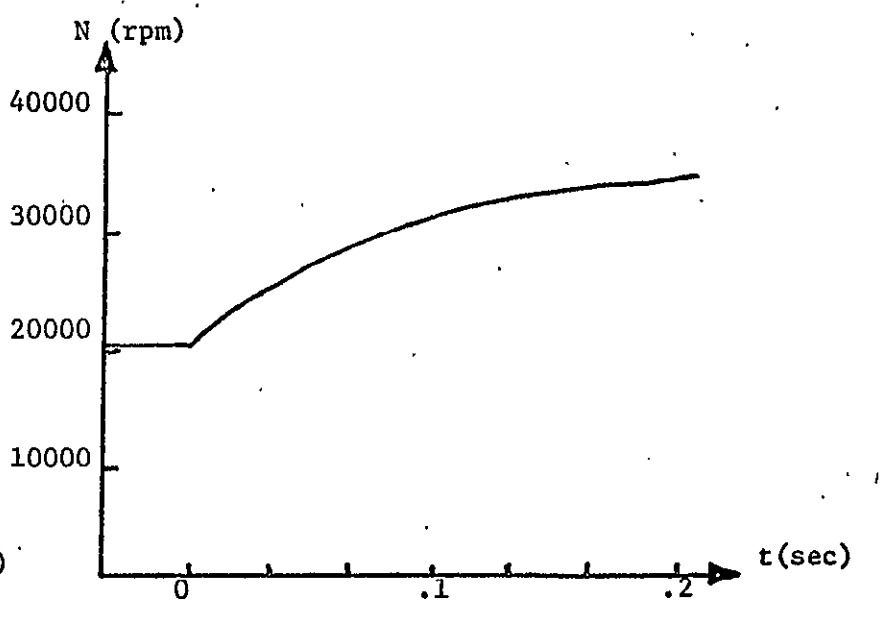
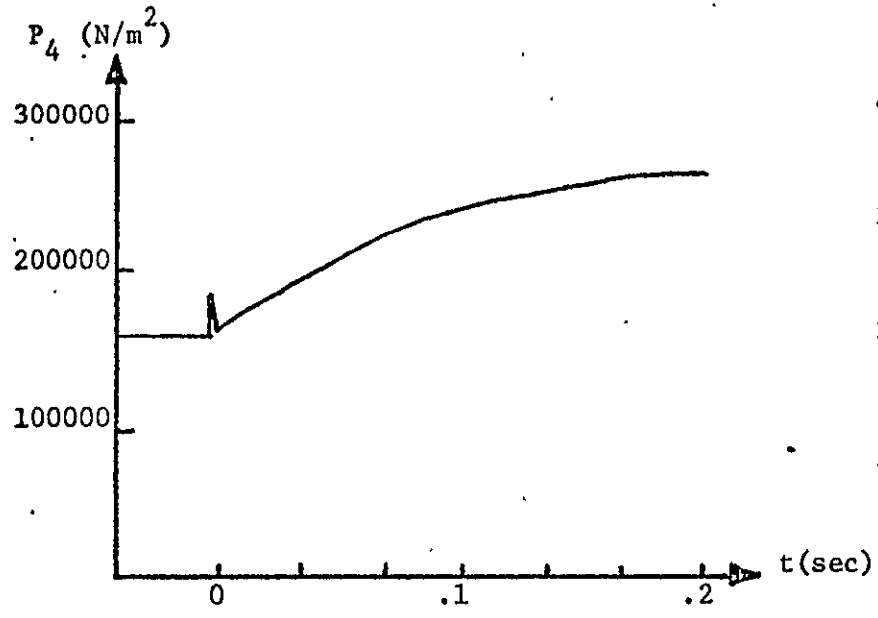
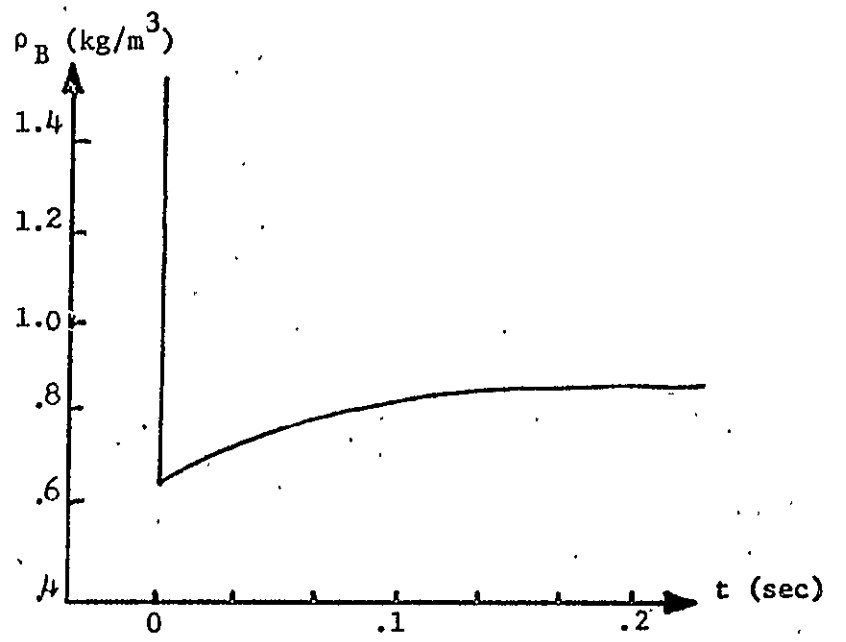
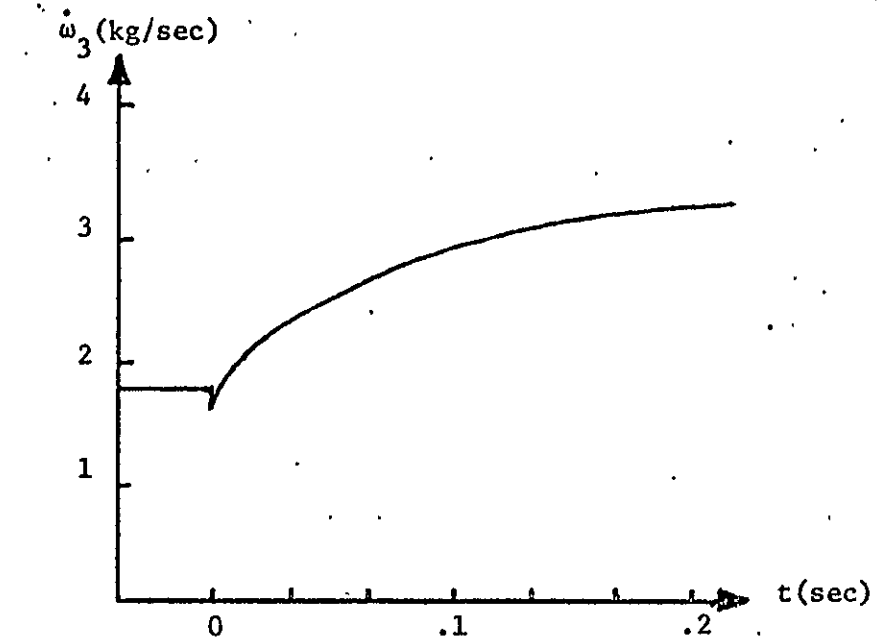


FIGURE 31. Acceleration transients, System C, Control 4.

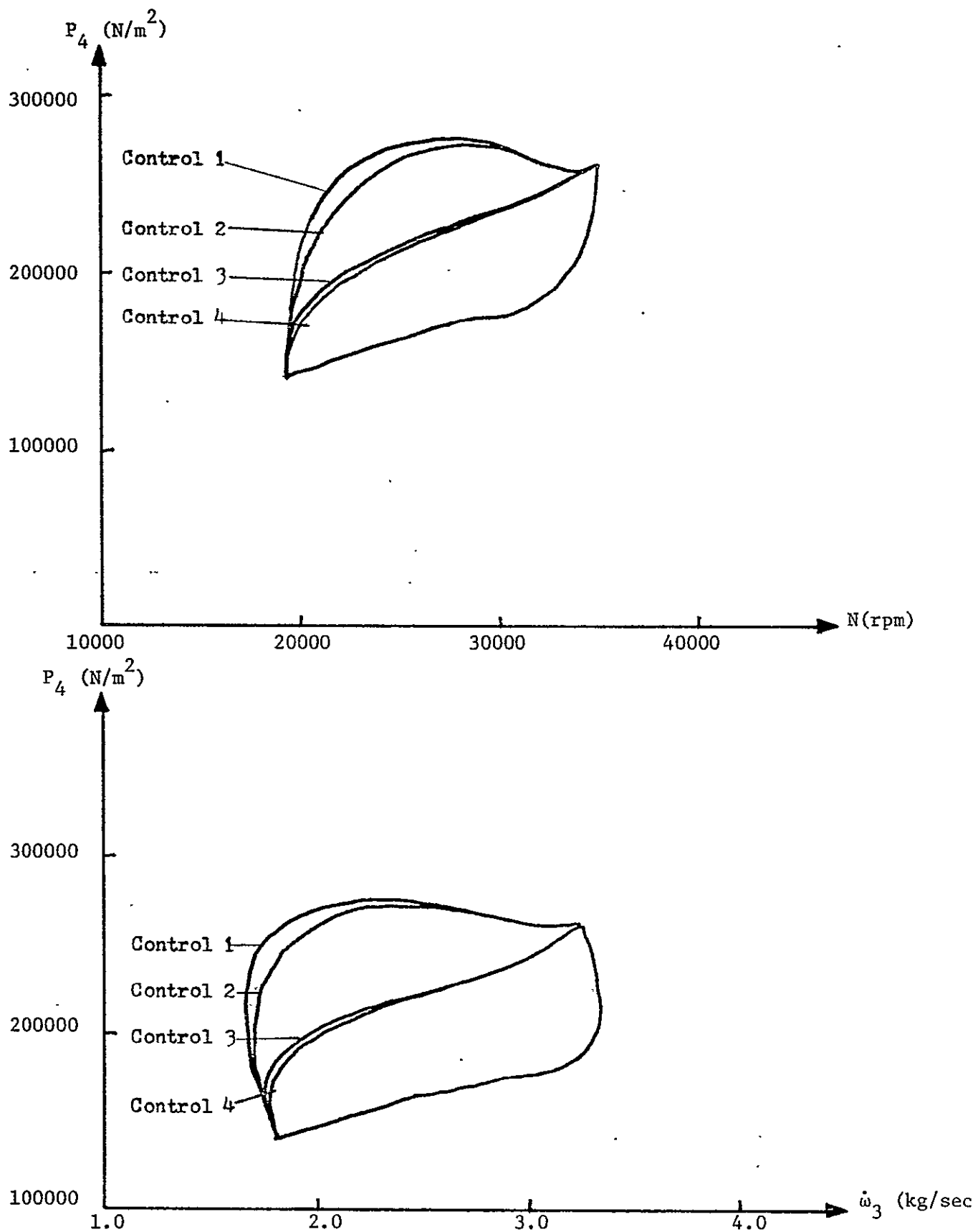


FIGURE 32. Graphs of surge margin studies of all four controls using System A.

REPRODUCIBILITY OF THE ORIGINAL PAGE IS POOR

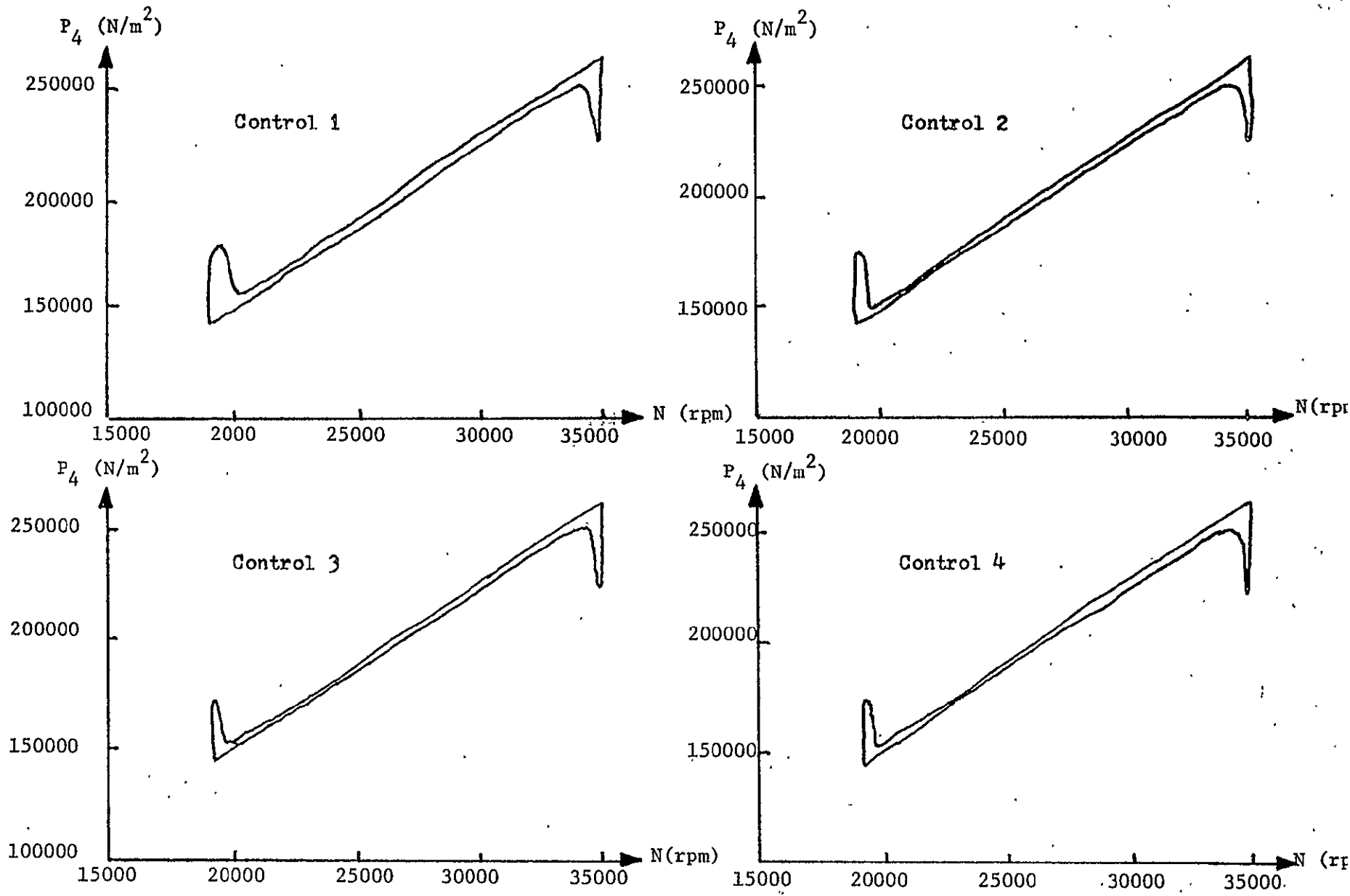


FIGURE 33. P_4 vs. N coordinate system plots of surge margin studies using System C.

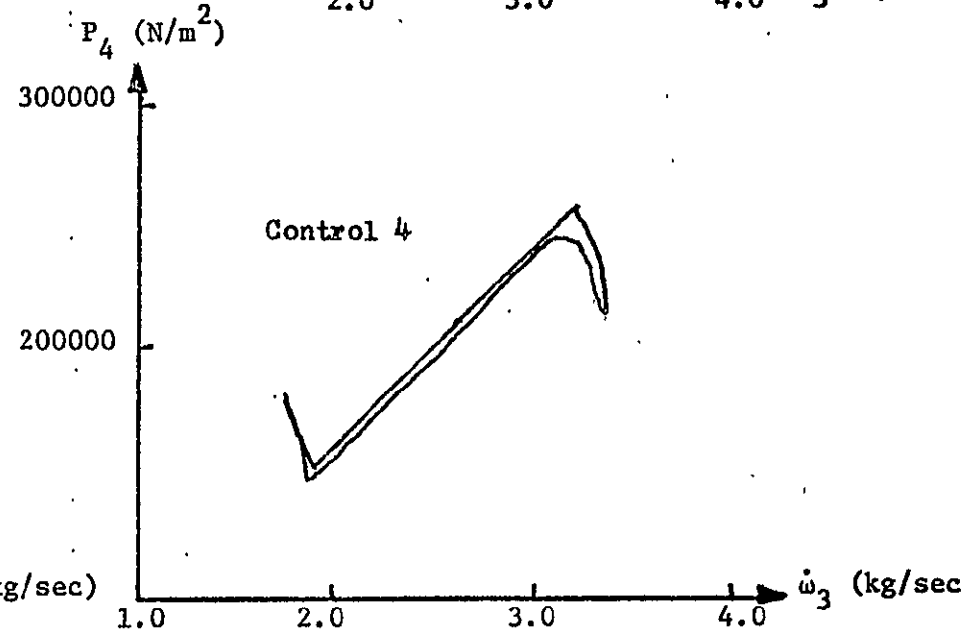
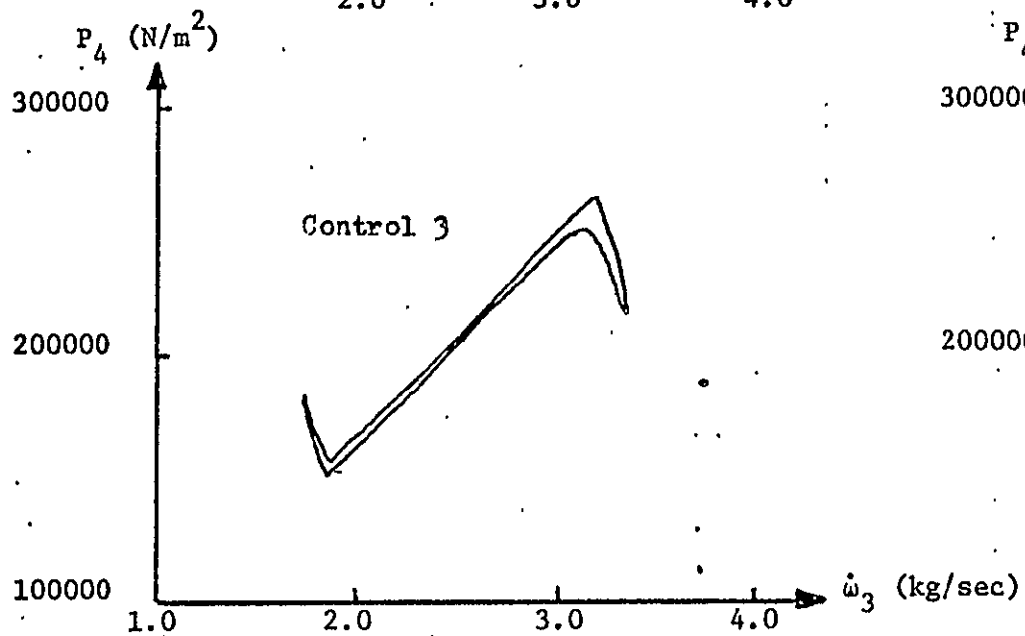
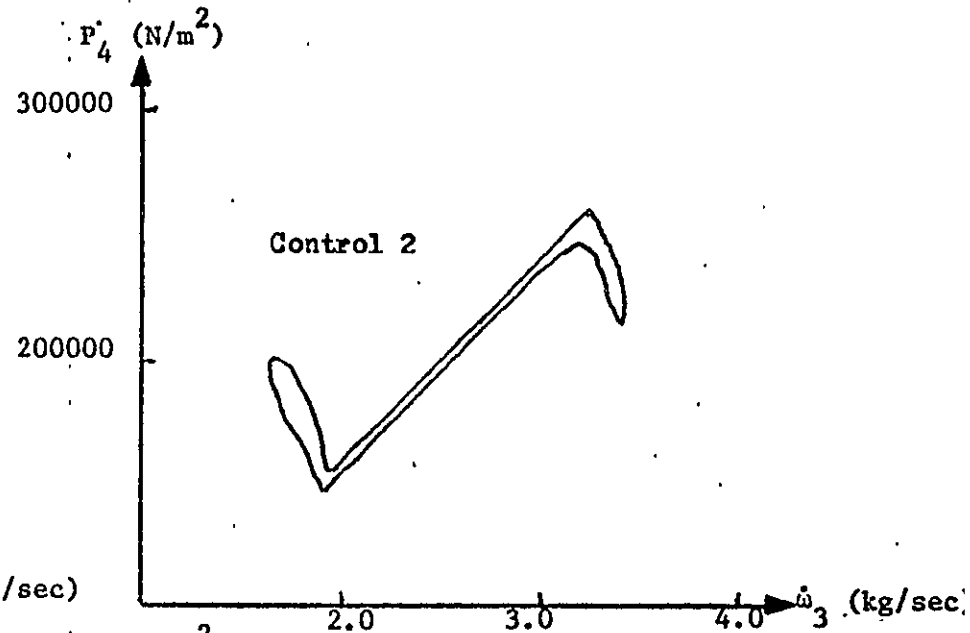
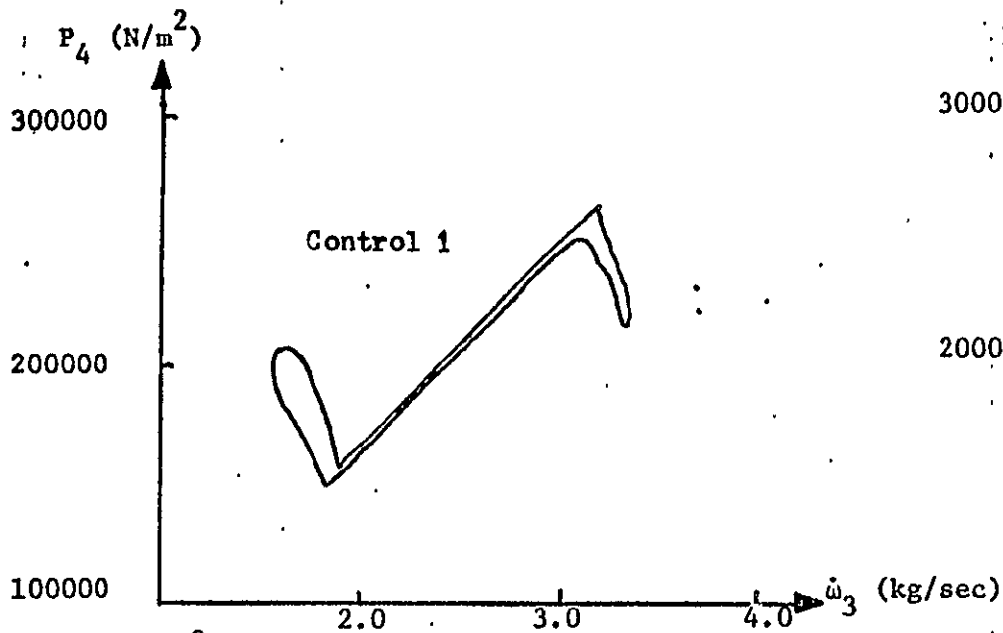


FIGURE 34. P_4 vs. \dot{w}_3 coordinate system plots of surge margin studies using System C.

REPRODUCIBILITY OF THE
ORIGINAL PAGE IS POOR

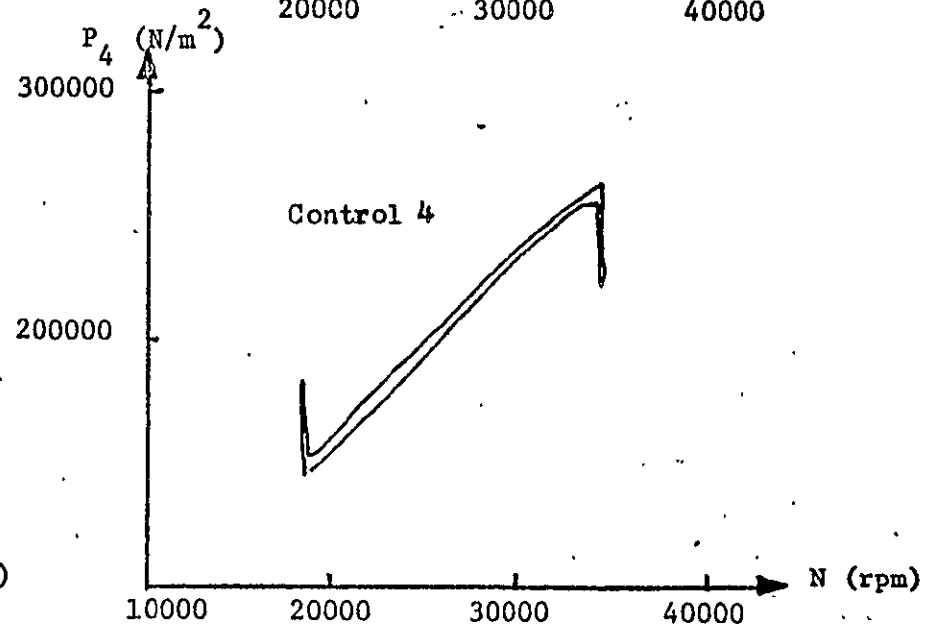
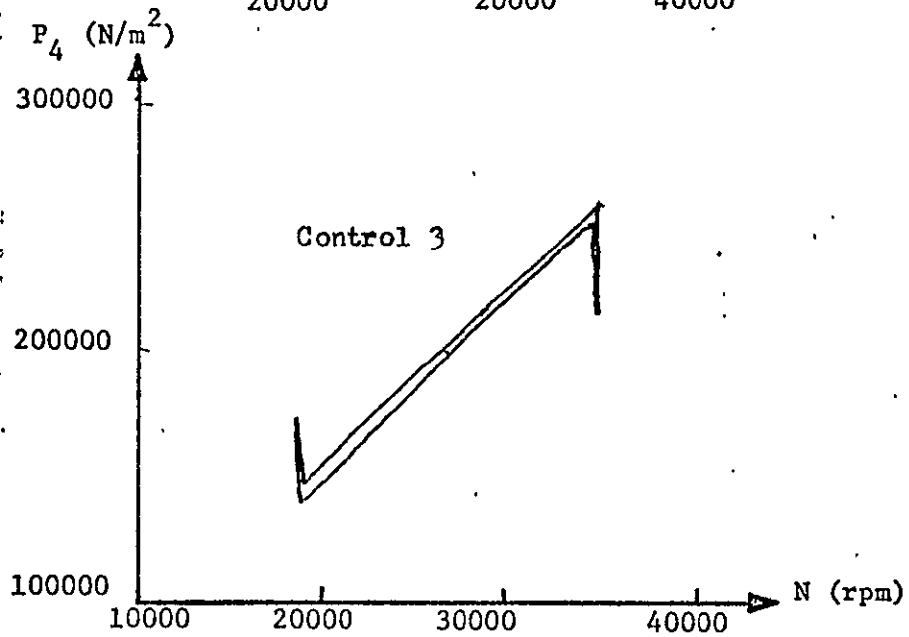
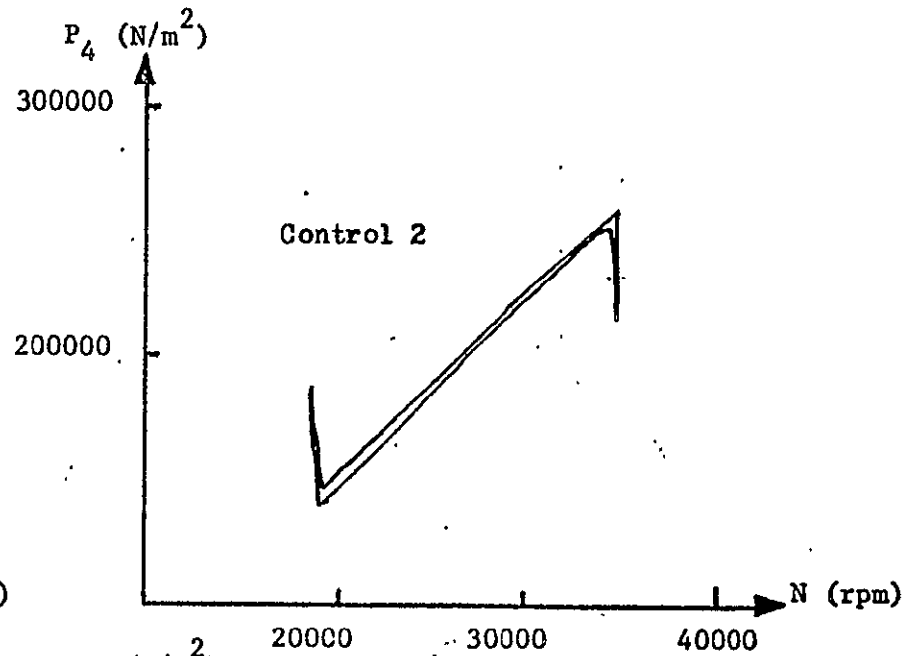
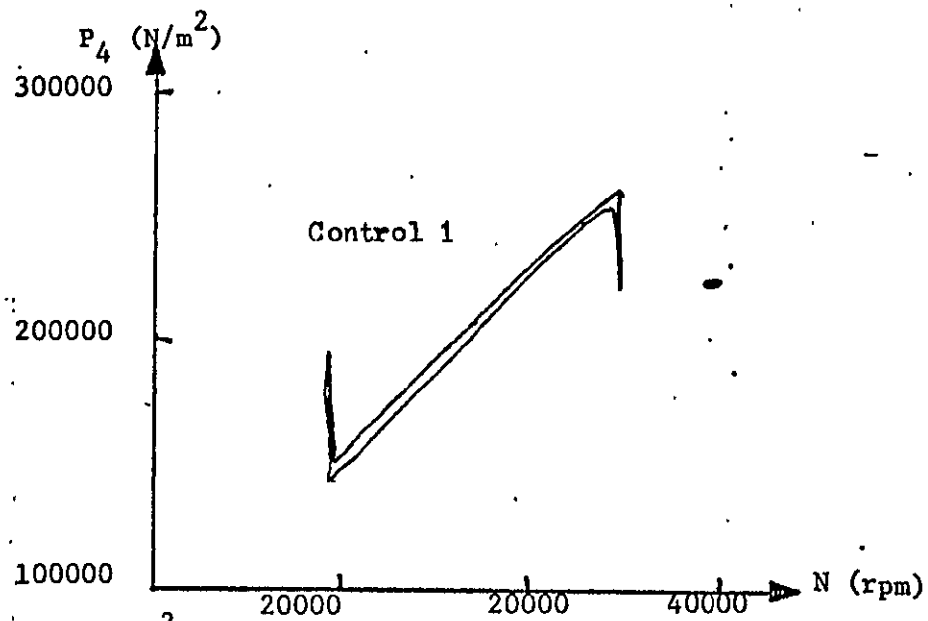


FIGURE 35. P_4 vs. N coordinate system plots of surge margin studies using System P.

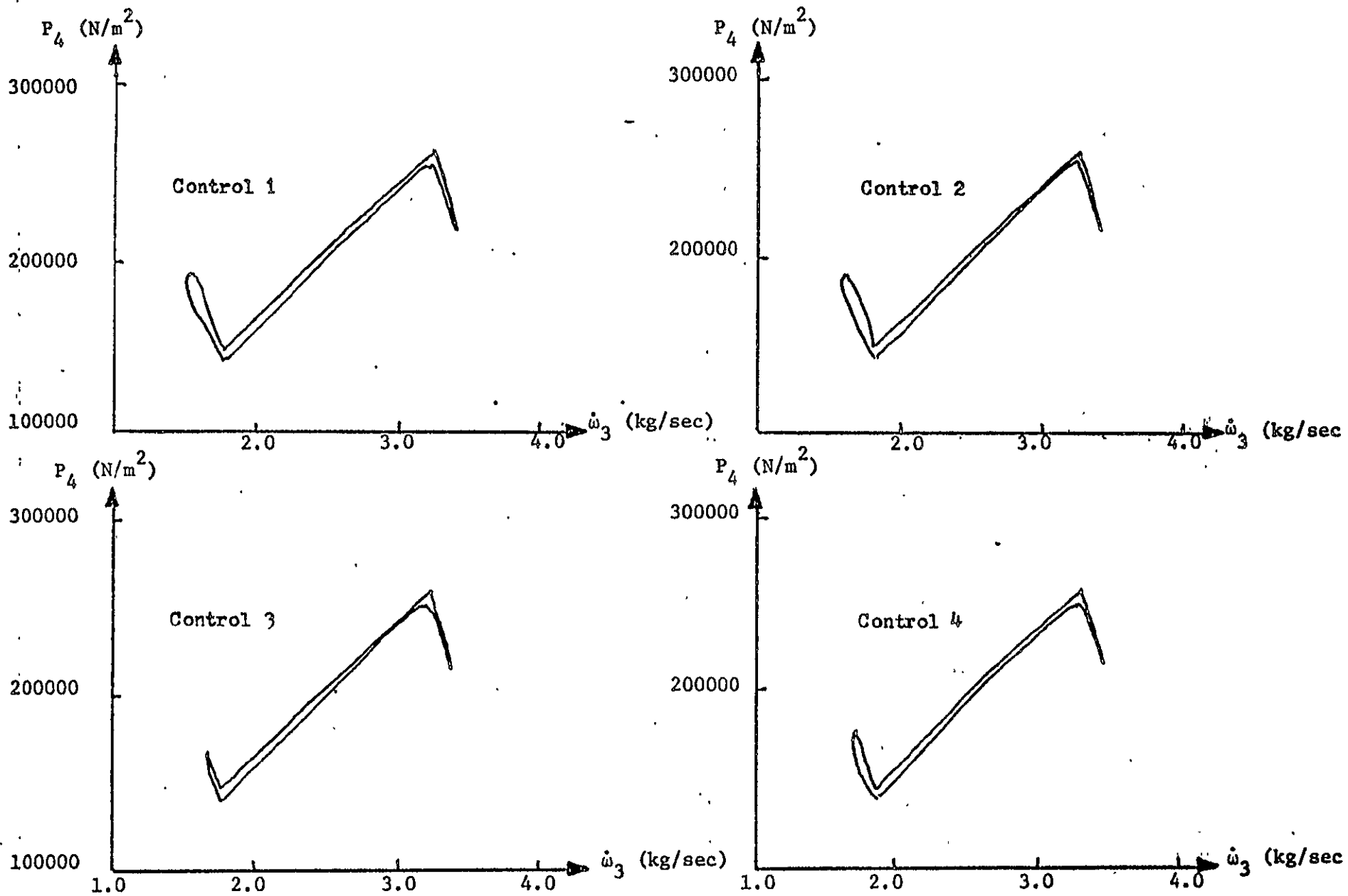


FIGURE 36. P_4 vs. \dot{w}_3 coordinate system plots of surge margin studies using System D.

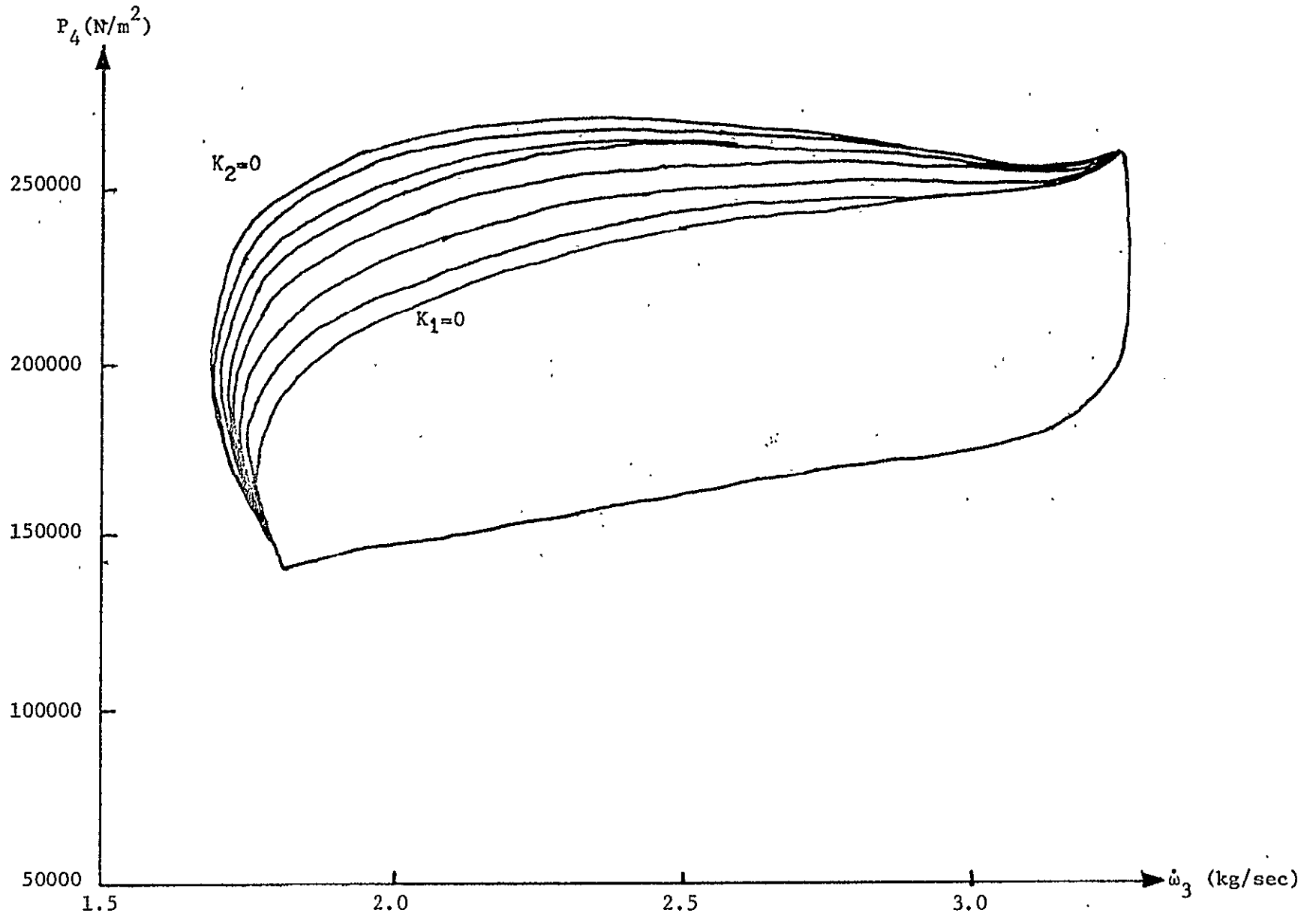


FIGURE 37. Surge margin constraint studies using a linear combination of controls 1 and 4. It is of the form $\dot{w}_f = K_1 \times (\text{Control 1}) + K_2 (\text{Control 2})$ where $K_1 + K_2 = 1$.

APPENDIX C

DETAILS OF SEVENTH ORDER ANALOG SIMULATION MODEL.

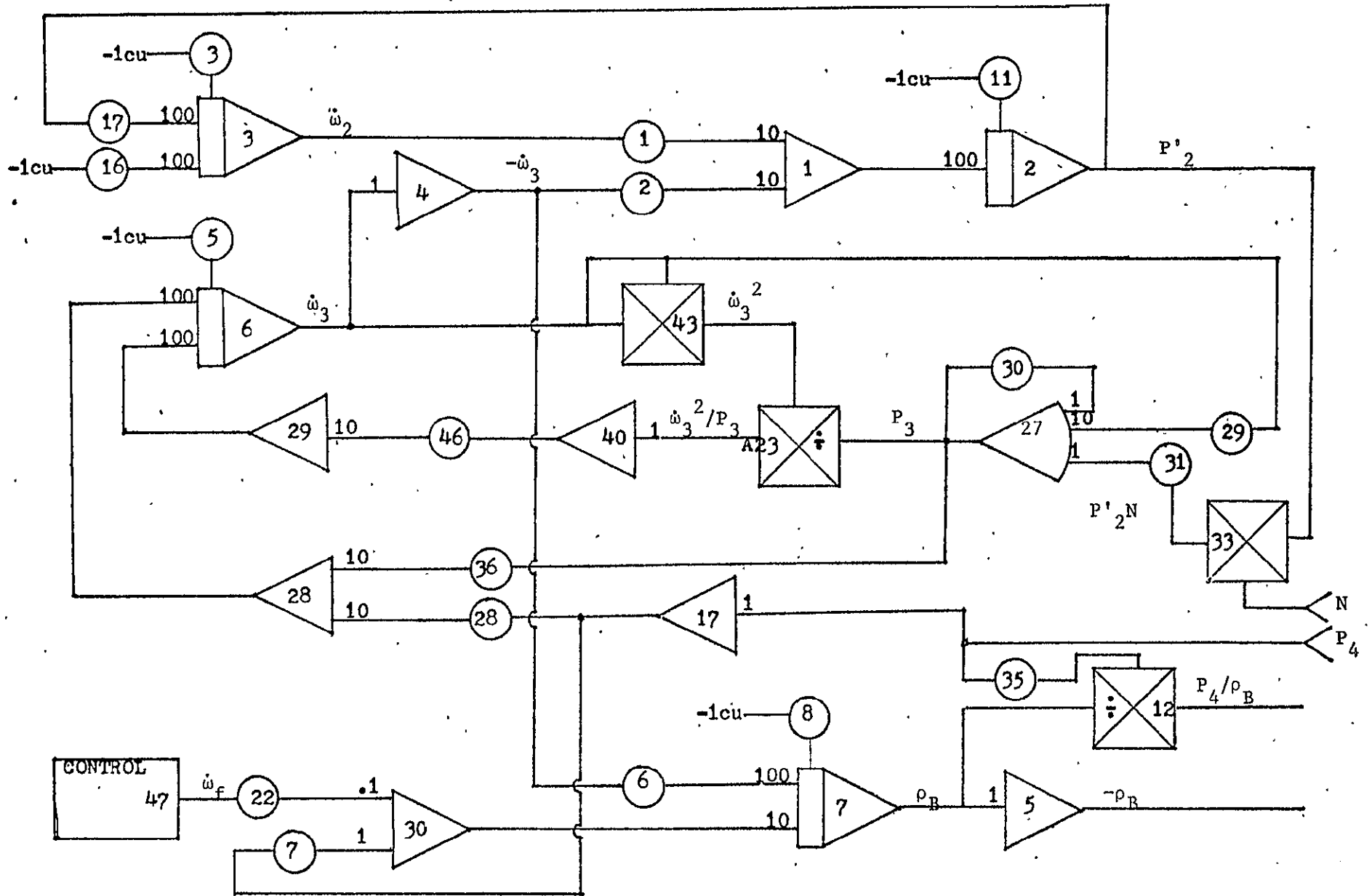


FIGURE 38. Part 1 of seventh order model patching diagram.

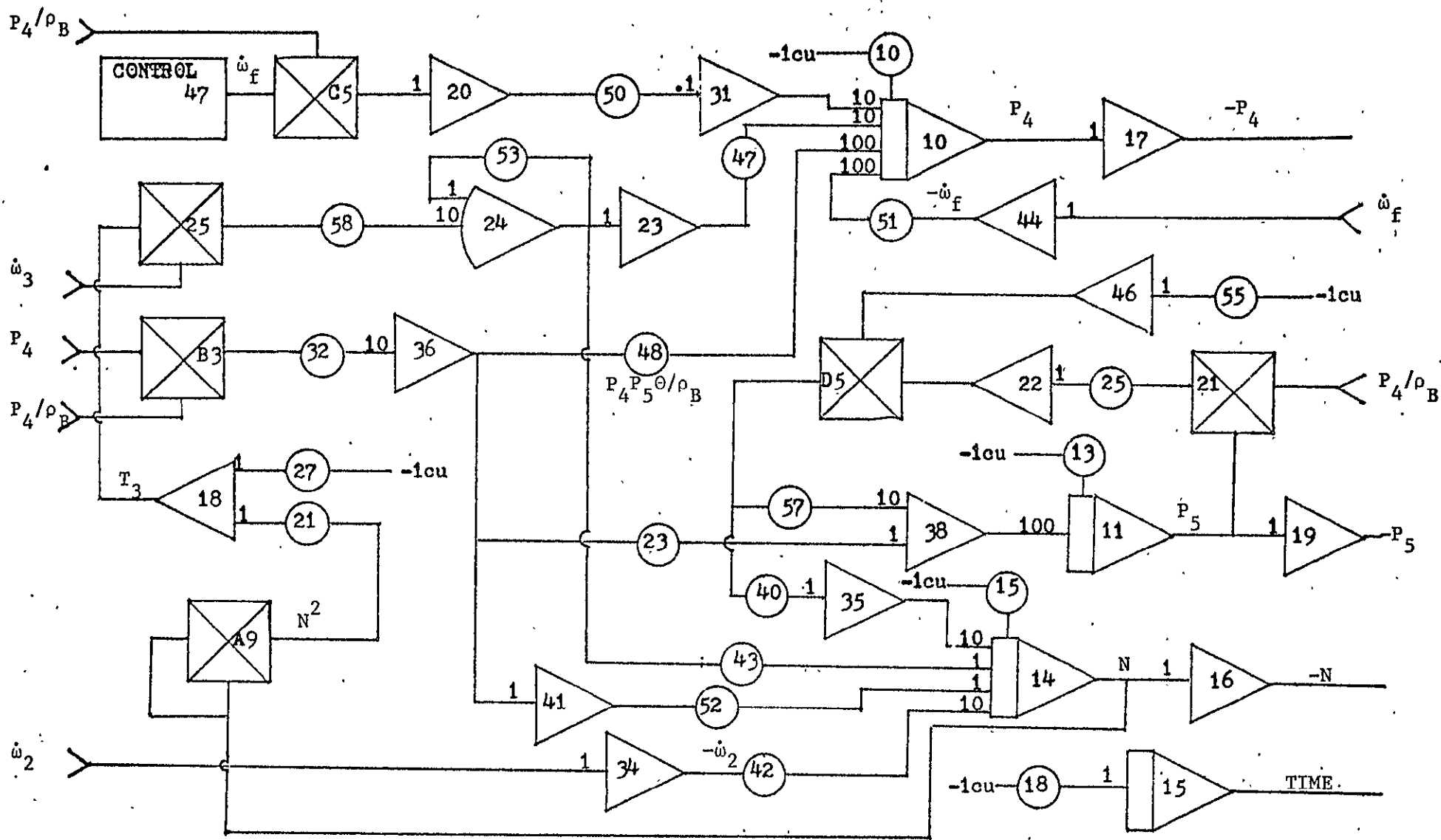


FIGURE 39. Part 2 of seventh order model patching diagram.

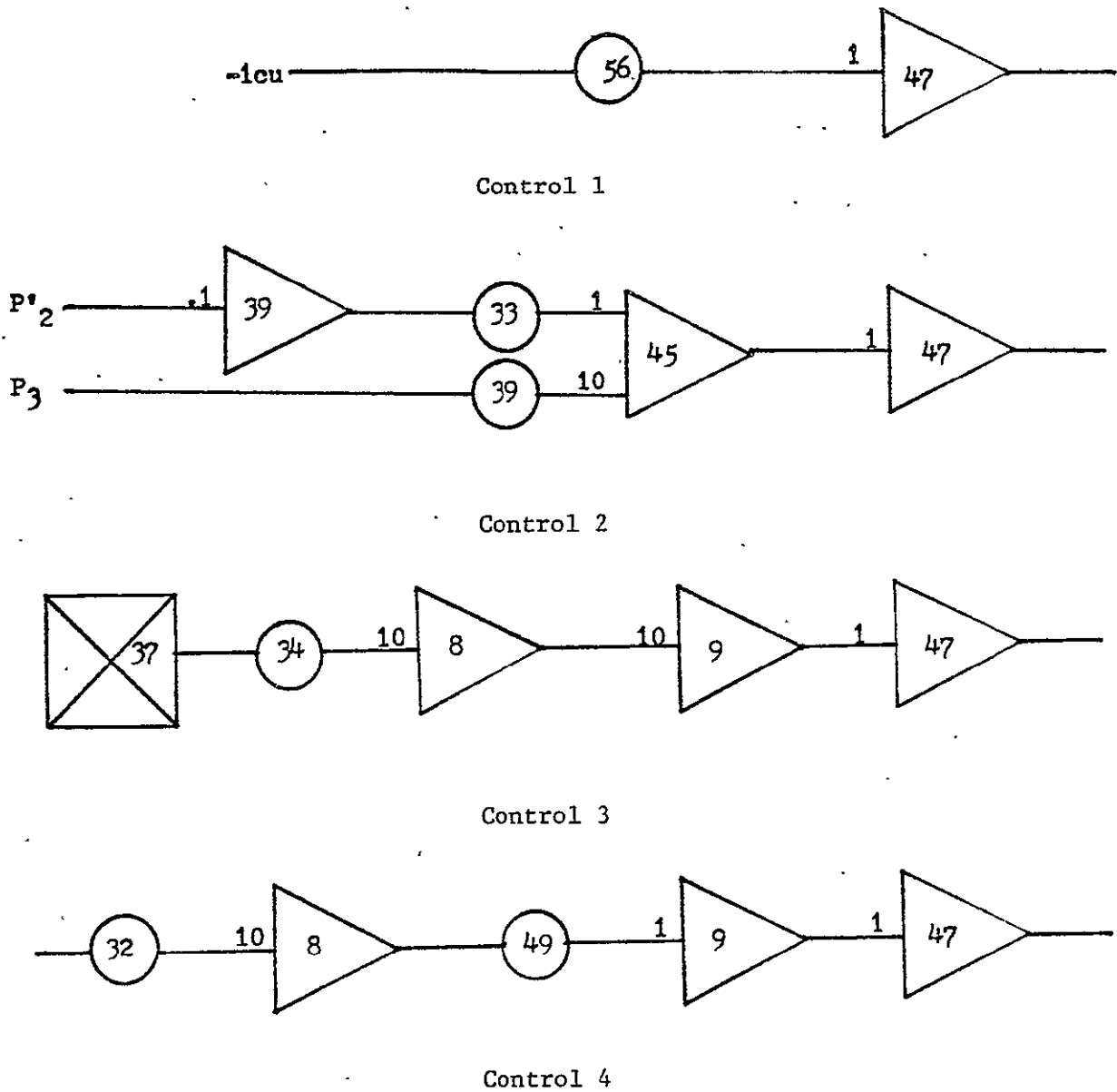


FIGURE 40. Analog diagrams of the four controls considered in this study.

TABLE VI
POT SETTINGS

POT	VALUE
01	.3758
02	.1879
03	.0405
05	.0810
06	.6667
07	.6212
08	.4288
10	.8847
11	.8862
13	.9627
15	.8700
16	.2954
17	.3333
21	.4132
22	.1333
23	.2421
25	.1200
27	.5612
28	.2500
29	.1960
30	.1000
31	.2667
32	.1200
35	.3750
36	.5000
40	.2662
42	.2956
43	.1976
46	.9132
47	.6697
48	.1933
50	.4978
51	.1294
52	.6608
53	.1000
55	.2000
57	.1112
58	.1333

REPRODUCIBILITY OF I...
ORIGINAL PAGE IS POOR.

TABLE VII
STATIC CHECK

AMPLIFIER	VALUE
01	.0000
02	.8860
03	.0405
04	-.0810
05	-.4288
06	.0810
07	.4288
10	.8847
11	.9627
12	-.7737
14	.8700
15	TIME
16	-.8700
17	-.8847
18	.8740
19	-.9627
20	.5546
21	.7747
22	.8937
23	-.9439
24	.9439
25	.0707
27	.4679
28	-.1280
29	.1280
30	.5400
31	.0270
33	.7709
34	-.0405
35	.4754
36	.8213
38	.0000
39	.0880
40	-.0140
41	-.8213
43	-.0065
44	-.7169
46	.2000
47	.7169
A23	.0140
A9	-.7568
B3	-.6843
C5	-.5540
D5	-.1786

TABLE VIII
SCALE FACTORS FOR SEVENTH ORDER MODEL

Variable	Scale Factor
P'_2	80000
$\dot{\omega}_2$	80
$\dot{\omega}_3$	40
ρ_B	2
P_4	300000
P_5	150000
N	40000
T_3	500
$T_3 \dot{\omega}_3$.015
P_4 / ρ_B	.4
$P_4 P_5 \theta / \rho_B$.05
P_3	600000
P_4^2 / ρ_B	.1
θ	5
$\dot{\omega}_f$.08

Beta = 30

REPRODUCIBILITY OF
ORIGINAL PAGE IS POOR

APPENDIX D.**DETAILS OF THIRD ORDER ANALOG SIMULATION MODEL.**

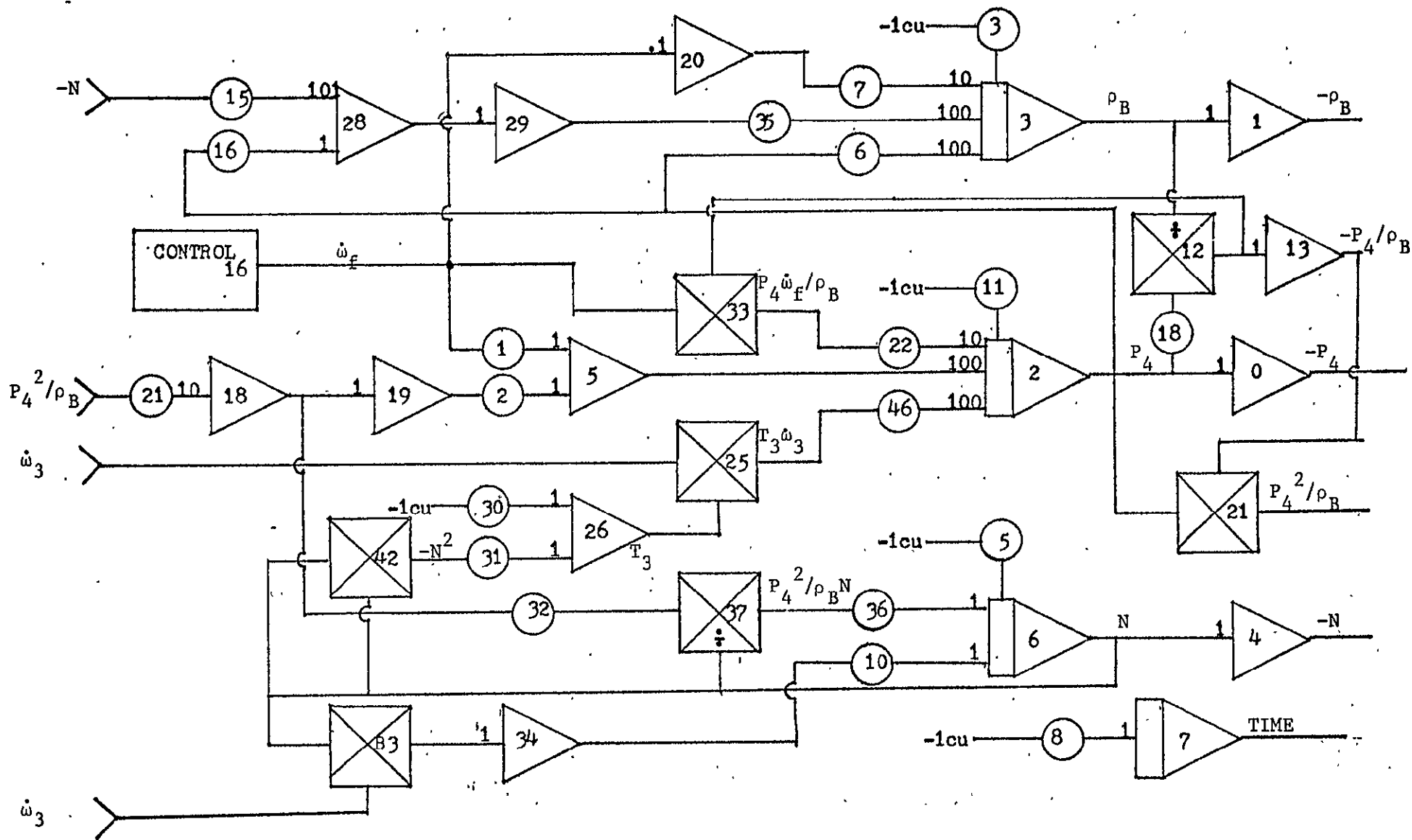


FIGURE 41. Patching diagram for third order model.

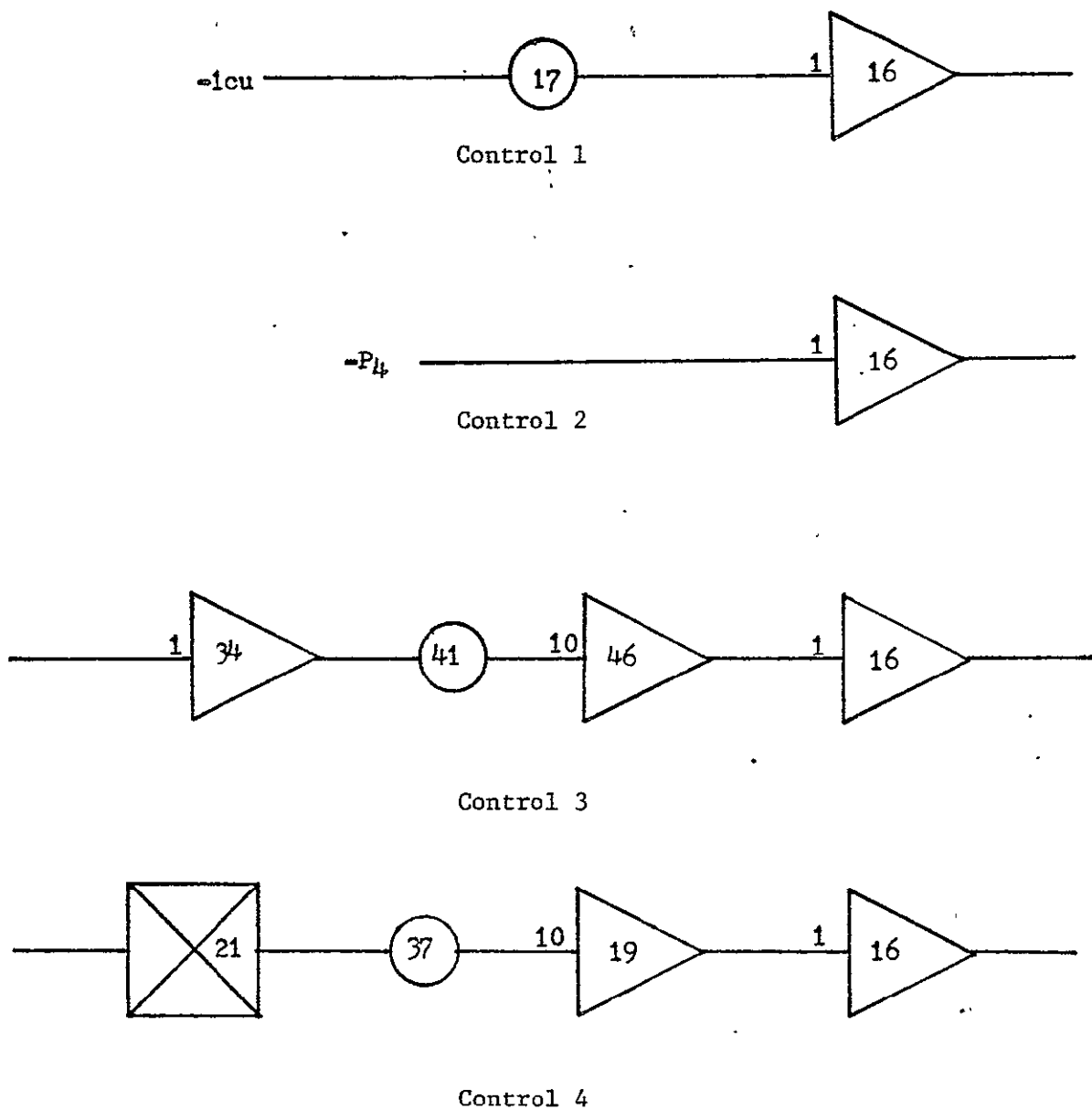


FIGURE 42. Analog diagrams of the four controls considered in this study.

TABLE IX
POT SETTINGS

POT	VALUE
01	.3936
02	.6733
03	.5000
05	.5000
06	.4806
07	.8356
08	.1250
10	.3146
11	TIME
15	.1295
16	.2946
18	.6667
21	.1500
22	.1155
30	.3211
31	.7158
32	.6667
35	.4722
36	.1180
46	.5359

TABLE X
STATIC CHECK

AMPLIFIER	VALUE
00	-.5000
01	-.5000
02	.5000
03	.5000
04	-.5000
05	.1480
06	.5000
07	TIME
12	.6667
13	-.6667
16	.5000
18	.5000
19	-.5000
20	-.0500
21	-.3332
24	.2500
25	-.2500
28	.5000
29	-.5000
33	-.3332
34	.2500
37	-.6666
42	-.2500
B3	.2500

REPRODUCIBILITY OF THE
ORIGINAL PAGE IS POOR

TABLE XI
SCALE FACTORS FOR THIRD ORDER MODEL

Variable	Scale Factor
\hat{P}_4	.5
$\hat{\rho}_B$.5
\hat{N}	.5
$\hat{\omega}_3$.5
\hat{T}_3	.5
$\hat{\omega}_f$.5
$\hat{P}_4/\hat{\rho}_B$	1.5

Beta = 3

APPENDIX E.

SUMMARY OF REFERENCE [4]

A private communication from B. Lehtinen and K. Seldner dated June, 1975.

SIMPLIFIED DRONE SIMULATION w/VARIABLE NOZZLE

i SEA LEVEL STATIC CONDITIONS (recommended conditions)

$$P_2 = 10.13 \text{ N/cm}^2$$

$$T_2 = 288.3 \text{ degK}$$

$$\Theta_2 = \delta_2 = 1$$

ii PARAMETER VALUES

$$\eta_c = 86\% \text{ (constant)}$$

$$\eta_4 = 100\% \text{ (constant)}$$

$$\eta_5 = 85\% \text{ (constant)}$$

$$V_4 = .006354 \text{ m}^3 \text{ (.2244 ft}^3\text{)}$$

$$V_5 = .001099 \text{ m}^3 \text{ (.03880 ft}^3\text{)}$$

$$I = .0305 \text{ N-m-sec}^2 \text{ (.0225 lb-ft-sec}^2\text{)}$$

$$h_c = 4.256 \times 10^7 \text{ J/kg}$$

$$C_p = .25 \text{ (4187.57)} = 1046.9$$

$$\gamma = 1.4$$

iii OPERATING POINT DATA TO USE FOR LINEARIZATIONS

a) Use Data given in Table I, column 1 of TMX-2537 [1].

Notes:

a) Use SLS condition and un-corrected variables.

- b) In the following write-up, "Eq D-" refers to a TMX-2537 equation number and "Eq J-" refers to a TND-6610 [2] equation number.

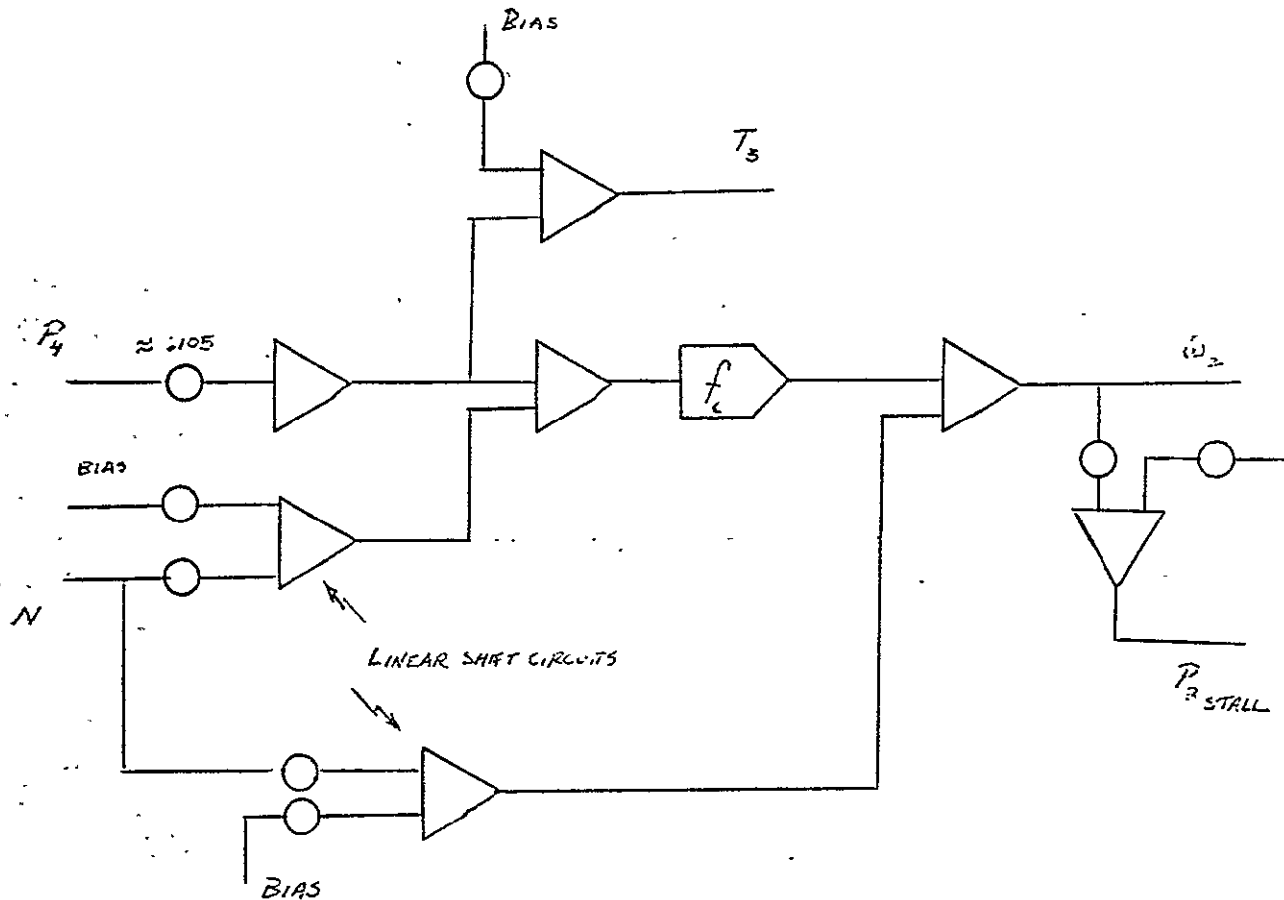


FIGURE 43. Compressor Simulation

- ① All dynamics in compressor are neglected.
- ② f_c is one "representative" speed line obtained from Fig. D-3, the overall compressor map.

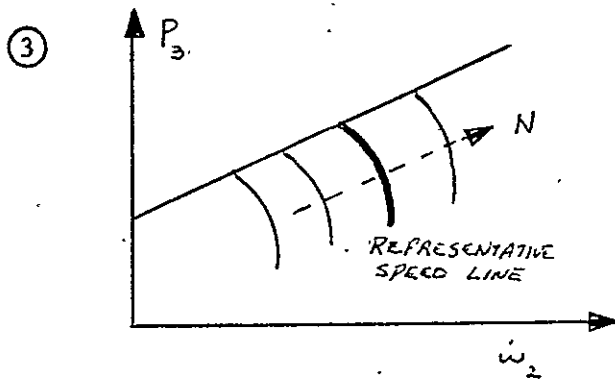


FIGURE 44. Compressor Map

Fit the map of Fig. D-3 by linearly shifting the one "representative" speed line with N. "Bias" is adjusted to null out shifts when operating at the "representative" speed.

Generate a linear approximation to the stall line, as shown ($P_{3\text{STALL}}$). This is used only as a stall indicator.

- ④ Assume constant efficiency ($\eta_c = \text{constant}$). Obtain T_3 as a function of P_3 using eq J-7 & J-8.

$$\frac{T_3 - T_2}{T_2} = \frac{(P_3/P_2)^{2/7}}{\eta_c}$$

Linearize this relationship as shown.

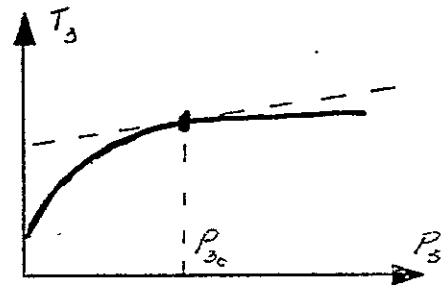


FIGURE 45. T_3 Relation

- ⑤ Obtain P_3 from P_4 assuming 5% pressure drop ($P_3 \approx 1.05 P_4$).

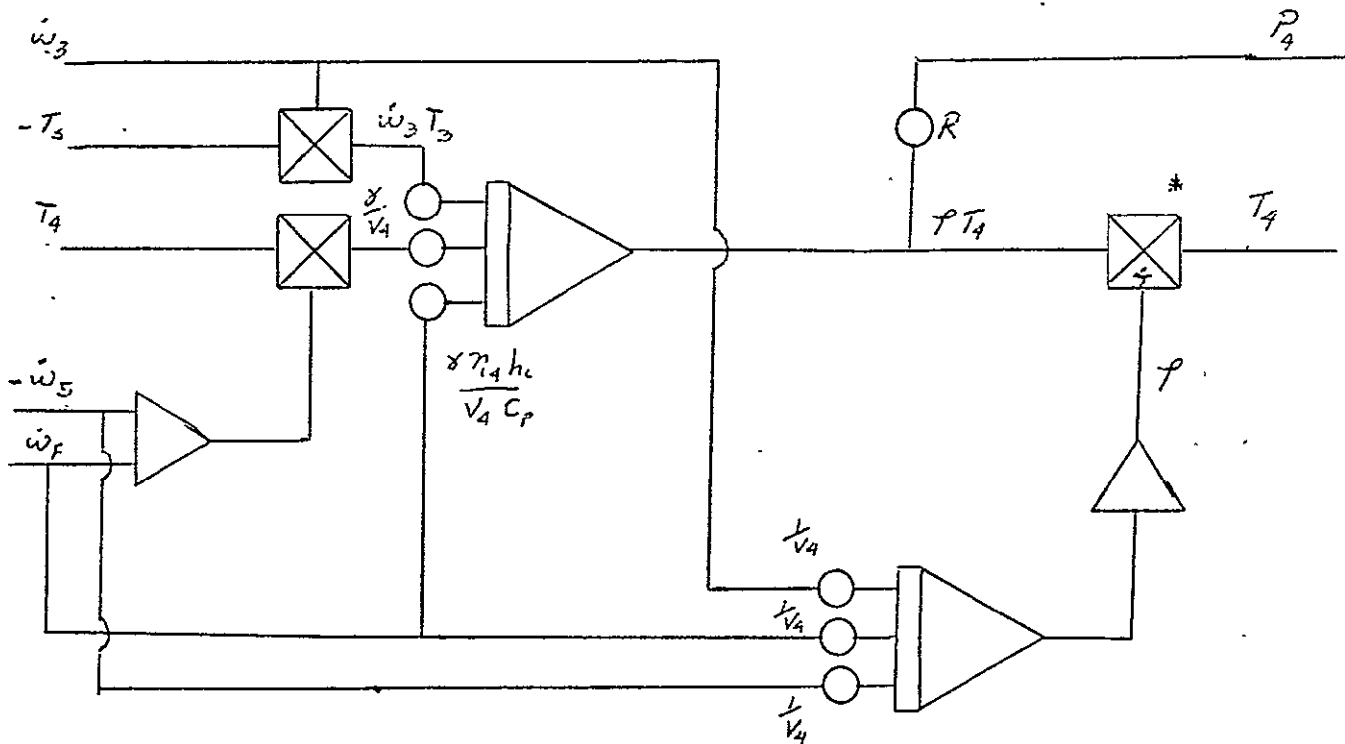


FIGURE 46. Combustor Simulation

REPRODUCIBILITY OF ORIGINAL PAGE IS POOR

(11) Continuity eq (eq D-B14)

$$\frac{dP_5}{dt} = \frac{R}{V_5} T_5 (\dot{\omega}_5 - \dot{\omega}_8)$$

(12) Energy eqs

$$T_4 - T_5 = \frac{\Delta h_a}{C_p} \quad (\text{Eq D-B13})$$

$$\Delta h_i = C_p T_4 \left[1 - \left(\frac{P_5}{P_4} \right)^{2/7} \right] \quad (\text{Eq D-B15})$$

Assume constant turbine efficiency; $\eta_5 \approx \text{constant}$

$$\Delta h_a = \eta_5 \Delta h_i$$

Combining, we obtain

$$\frac{T_4 - T_5}{T_4} = \eta_5 \left[1 - \left(\frac{P_5}{P_4} \right)^{2/7} \right]$$

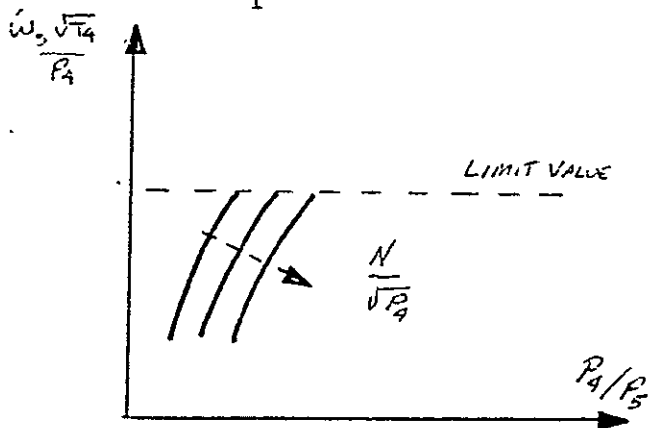
Linearize this temperature-pressure relationship, as was done for the compressor (item (4)).

(13) Turbine map (f_T)

use eq D-B11

$$\frac{\dot{\omega}_5 \sqrt{T_4}}{P_4} = f \left(\frac{P_4}{P_5}, \frac{N}{\sqrt{T_4}} \right)$$

Let f_T be a representative corrected speed line from Fig. D-21.



Assume a linear shift in this speed line with $N/\sqrt{T_4}$. Use a limiter on the output of the multiplier as shown on the analog diagram.

FIGURE 48. Turbine Map

- ⑭ Linearize $\sqrt{T_4}$ about operating point.

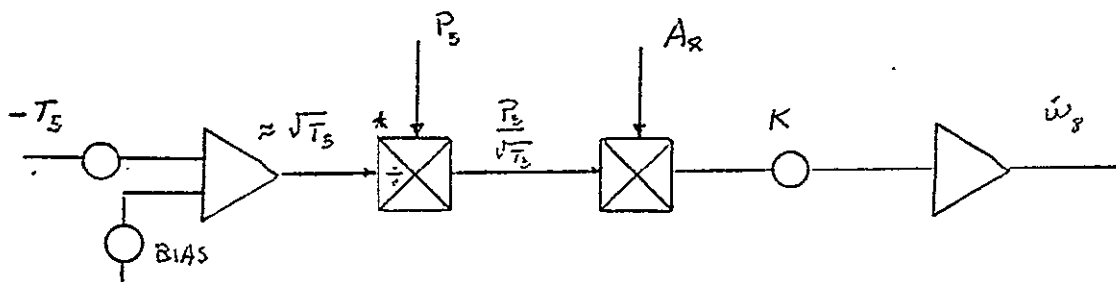


FIGURE 49. Nozzle

- ⑮ Assume choked flow in Nozzle ($0 \leq P_0/P_5 \leq 0.53$)

$$\frac{\dot{\omega}_8 \sqrt{T_5}}{P_5 A_8} = \sqrt{\frac{\gamma_g}{R} \left(\frac{2}{\gamma+1} \right)^{\frac{\gamma+1}{\gamma-1}}} \quad \text{eq D-B16}$$

- ⑯ Linearize $\sqrt{T_5}$ about operating point.

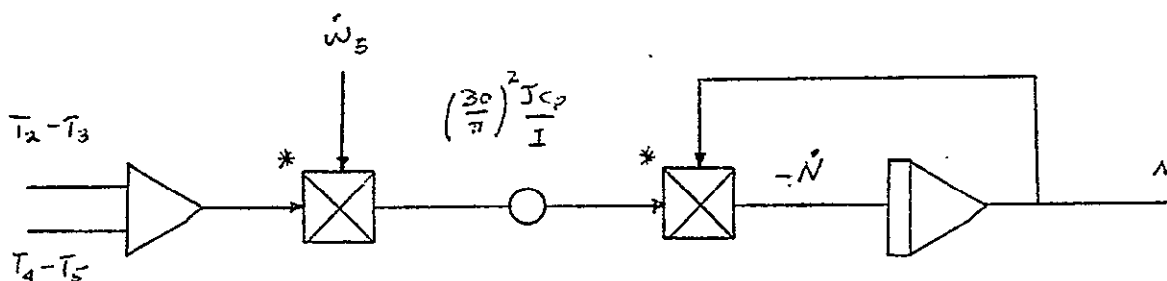


FIGURE 50. Rotor Dynamics

- ⑰ Assume: $\dot{\omega}_5 = \dot{\omega}_8$
 $\dot{\omega}_2 = \dot{\omega}_3$
 and $\dot{\omega}_2 = \dot{\omega}_5$

Also assume:

$$h_4 = C_p T_4$$

$$h_5 = C_p T_5$$

Eq (D-B21) then becomes

$$\frac{dN}{dt} = \left(\frac{30}{\pi} \right)^2 \frac{J_c P}{I} \frac{\dot{\omega}_5}{N} (T_2 - T_3 + T_4 - T_5)$$

(18) Nonlinear Complement is 14 multipliers and 2 DFG'S.

To reduce multiplier complement to 6, linearize the multiplier functions denoted by "*" in the diagrams;

for example, on page 3:

$$\begin{aligned} \frac{\rho T_4}{T_4} &\approx \rho_o + \frac{1}{T_{4o}} (\rho T_4 - \rho_o T_{4o}) - \frac{1}{T_{4o}^2} \rho_o T_{4o} (T_4 - T_{4o}) \\ &= \rho_o + \frac{1}{T_{4o}} (\rho T_4) - \frac{\rho_o}{T_{4o}} T_4 \end{aligned}$$

(19) Note that throughout the simulation diagrams, no attention has been paid to scaling or sign conventions.

REFERENCES

1. Seldner, Kurt; Geysler, Lucille C.; Gold, Harold; Walker, Darrel; and Burgner, Gary. "Performance and Control Study of a Low-Pressure-Ratio Turbojet Engine for a Drone Aircraft." NASA TM X - 2537, 1972.
2. Seldner, Kurt; Mihaloew, James R.; and Blaha, Ronald J. "Generalized Simulation Technique for Turbojet Engine System Analysis." NASA TN D-6610, 1972.
3. Zucrow, M. J. Aircraft and Missile Propulsion. New York: John Wiley and Sons, Inc. 1958.
4. Lehtinen, Bruce, and Seldner, Kurt. Letter to R. J. Leake, June 9, 1975.
5. Sellers, James F. and Daniele, Carl J. "Dyngen - A Program for Calculating Steady - State and Transient Performance of Turbojet and Turbofan Engines." NASA TN D-7901, 1975.
6. Crowley, Mark. "Ansir 3: A Digital Language for HYBRID Simulation and Patching," Masters Thesis, Department of Electrical Engineering, University of Notre Dame, Notre Dame, Ind., August, 1975.